RELATIONS BETWEEN CLIMATE VARIABILITY AND GROUNDWATER FLUCTUATIONS IN U.S. PRINCIPAL AQUIFERS

A Thesis submitted to the faculty of
San Francisco State University
In partial fulfillment of
the requirements for
the Degree

Master of Science

In

Geosciences

by

Elzie Monique Lapuz Velasco

San Francisco, California

May 2015

CERTIFICATION OF APPROVAL

I certify that I have read Relations Between Climate Variability and Groundwater Fluctuations in U.S. Principal Aquifers by Elzie Monique Lapuz Velasco, and that in my opinion this work meets the criteria for approving a thesis submitted in partial fulfillment of the requirement for the degree Master of Science in Geosciences at San Francisco State University.

Dr. Jason J. Gurdak Ph.D.
Assistant Professor

Dr. Leonard Sklar Ph.D.
Professor

John P. Monteverdi

Dr. John P. Monteverdi Ph.D.
Professor

RELATIONS BETWEEN CLIMATE VARIABILITY AND GROUNDWATER FLUCTUATIONS IN U.S. PRINCIPAL AQUIFERS

Elzie Monique Lapuz Velasco
San Francisco, California
2015

The response of groundwater to interannual to multidecadal climate oscillations has important implications for water-resource sustainability, however, there is a poor understanding of how physical processes in the vadose zone dampen and filter climate variability signals prior to recharging the water table. This thesis addresses this knowledge gap by quantifying the teleconnections between six modes of quasi-periodic climate variations and precipitation and groundwater level fluctuations within seven sand and gravel principal aquifers (PAs) in the United States. The six modes of climate variability are the Atlantic Multidecadal Oscillation (50–80 year cycle), Pacific Decadal Oscillation (15–30 year cycle), El Niño-Southern Oscillation (2–7 year cycle), North Atlantic Oscillation (3–6 year cycle), Pacific/North American Oscillation (<1–4 year cycle), and Arctic Oscillation (6–12 month cycle). Singular Spectrum Analysis was used to quantify climate variability signals in climatic and hydrologic time series, and the influence of soil texture, vadose zone thickness, mean infiltration flux, and infiltration period on the damping of sinusoidal signals in the vadose zone was explored using an analytical model. Results indicate that each PA reflects some influence from each of the six modes of climate variability and that the effects of these climate variations on groundwater fluctuations can be characterized spatially based on the degree of damping. There is a consistent increase (decrease) in average percent variance and lag correlation coefficients with longer (shorter) fluctuation periods. These findings highlight the importance of low frequency climate variations on hydrologic fluctuations and indicate that considering these long-term patterns will help with water resource management.

I certify that the Abstract is a correct representation of the content of this thesis.

Chair, Thesis Committee

5-19-2015
Date

ACKNOWLEDGEMENTS

Foremost, I would like to express my sincere gratitude to my thesis advisor, Dr. Jason Gurdak, for his guidance, trust, and encouragement. He supported me through all my years at SFSU and helped me attain many great academic and professional opportunities. It was a pleasure and honor to have worked with him on this research project. I would also like to thank the rest of my thesis committee, Dr. Leonard Sklar and Dr. John Monteverdi, for their enthusiasm, insightful comments, and stimulating questions. My sincere thanks goes to Jesse Dickinson, hydrologist at the USGS Arizona Water Science Center, and Dr. Ty Ferre, professor in the Department of Hydrology and Water Resources at the University of Arizona, for their incredible knowledge and collaboration. I must also acknowledge the National Science Foundation, the ARCS Foundation, and Doris and David Dawdy for their generous financial support of my research. I would like to recognize my fellow grad student Claudia Corona for her positivity and friendship. I am also indebted to Dr. Karen Grove because without her belief in me I would not have made the wonderful decision to move to the Bay Area to pursue my love of geology. Finally, I am eternally grateful for the love and support of my parents, Joaquin and Elizabeth, my brothers, J.B. and Jober, and my best friend, Giovana Constantino.

TABLE OF CONTENTS

TABLE OF CONTENTS (CONTINUED)

TABLE OF CONTENTS (CONTINUED)

LIST OF TABLES

LIST OF TABLES (CONTINUED)

LIST OF FIGURES

LIST OF FIGURES (CONTINUED)

LIST OF APPENDICES

1.0 INTRODUCTION

The potential effects of natural climate variability on water resources has been an increasingly urgent water management issue on local to global scales and especially in the United States (U.S.). Interannual to multidecadal climate variability impacts the hydrologic cycle and has been associated with changes in patterns of precipitation, snowmelt, streamflow, and drought occurrence (e.g. Beebee and Manga, 2004; Brabets and Walvoord, 2009; Hanson et al., 2004; Mantua et al., 1997; McCabe et al., 2004; Ropelewski and Halpert, 1986; Vicente-Serrano et al., 2011). However, it is still poorly understood how climate variability affects subsurface hydrologic processes and groundwater quantity, particularly in many of the principal aquifers (PAs) of the U.S., which are important regional sources of potable water (Gurdak et al., 2009, 2007; Hanson et al., 2006). Groundwater is the largest accessible source of freshwater and plays a critical role in maintaining adequate water supplies for human consumption, agricultural irrigation, and ecosystem function. Therefore, it is essential to understand how long-term climate variations impact groundwater levels in our nation's PAs. This knowledge will better inform practices and policies in water management and sustainability, particularly within the context of increasing groundwater use due to population growth, agricultural needs, and the possible impacts of climate change and variability (Earman and Dettinger, 2011; Gurdak et al., 2007; Hanson et al., 2006; Holman, 2006; Wada et al., 2010).

This thesis focuses on six measures of pressure teleconnections that have been shown statistically to relate to interannual to multidecadal climate oscillations and to anomalous shifts in weather patterns in many parts of the world including in the U.S. These six indices, or climate variability modes, are the Atlantic Multidecadal Oscillation (AMO), the Pacific Decadal Oscillation (PDO), the El Niño-Southern Oscillation (ENSO), the North Atlantic Oscillation (NAO), the Pacific/North American Oscillation (PNA), and the Arctic Oscillation (AO). Each mode of climate variability has a quasi-periodic cycle to the negative and positive phases of the index. The AMO has a 50 to 80 year cycle, the PDO has a 15 to 30 year cycle, the ENSO has a 2 to 7 year cycle, the NAO has a 3 to 6 year cycle, the PNA has a <1 to 4 year cycle, and the AO has a 6 to 12 month cycle. These modes of climate variability have been associated with changes in the amount, timing, and spatial distribution of precipitation, air temperature, and evapotranspiration (e.g. De Vita et al., 2012; Ropelewski and Halpert, 1986; Sabziparvar et al., 2011; Shang et al., 2011; Tremblay et al., 2011). Climate variability therefore has important implications for recharge rates and changes in groundwater storage (e.g. Fleming and Quilty, 2006; Gurdak et al., 2007; Hanson et al., 2006, 2004; Kuss, 2011).

There is abundant literature that link interannual and multidecadal climate oscillations to changes in various hydrologic processes in surface water such as streamflow, surface water storage, and flooding (e.g. Bayari and Yildiz, 2012; Brabets and Walvoord, 2009; Kondrashov et al., 2005; Maheu et al., 2003; Mazouz et al., 2012). Some studies have also inferred teleconnections between climate variability and groundwater levels in local areas around the world (e.g. Anderson and Emanuel, 2008; Dickinson et al., 2004; Fleming and Quilty, 2006; Gurdak et al., 2007; Hanson et al., 2006, 2004; Holman et al., 2011; Perez-Valdivia et al., 2012; Pool, 2005; Tremblay et al., 2011; Venencio and García, 2011). However, groundwater responses to interannual to multidecadal climate oscillations are still poorly monitored, understood, and quantified (Earman and Dettinger, 2011; Gurdak et al., 2007). This knowledge gap is driven by a poor understanding of how physical processes in the vadose zone dampen and filter interannual to multidecadal climate variability signals during infiltration, percolation, and recharge to the water table (Dickinson et al., 2014a).

To address this knowledge gap, this thesis answers the following three questions: 1) How does soil texture, vadose zone thickness, infiltration flux, and infiltration periodicity control the damping and filtering of climate variability signals in the vadose zone?; 2) How does the damping and filtering of signals affect correlations and lag times between variations in climate, precipitation, and groundwater?; and 3) What are the national-scale patterns of climate variability effects on select PAs in the U.S.? More specifically, this thesis quantifies the teleconnections between quasi-periodic climate variations as measured by the AMO, PDO, ENSO, NAO, PNA, and AO and precipitation and groundwater level fluctuations within seven unconsolidated to semi-consolidated sand and gravel PAs in the U.S. The seven PAs are the California Coastal Basins, Rio Grande, Coastal Lowlands, Mississippi Embayment, Surficial, Glacial, and aquifers of the Pacific Northwest region (Figure 1). Co-located precipitation and groundwater sites were selected within the bounds of each PA, and then spectral analysis techniques were used to identify quasi-periodic oscillations, or reconstructed components (RCs), in the long-term precipitation and groundwater records that are possibly related to the modes of climate variability. Next, the time series of RCs for climate variability indices, precipitation, and groundwater levels were correlated to determine the lag times in the response of precipitation and groundwater to these climate variations. Finally, an analytical model of periodic flow in the vadose zone called DAMP (Dickinson et al., 2014a) was used to explore the influence of soil texture, vadose zone thickness, and infiltration flux and periodicity on the damping and filtering of climate variability signals in the vadose zone.

Identifying the presence of climate variability signals in hydrologic time series, lag correlating the data sets, and then linking these findings to select infiltration and vadose zone properties provides insight into how the vadose zone may be altering the climate variability signals within infiltrating water and thus modifying the teleconnection between climate variations and groundwater fluctuations. Results from these PAs are compared to findings from other climate variability investigations including those of Gurdak et al. (2007) and Kuss (2011) that focused on the impact of climate variability on the Central Valley, Basin and Range, High Plains, and North Atlantic Coastal PAs. This thesis will provide a more comprehensive analysis of national-scale trends of the effects of interannual to multidecadal climate variability on groundwater levels in PAs across the U.S. These findings can be used to help make water-resource management plans and policies better adapted to potential changes in the global climate. It will also help ensure that water resources and particularly groundwater are used more sustainably and that increasing water demands in the U.S. can continue to be met in future years.

2.0 BACKGROUND

2.1 Climate Variability

Climate variability refers to natural variations about the mean state of the climate that occur on various temporal and spatial scales beyond that of individual weather events (Baede, 2001; Ghil, 2002). Indices for each mode of climate variability are created using various climatic anomalies in key locations, including but not limited to sea surface temperatures (SSTs), sea level pressures (SLPs), geopotential heights, and wind speeds (Ghil, 2002; NOAA, 2015). These indices are used to define positive, negative, and neutral phases of a climate variability mode and to identify the strength of the phases. Additionally, positive and negative phases are associated with anomalous weather patterns in certain areas of the world.

2.2 Climate Variability Modes in the Pacific Region

2.2.1 The Pacific Decadal Oscillation (PDO)

The PDO is characterized by anomalies in SSTs in the North Pacific Ocean that occur every 15 to 30 years (Mantua et al., 1997; Mantua and Hare, 2002). The PDO index (Figure 2a) is calculated as the leading principal component of detrended monthly SST anomalies in the Pacific Ocean poleward of 20° north latitude (Zhang et al., 1997).

During the positive (negative) phase of the PDO, SSTs are cooler (warmer) than normal in the central North Pacific while SSTs are anomalously warmer (cooler) than normal along the west coast of North America. The positive phase of the PDO is associated with ridging in the middle and upper troposphere over the eastern Pacific with the polar jet stream and surface cyclones directed into Alaska. During the negative phase, there is a tendency for high amplitude troughs in the middle and upper troposphere over the eastern Pacific with an accompanying southward shift of the average track of frontal cyclones into the West Coast and a greater frequency of surface cyclones in the eastern Gulf of Alaska (Hanson et al., 2006; Mantua et al., 1997; Mantua and Hare, 2002). As a result, positive PDO has been associated with decreased winter precipitation and sustained droughts from the Pacific Northwest region through the northwest Great Plains, Great Lakes, and Ohio Valley, and wetter than normal conditions in the western and southwestern U.S. (Hanson et al., 2006; Higgins et al., 2007; Mantua et al., 1997; Mantua and Hare, 2002). During the negative PDO, the precipitation patterns in these areas are reversed. The PDO was in a positive phase during the periods 1925 to 1946 and from 1977 through the late 1990s, and in a negative phase from 1890 to 1924, 1947 to 1976, and since 1999 (Figure 2a) (Mantua and Hare, 2002; McCabe et al., 2004).

2.2.2 The El Niño-Southern Oscillation (ENSO)

The ENSO is characterized by anomalies in SSTs and SLPs in the equatorial Pacific that occur every 2 to 7 years (NOAA, 2015). Several different ENSO indices have developed over time, however, the Multivariate ENSO Index (MEI) (Figure 2b) is favored over other indices because it combines the significant features of all observed surface fields in the tropical Pacific: SLP, SST, zonal and meridional winds, air temperature, and total cloudiness (Wolter and Timlin, 1998, 1993). During the positive phase of the ENSO, also known as an El Niño, the equatorial Pacific experiences abnormally low SLP in the east and high SLP in the west. This allows for the warm waters of the western Pacific to migrate eastward, creating increased SSTs in the east. The warmer SSTs in the eastern tropical Pacific then create height and pressure anomalies in the middle and upper troposphere in the subtropics in such a fashion that the polar jet stream is strengthened and shifted south, driving storms from California to Florida. Consequently, moisture is advected ahead of advancing frontal systems from the tropical Pacific into the southeastern U.S. (Kiladis and Diaz, 1989; NOAA, 2005; Ropelewski and Halpert, 1986; Vega et al., 1998). However, while the western and southwestern U.S. experience above average precipitation during an El Niño, the Pacific Northwest and Ohio Valley experience below average precipitation (Higgins et al., 2007; McCabe and Dettinger, 1999; Pool, 2005; Ropelewski and Halpert, 1986; Schonher and Nicholson, 1989). During the negative phase (La Niña), the SLP pattern is reversed (high SLP in the east and low SLP in the west), leading to relatively cool SSTs in the east and a weakened polar jet stream that is shifted more northward. This causes drier than normal conditions across the southern U.S. Thus, the ENSO is associated with a U.S. coast-to-coast continuity of either increased or decreased precipitation.

The ENSO is one of the most important patterns of natural interannual variability in the Earth's climate because of its relatively high frequency, persistent effects on weather through multiple seasons, and its global impact on average and extreme weather events (Cayan et al., 1999; McCabe and Dettinger, 1999; Ropelewski and Halpert, 1987). At least eight strong El Niño events have occurred since 1871, with the most extreme events occurring in the periods 1877–1878, 1982–1983, and 1997–1998 (Figure 2b) (Wolter and Timlin, 2011, 1998). The results of such strong El Niño events in the U.S. include catastrophic flooding, severe ice storms, intense tornadoes, and landslides. Fortunately, compared to other climate variability modes, the ENSO is the most reliable climate oscillation in terms of prediction (Cayan et al., 1999).

2.2.3 The Pacific/North American Oscillation (PNA)

The PNA is an index (Figure 2c) that oscillates with a <1 to 4 year periodicity and is based upon the periodic fluctuations of 500 millibar heights over the eastern Pacific and North American continent (NOAA, 2015). It is created by projecting the PNA loading pattern to the daily anomaly 500 millibar height field over 0° to 90° north latitude. During the positive (negative) phase of PNA, there is above (below) average geopotential heights near Hawaii and in western Canada, and below (above) average geopotential heights south of the Aleutian Islands and in the southeastern U.S. This creates a stronger (weaker) ridge in the middle and upper troposphere over western Canada and a stronger (weaker) trough in the middle and upper troposphere over the eastern Gulf of Alaska (Bridgman and Oliver, 2006). These features in the troposphere then feed back to surface pressure patterns with a stronger (weaker) surface anticyclone over western Canada and a stronger (weaker) average cyclone in the Gulf of Alaska. Thus, during the positive phase, the polar jet stream over eastern Asia strengthens and extends eastward toward the western U.S., while the negative phase is associated with a retraction of the jet toward East Asia (Wallace and Gutzler, 1981). The positive phase of the PNA is associated with above average temperatures in the extreme western U.S. and below average temperatures across the south-central and southeastern U.S. Additionally, the positive phase of the PNA is associated with below average precipitation the Pacific Northwest and across the eastern half of the U.S. during the winter season (Dahlman, 2009). During the negative phase, temperature and precipitation patterns are reversed in these locations.

2.3 Climate Variability Modes in the Atlantic Region

2.3.1 The Atlantic Multidecadal Oscillation (AMO)

The AMO is characterized by anomalies in SSTs in the North Atlantic Ocean that occur every 50 to 80 years (Wyatt et al., 2012). The AMO index (Figure 3a) is calculated from detrended monthly SST anomalies averaged over the Atlantic Ocean from 0° to 70° north latitude (Enfield et al., 2001). During the positive (negative) phase, North Atlantic SSTs are warmer (cooler) than average which has been associated with a faster (slower) thermohaline circulation and resulting in more (less) transport of warm equatorial waters to higher latitudes (Enfield et al., 2001; Knight et al., 2006; Wang and Zhang, 2013). In

North America, the AMO has been shown to primarily affect climatic phenomenon in the summer, with positive AMO associated with below normal summer rainfall and greater occurrence of drought for most of the U.S., with large dry regions in the Southwest, Midwest, central and southern Great Plains, and southern Texas (Enfield et al., 2001; Feng et al., 2011; Hu et al., 2011; McCabe et al., 2004; Sutton and Hodson, 2005). In the Pacific Northwest and U.S. East Coast, however, positive AMO has been associated with increased precipitation and increased number of major hurricanes, respectively (Enfield et al., 2001; Knight et al., 2006; Yan et al., 2014). During negative AMO, the precipitation patterns in the previously mentioned locations are reversed. Positive AMO phases occurred during the periods 1860 to 1880, 1930s to early 1960s, and since the mid-1990s, with the AMO being linked to the 1930s Dust Bowl and the 1950s drought, and negative phases occurred from the early-1900s to 1920s and mid-1960s to mid-1990s (Figure 3a) (Enfield et al., 2001; Knight et al., 2006; McCabe et al., 2004; Nigam et al., 2011; Peings and Magnusdottir, 2014).

2.3.2 The North Atlantic Oscillation (NAO)

The NAO is an index (Figure 3b) that is a function of height anomalies in the middle troposphere over the Atlantic between the polar region and the subtropics. These height anomalies relate to variations in the strengths and positions of the Icelandic Low and the Azores High pressure systems. These variations occur every 3 to 6 years with a less significant periodicity of 8 to 10 years (Hurrell, 1995; Hurrell et al., 2003; Van Loon and Rogers, 1978; Walker, 1924; Walker and Bliss, 1932). The NAO index is obtained by projecting the NAO loading pattern to the daily anomaly 500 millibar height field over 0° to 90° north latitude (NOAA, 2015). During the positive (negative) phase of NAO, the Icelandic Low and Azores High pressure systems strengthen (weaken), resulting in an increased (decreased) south-to-north pressure gradient over the North Atlantic that causes the surface westerlies between those features to increase (decrease) in speed. When the speed of the surface westerlies increases, cold air drains off the North American continent eastward rather than southward, and the stronger than normal polar jet stream shunts cold Arctic Air eastward, thus preventing it from entering the lower latitudes and resulting in mild and possibly wet winters in the eastern U.S. Conversely, when the westerlies slow down, cold air builds up over Canada and a shift in the jet stream southward results in more cold air invasions and winters that are much harsher in the eastern U.S., i.e. colder temperatures and above average snowfall (Bridgman and Oliver, 2006; Hurrell, 1995; Stoner et al., 2009). Therefore, the NAO tends to affect winter climate phenomenon primarily in eastern North America.

2.4 Climate Variability Modes in the Arctic Region

2.4.1 The Arctic Oscillation (AO)

The AO is characterized by a seesaw of atmospheric pressure anomalies between the Arctic Basin and the zonal ring around the mid-latitudes with a 6 to 12 month periodicity (Kutzbach, 1970; Lorenz, 1951; Thompson and Wallace, 1998; Wallace and Gutzler, 1981). The AO index (Figure 4) is obtained by projecting the AO loading pattern to the daily anomaly 1000 millibar height field over 20° to 90° north latitude (NOAA, 2015). During the positive phase, SLP in the polar region is below average and SLP in the mid-latitude region is above average, creating a ring of strong winds circulating the North Pole that confines cold air and storms to the north. Also, during the positive phase, the polar jet stream tends to be zonal, with few excursions into the subtropical regions. During the negative phase, SLP is above average in the polar region and below average in the mid-latitude region. This tends to be associated with a meridional flow pattern with high amplitude ridges and troughs in the polar jet stream. In such a flow pattern, surface wave cyclones can track frequently across the middle latitudes and storminess tends to occur further south (Bridgman and Oliver, 2006; NOAA, 2015; Stoner et al., 2009).

2.5 Interactions of Climate Variability Modes

The interaction of certain climate variability modes has also been known to enhance or reduce different climate variability effects. For example, during a positive AMO phase, El Niño events tend to weaken which has been noted to accentuate the dryness over the south Ohio River drainage, and during a negative AMO, El Niño events are strengthened which diminishes the area of dryness south of the Great Lakes (Enfield et al., 2001; McCabe et al., 2004). Hunter et al. (2006) also found that in Oregon the negative AMO phase not only enhances the effects of El Niño, resulting in a greater reduction of snow water equivalent (SWE), but also enhances the effects of La Niña, resulting in a greater increase of SWE. The ENSO influence can also be enhanced by the

PDO when both modes are in the same phase (Cole et al., 2002; Gershunov and Barnett, 1998; Hamlet and Lettenmaier, 2007; Hunter et al., 2006; McCabe and Dettinger, 1999). During a positive PDO, El Niño events exhibit a more robust pattern of wetter (drier) winters in the southern (northern) tier of the contiguous U.S. (Gershunov and Barnett, 1998). Additionally, during a positive PDO, there tends to be a greater occurrence of El Niño events, whereas during a negative PDO, La Niña events are more frequent (Gutzler et al., 2002; Lapp et al., 2013). Similarly, Peings and Magnusdottir (2014) found that the positive AMO phase tended to result in more frequent negative NAO phases, leading to more cold weather systems existing over the eastern U.S. Song et al. (2009) also found that the NAO tended to be negative (positive) when the PNA was extremely positive (negative).

The spatial patterns of climate variability effects can also be modified by interacting modes. For example, increased drought frequency was found to be located more in the southwestern U.S. during a positive AMO and negative PDO period but located more across the northern U.S. during a positive AMO and positive PDO period (Hidalgo, 2004; McCabe and Palecki, 2006). During a negative AMO and positive PDO, McCabe et al. (2004) found that above normal drought frequency was constrained to the regions of the Pacific Northwest and Maine, whereas during negative AMO and negative PDO, frequent drought occurrence was centered in Southern California and the central High Plains. Thus, the broad regional drought patterns that occur with AMO or PDO alone become constrained to smaller areas when these climate variability modes interact.

There are many other studies that explore the hydroclimatic results of these climate variability pairings as well as other combinations of modes (e.g. Bonsal and Shabbar, 2011; Renwick and Wallace, 1996). While all the ways these six modes of climate variability affect each other is not completely understood, it is nonetheless important to acknowledge the modifications that can occur to expected hydroclimatic patterns when different climate variability modes interact.

2.6 Processes in the Vadose Zone that Influence the Propagation of Climate Signals

Sinusoidal infiltration fluxes at land surface are known to damp with depth in the vadose zone (Bakker and Nieber, 2009; Gardner, 1964; Nimmo, 2005). Recently, Dickinson et al. (2014a) demonstrated that soil type, thickness of the vadose zone, mean infiltration flux, and the period of the flux variation partially control the damping depth of sinusoidal infiltration fluxes at land surface. Damping depth is defined as the depth in the vadose zone below which <5% of the infiltration flux variation is preserved (Dickinson et al., 2014a). Greater damping depths occur with coarser soil textures, larger mean fluxes, and/or longer periods, and these conditions preserve more of the flux variation in the water table. The thickness of the vadose zone is inversely related to damping depth—relatively thinner vadose zones tend to preserve more of the flux variation in the water table and relatively thicker vadose zones tend to preserve less of the flux variation. Furthermore, because infiltration fluxes with different periods are damped at different depths, the vadose zone has a filtering effect that allows some signals to propagate further through the subsurface than others. Thus, the damping depth is an important consideration because it provides a physical mechanism that helps explain which aquifers will reflect the incidence of rainstorms and how long until such fluxes become apparent in the water table (Rijtema and Wassink, 1968).

The work of Dickinson et al. (2014a) provides the main conceptual framework in this thesis for understanding processes in the vadose zone that can control the climate variability-groundwater teleconnection patterns. However, other concepts may be pertinent to interpreting lag times between precipitation events and groundwater response. For example, quick groundwater response times to a precipitation event can occur due to the propagation of pressure waves in the vadose zone that push older water already residing in the soil column downward (Rimon et al., 2007; Sophocleous, 1991; Waswa et al., 2013). Additionally, with multiple rain events, a piston-like flow can develop whereby water movement takes place in a layered form (Li et al., 2007; Sukhija et al., 2003). Therefore, in some cases, rapid groundwater response is not a result of water directly from the precipitation event recharging the aquifer.

The volume of infiltrating water can also influence groundwater response time to that surface flux. In a study of water percolation through the deep vadose zone of a coastal plain in Israel, Rimon et al. (2007) found that multiple rainfall events were needed to initiate percolation at the deepest sensor in the soil column and thus generate recharge. In the case of a sandy vadose zone 21 meters thick, it took five discrete precipitation events and a cumulative rainfall of 382 millimeters to enable the initial precipitation event to reach the water table 3 months later. Similarly, Gurdak et al. (2007) found that in the High Plains PA, fluctuations in matric potential and water content in the vadose zone were limited to the top 1 or 2 meters of the soil column and only when there was a significant precipitation event were fluctuations recorded at depths of 7 to 11 meters.

Finally, Townley (1995) demonstrated that saturated zone properties can also influence the timing of groundwater response. He determined that the amplitude and lag time of water table fluctuations to a periodic forcing depended on a ratio of the form $\frac{L^2S}{TP}$, where L = length of the aquifer [L], S = aquifer storativity (or storage coefficient) [dimensionless], T = aquifer transmissivity [L^2/T], and P = periodicity of the applied forcing [T]. Ratios greater than 1 indicate a slow aquifer response to dynamic forcing, and many aquifers fall into this category (Townley, 1995). The periodicity of the applied forcing is pertinent to this thesis, and with all aquifer properties held constant, then the longer (shorter) the period of the forcing, the faster (slower) the response of groundwater to that forcing.

2.7 Site Descriptions

The aquifers chosen for this study are PAs of the U.S., as defined by the U.S. Geological Survey (USGS), that are generally unconfined and formed from unconsolidated to semi-consolidated sand and gravel material, which gives them moderate to high hydraulic conductivity (USGS, 2014a). The Central Valley, Basin and Range, High Plains, and North Atlantic Coastal PAs were analyzed in previous climate variability investigations, therefore, this study improves the spatial coverage across the

U.S. and focuses on the California Coastal Basins (CC), Rio Grande (RG), Coastal Lowlands (CL), Mississippi Embayment (ME), Surficial (SR), and Glacial (GL) aquifers (Figure 1). Due to the large extent of the GL aquifer, this study splits the aquifer into a western (GLW) and eastern (GLE) section. There are also several PAs in the Pacific Northwest region of the U.S., however, groundwater data suitable for this investigation was sparse in any one PA. Therefore, this study used the Pacific Northwest, Willamette Lowland, Columbia Plateau, and Northern Rocky Mountains Intermontane Basins aquifers as a group to represent the Pacific Northwest (PN) region.

To make regional comparisons across the U.S., PAs that were considered as being located in the western U.S. were the CC, PN, and RG aquifers. PAs that were considered as being in the central U.S. were the GLW, CL, and ME aquifers. Finally, PAs that were in the eastern U.S. were the GLE and SR aquifers. In addition, PAs in the northern half of the U.S. were the PN and GL aquifers, and the remaining aquifers were located in the southern half of the U.S.

In the following sections, the details on each aquifer are derived primarily from the USGS *Ground Water Atlas of the United States*, which is a publication that describes the location, extent, and geologic and hydrologic characteristics of the important aquifers of the U.S. The online version of the atlas is available at http://pubs.usgs.gov/ha/ha730/gwa.html.

2.7.1. Principal Aquifers in the Western U.S.

Both the CC and RG aquifers are basin-fill aquifers composed of various intermontane, structurally formed depressions. The CC is formed of many individual basins located along the coast of California (Figure 5a) and is composed of marine and alluvial sediments. However, most of the freshwater available in the CC aquifer is contained in continental deposits of sand and gravel that might be interbedded with some layers of silt and clay. The climate along the California Coast is Mediterranean with cool winters and warm summers. Rainfall is greatest during the late autumn, winter, and early spring, and precipitation amounts are greatest in northern California and progressively decrease southward.

The RG is located primarily in central New Mexico but stretches northward into southern Colorado and southeast into a small section of western Texas (Figure 5b). The RG is composed of alluvial and flood-plain sediments. Additionally, in Colorado's San Luis Valley, there is a confining unit as much as 365 meters thick that extends through the subsurface of the valley and consists of interlayered clay, silt, sand, and unfractured volcanic rocks. In the arid climate of the Rio Grande Valley, the average rate of pan evaporation exceeds the average rate of precipitation by as much as 10 times in any one month. Therefore there is insufficient precipitation for the growth of most commercial crops, requiring the area to be heavily irrigated.

Both the Pacific Northwest and Northern Rocky Mountains Intermontane Basins aquifers are systems of many individual, structural or erosional basins (Figure 5c). The Pacific Northwest aquifer is located in Northern California, Oregon, Washington, and Idaho, and is composed mostly of alluvium, but in some places contain eolian, glacial, or volcanic deposits. Therefore, some areas of the aquifer have confining units and/or low permeability, but overall it is the most productive aquifer in the Pacific Northwest area. The Northern Rocky Mountains Intermontane Basins aquifer is located in Idaho and Montana and is formed mainly from alluvium derived from the weathering and erosion of consolidated rocks that underlie the mountains that border the basins. The basins also contain materials deposited by alpine glaciers and some lacustrine deposits of clay and silt that can form confining units. The Columbia Plateau aquifer is a single structure that extends across northeastern Oregon, southeastern Washington, and northern Idaho (Figure 5c) and is composed of Miocene basaltic-rock overlain by unconsolidated deposits that are mainly glacial outwash. In some places, the unconsolidated deposits are more important aquifers than the basaltic-rock aquifers. The Willamette aquifer underlies the Willamette River Valley which extends southward from the Columbia River to central Oregon (Figure 5c). Like the Columbia Plateau aquifer, the Willamette aquifer is composed of Miocene basaltic-rock and unconsolidated sand and gravel deposits. Overall, the unconsolidated deposit aquifers of the Pacific Northwest region contain mostly sand and gravel and are the most productive aquifers across the states of Washington, Oregon, and Idaho.

The climate of the Pacific Northwest region is divided by the Cascade Mountain Range. West of the Cascades, the climate is more influenced by the maritime environment and is characterized by dry summers and abundant rain in the winters. Average annual precipitation in most places west of the Cascades is more than 762 millimeters. The rainshadow created by the Cascades makes the climate east of the mountain range more continental with drier conditions being more common. Average annual precipitation east of the Cascades is generally less than 508 millimeters, with some places receiving as little as 178 millimeters (Climate Impacts Group, 2014).

2.7.2 Principal Aquifers in the Central U.S.

The GL aquifer is composed of glacial outwash and stream alluvium, which are generally extremely permeable, and some fine-grained lake deposits and glacial till that have minimal permeability and commonly form local confining units. The majority of the GL aquifer is located in the northern section of the U.S. where the climate is continental and humid with significant precipitation in all seasons (Kottek et al., 2006). The western half of the GL aquifer resides in multiple states stretching from Montana in the west, to the southern tip of Illinois, and to the western edge of Pennsylvania in the east (Figure 6a). Meltwater deposits, which are generally stratified deposits of sand and gravel, are the primary source of water for wells in the states of Minnesota, Wisconsin, Michigan, and Iowa.

The CL and ME aquifers are both semi-consolidated PAs located in the region of the U.S. that has a humid and temperate climate (Kottek et al., 2006). The CL aquifer stretches across the U.S. coast from the southern tip of Texas to the western section of the Florida Panhandle (Figure 6b). The CL aquifer consists primarily of sediments deposited in a deltaic to marginal marine environment. The aquifer thickens gulfward and undergoes a progressive facies change from permeable deltaic sands to prodelta silts and clays. The complex layering of the CL aquifer is compounded by numerous oscillations of ancient shorelines that resulted in an overlapping mixture of sand, silt, and clay.

The ME aquifer is located mainly within Mississippi, Louisiana, and Arkansas, and extending eastward into Alabama and northward into Tennessee, Kentucky, and Missouri (Figure 6c). Similar to the CL aquifer, the ME aquifer is composed of interbedded fluvial, deltaic, and marine deposits. Layering in the ME aquifer also consists of thick, regionally-extensive clay and shale confining units that separate the PA into zones of homogeneous sand.

2.7.3 Principal Aquifers in the Eastern U.S.

The eastern section of the GL aquifer resides in the states from Pennsylvania and New Jersey in the south, to Maine in the north (Figure 7a). The majority of the GLE aquifer is characterized by valley-fill deposits of coarse-grained glacial outwash, ice-contact material, and alluvial sediments which are primarily sand and gravel. In the Cape Cod and Long Island areas, the GLE aquifer was formed from sheet-type glacial outwash.

The SR aquifer is located along the U.S. East Coast from North Carolina southward into Florida and extending slightly westward into southern Alabama (Figure 7b). Beds of unconsolidated sand, shelly sand, and shell comprise the SR aquifer. Thin clay beds in some areas create confined or semi-confined conditions in the aquifer, and limestone beds are also present in the PA in southwestern Florida. Therefore, the PA has a complex interbedding of fine- and coarse-textured rocks. Most of the area where the SR aquifer is located experiences a humid, temperate climate, but at the southern end of Florida, the climate is tropical with monsoonal as well as wet and dry season precipitation patterns (Kottek et al., 2006).

3.0 METHODOLOGY

3.1 Data Selection

Three data types were evaluated in this study: climate indices, groundwater levels, and precipitation amounts. Climate indices were obtained from the Earth System Research Laboratory, Physical Sciences Division of NOAA (http://www.esrl.noaa.gov/psd/data/climateindices/list/). With the exception of the AMO index which covers the period from 1856 to 2013, the remaining indices generally cover the period from 1950 to 2013.

Groundwater level data, spanning the years from 1926 to 2014, were obtained from monitoring wells in the USGS National Water Information System (NWIS) (http://nwis.waterdata.usgs.gov/usa/nwis/gwlevels) (Tables 1–8). Monitoring wells within each PA were selected based on various criteria including length and completeness of water level record, well depth, and surrounding land use patterns. The minimum permitted record length was 28 years, to capture climate variability signals up to the PDO periodicity (15 to 30 years), since groundwater level records long enough to capture the AMO periodicity (50 to 80 years) are not common. Well depths were preferably less than 60 meters, in order to maintain confidence that there would be a hydraulic connection between infiltrating rainfall and groundwater fluctuations. However, some wells that were deeper than 60 meters were included in the analysis where more sampling points were needed. To select wells that would be away from developed and irrigated areas in order to remove the possible influence of human pumping, ArcGIS was used to overlay the well locations on land cover data from the 2006 National Land Cover Database (Fry et al., 2011). Finally, wells were selected so as to maximize spatial coverage across the extent of each aquifer.

Precipitation data, spanning the years from 1884 to 2014, were obtained from meteorological stations that are part of NOAA's Global Historical Climatology Network (Tables 9–16). The data were downloaded from the agency's National Climatic Data Center, Climate Data Online (CDO) portal (http://www.ncdc.noaa.gov/cdo-web/). Each meteorological station was selected to be co-located with a groundwater well (Figures 5–7) and to have an annual average precipitation similar to that of the groundwater well location. Data on annual average precipitation for the conterminous U.S. was obtained from a map of 30-year (1981 to 2010) normals (PRISM Climate Group, 2014).

Additionally, the precipitation records were required to be mostly complete and longer than the co-located groundwater level record. Because the precipitation data were in daily measurements, monthly sums were computed to maintain consistency with climate indices and groundwater level measurement frequency.

Each well and meteorological station was given a site ID that includes the following three details: the aquifer name (CC, California Coastal Basins; RG, Rio Grande; PN, Pacific Northwest; CL, Coastal Lowlands; ME, Mississippi Embayment; SR, Surficial; and GL, Glacial), the type of site (PR, precipitation; GW, groundwater), and the relative location (an ordinal number representing its position in a west to east or north to south ordering of sites across the aquifer). The location number also indicates which sites are co-located. For example, CC_PR_01 is co-located with CC_GW_01 and both are the northernmost sites in the CC aquifer, whereas CC_PR_08 and CC_GW_08 are co-located sites that are the furthest south in the PA. Distances between co-located sites are listed in Appendix A.

3.2 Time Series Analysis

Time series analysis was performed using the USGS Hydrologic and Climatic Analysis Toolkit (HydroClimATe). HydroClimATe is a computer program that brings together and automates the use of various objective methods for assessing relations between hydrologic and climatic time series that vary in time and space (Dickinson et al., 2014b). Some of the functions in HydroClimATe include data pre-processing, Fourier analysis, Empirical Orthogonal Function analysis, Singular Spectrum Analysis (SSA), and time series regression, correlation, and projection. This thesis uses HydroClimATe to first pre-process the data, then perform SSA, and finally calculate lag correlations.

3.2.1 Data Pre-Processing

Data were pre-processed following steps outlined in Hanson et al. (2004). First, each time series was interpolated with a monthly spline to integrate any irregularly sampled records. The interpolated time series were then converted into a cumulative departure series using the monthly mean. To remove potential influences from human activities, such as persistent decline in groundwater levels due to pumping, and from possible climate cycles longer than the AMO, a regression-fitted low-order (cubic) polynomial was subtracted from the time series in order to obtain the residuals of the monthly cumulative departure series. This detrending of the time series eliminates much of the lowest frequency cycles that are not of interested in this study and that would otherwise dominate the variance of the time series. Finally, the detrended time series were normalized by the historic mean to form normalized departures (unitless) which allows for statistical comparisons to be performed between different data types.

3.2.2 Singular Spectrum Analysis (SSA)

SSA, a nonparametric spectral estimation method, has been commonly used to analyze long-term variations in short and noisy hydrologic time series (e.g. Enfield et al., 2001; Gurdak et al., 2007; Hanson et al., 2006, 2004; Kuss, 2011; McCabe et al., 2004).

SSA employs an eigenanalysis of a lagged covariance matrix to obtain temporal structures that explain the maximum possible amount of covariance in time for a single time series (Broomhead and King, 1986; Vautard et al., 1992). These structures are often called temporal empirical orthogonal functions (T-EOFs) and the manner in which the T-EOFs change through time is described by the temporal principal components (T-PCs) (Dickinson et al., 2014b). The T-EOFs and T-PCs are linearly combined to form reconstructed components (RCs) that rebuild the phase information, oscillatory modes, and noise of the time series. RCs represent the dominant frequencies in a time series and are listed in order of decreasing variance and labeled with a sequential number starting with 1 (Ghil et al., 2002; Vautard et al., 1992). The variability in most hydrologic time series can almost be entirely described using RCs 1 through 10 (Hanson et al., 2004).

SSA was applied to the normalized departure time series of all data sets in this study. Within the first 10 RCs of each time series, the Ghil and Mo significance test was used to determine which of these RCs were statistically significant against a red-noise null hypothesis (Ghil and Mo, 1991). Then for each time series, composite RCs were created by taking only the statistically significant RCs and grouping and summing them together according to the following period ranges: 40 to 80 years (AMO-like), 12 to 35 years (PDO-like), 1.9 to 7.3 years (ENSO-like), 2.9 to 6.2 years (NAO-like), 0.5 to 4.2 years (PNA-like), and 0.4 to 1.2 years (AO-like). These ranges were slightly extended beyond the established periodicities of the climate variability modes in order to be more liberal in capturing signals potentially related to the climate variability modes of interest.

The composite RCs are used in all subsequent lag correlations and represent statistically significant oscillatory modes within each of the hydrologic time series that are consistent with the AMO, PDO, ENSO, NAO, PNA, and AO.

3.2.3 Lag Correlations

When a system has a delayed response to a forcing, it is useful to calculate lag correlation coefficients that indicate the strength of association between these two variables at different time shifts (Helsel and Hirsch, 2002). In this study, lag correlations were performed between each unique pair of data types, i.e. between climate indices and precipitation, between precipitation and groundwater, and between climate indices and groundwater, where the first data type in each pair is the independent variable and the latter is the dependent variable. Before each lag correlation, the two composite RCs to be correlated were truncated to give them the same starting and ending dates while also maximizing the length of the record. HydroClimATe allows the user to specify the maximum forward and backward lags between two time series, which is useful when there is an *a priori* expectation that a lag cannot be greater or less than a certain amount (Dickinson et al., 2014b). Here, only forward lags are considered. Additionally, in contrast to the previous climate variability studies of Gurdak et al. (2007) and Kuss (2011), a 60 month (5 year) limit was set as the maximum possible forward lag for all correlations. This 60 month limit was chosen based on previous studies of water infiltration and groundwater recharge and because of the known lags between changes in atmospheric-ocean processes that in turn affect local precipitation. For example, the seminal work of Hanson et al. (2006, 2004), which looked at aquifers in the arid southwestern U.S., found that lag times of groundwater level correlations to the PDO and ENSO fell within a range of 7 months to 5 years. For water flow in general, Mattern and Vanclooster (2010) estimated a travel time of 0.9 to 3.1 years of percolating water through a deep (approximately 15 meters) vadose zone over an unconfined sandy aquifer in Belgium.

HydroClimATe returns both positive and negative lag correlation coefficients for each correlation. Therefore, the maximum lag correlation was selected based on known or assumed teleconnections between the two time series at certain locations. For example, the positive phase of the AMO is known to increase precipitation in the U.S. East Coast, therefore, only positive lag correlation coefficients were evaluated between the AMO composite RCs of the AMO index and the precipitation sites in the SR aquifer. In contrast, the positive phase of the AMO tends to decrease precipitation in the southwestern U.S., therefore, only negative lag correlation coefficients were evaluated between the AMO composite RCs of the AMO index and precipitation sites in the RG aquifer. The same patterns of signs in correlations between climate indices and precipitation apply to correlations between climate indices and groundwater, but for the relation between precipitation and groundwater, all correlations are positive under the assumption that increased (decreased) precipitation always leads to an increase (decrease) in groundwater levels. The final lag correlation results include the maximum lag correlation coefficient (unitless) and the lag time (years) for correlations that are statistically significant at the 95% confidence level.

3.3 Analysis of Percent Variance and Lag Correlation Results

To identify spatial patterns of possible hydroclimatic teleconnections, the SSA results for precipitation and groundwater composite RCs (percent variance, lag correlation coefficients, and lag times) were averaged and compared across PAs for each climate variability mode. On one set of graphs of aquifer averages, the PAs are plotted in a west to east order, with the CC aquifer as the westernmost PA and the GLE aquifer as the easternmost PA. A linear trend line was fit to the data on each of these plots. The R^2 value for the trend line is a statistical measure of how well the regression line approximates the data points. An R^2 value of 1 indicates that the linear model explains 100% of the variability of the data points around their mean, and an R^2 value of 0 indicates that the linear model explains none of the variability in the data points. SSA results were also averaged and compared by regions (west, central, and east; north and south) for each climate variability mode. Additionally, JMP, a statistical discovery computer program developed by the SAS Institute, was used to perform an analysis of variance on all these averages and apply the Tukey-Kramer Honestly Significant Difference test to identify statistically significant differences between the means at the 95% confidence level.

3.4 Analysis of Damping in the Vadose Zone

To assess how soil texture, vadose zone thickness, mean infiltration flux, and the period of sinusoidal fluctuation affect the damping of sinusoidal signals in the vadose zone, a USGS MATLAB computer program called DAMP was used that employs the analytical model of Bakker and Nieber (2009) on the damping of periodic flow in the vadose zone. DAMP creates two-dimensional nomograms of the damping factor. A damping factor of 1 equates to 100% of an original periodic signal preserved at a specified depth and a damping factor of 0 indicates a complete damping of the signal at a specified depth. The nomograms show how the damping of a surface-applied sinusoidal flux changes with depth in a user-constructed soil column. Additional information on the DAMP program is detailed in Dickinson et al. (2014a).

Four groups of nomograms were created by inputting various soil textures, depth to water values, average infiltration fluxes, and sinusoidal infiltration periods that would capture the range of aquifer conditions in this study. Because there is little field data on infiltration fluxes at each PA, these values were estimated by calculating the average annual precipitation at each meteorological site using the raw precipitation time series and then subtracting the estimated amount of evapotranspiration (ET), which was determined from ET maps created by Sanford and Selnick (2013) (Tables 9–16). The resulting infiltration fluxes were averaged for each aquifer and then converted to a measurement of meters per day (Table 17). The smallest average daily infiltration flux occurred at the RG aquifer with 7.6×10^{-5} meters per day while the greatest daily infiltration flux occurred at the GLE aquifer with 1.8 x 10^{-3} meters per day. These two fluxes as well as two intermediate fluxes (4.9 x 10^{-4} meters per day at the CC aquifer and 1.1 x 10^{-3} meters per day at the PN aquifer) were chosen to establish the four groups of nomograms.

Within each group of nomograms are plots for each soil type that was input into DAMP. The following six soil textures were selected for analysis: sand, sandy clay loam, clay, loam, silt, and silty clay loam. Compiling detailed information on the vadose zone soil types at each PA is beyond the scope of this project, therefore, the soil texture in the vadose zone above each PA was approximated using GIS data on hydrologic soil groups (HSGs) from the Natural Resources Conservation Service of the U.S. Department of Agriculture (Tables 1–8). Soils in the first HSG (A) are gravel or sand textures, have low runoff potential when thoroughly wet, and transmit water freely through the soil, whereas soils in the last HSG (D) have clayey textures, high runoff potential, and restricted water movement (USDA NRCS, 2009). The HSG was identified for each groundwater site using ArcGIS. Combined with background information on the PAs, one representative vadose zone soil type from the list of six analyzed soil types was then assigned to each PA (Table 17).

On the y-axis of each nomogram plot is a range of depth values and on the x-axis is a range of infiltration periods. Depth to water was chosen to be 2 to 30 meters, which represents the SR aquifer with the smallest average depth to water (1.6 meters) and the PN aquifer with the greatest average depth to water (27.1 meters) (Table 17). Finally, the infiltration period was selected to be 730 to 7,300 days (2 to 20 years), to capture fluctuations up to the PDO periodicity.

After the nomograms were generated, each PA was assigned to a nomogram that most closely represented the average infiltration and estimated vadose zone soil type at that PA. The thickness of the vadose zone for the assigned PA is indicated with a horizontal dashed line that intersects the y-axis at the average depth to water value for that PA. Thus, a dashed line specifies the damping factors for the range of periodic fluxes at the depth of the water table for a particular PA.

4.0 RESULTS AND DISCUSSION

4.1 Percent Variance

Results of the SSA showed that all the hydrologic time series contained statistically significant oscillations that are potentially related to the AMO, PDO, ENSO, NAO, PNA, and AO (Appendix B). The largest amount of variance in precipitation and groundwater time series was attributed to the PDO, which ranged from 2.3 to 99.8% (Table 18). The AMO also accounted for a large amount of variance, ranging from 41.6 to 96.6%. However, the AMO signal was the least frequently detected oscillation in the SSA compared to all other climate variability modes, which is likely a result of the limited length of the data records and the analysis method. SSA uses a window length that sets the dimension of the lag autocorrelation matrix to be constructed and diagonalized by SSA and the window length is required to be wide enough to contain the oscillatory component of interest (Dickinson et al., 2014b; Vautard et al., 1992). Because the AMO oscillation has a period of 50 to 80 years and many precipitation and groundwater time series were shorter than this length, the detection of AMO-like signals was limited. The next largest amount of variance was attributed to the ENSO (0.02 to 59.3%), followed by the NAO (0.02 to 40.6%), PNA (<0.01 to 27.7%), and AO (<0.01 to 18.6%) (Table 18). This is consistent with findings from Gurdak et al. (2007) and Kuss (2011) that longer-term climate variations accounted for greater amounts of the variance in hydrologic time series than shorter-term climate variations.

4.1.1 Spatial Patterns of Percent Variance in Precipitation RCs

The percent variance aquifer averages for precipitation RCs showed a variety of spatial patterns (Figure 8 and Tables 19 and 20). Only the AMO plot had a moderately good R^2 value of 0.42 for the linear trend line through the data (Figure 8a). The linear trend lines for all the other plots had very weak fits to the data ($R^2 \leq 0.09$) (Figures 8b to 8f). However, the negative trend of the AMO averages across aquifers indicates that the AMO influence on precipitation is strongest in the western U.S. and decreases going eastward (Table 20), which is the opposite pattern of what would be expected. There is not a strong west to east pattern of percent variance aquifer averages for the PDO (Figure 8b), but regional averages indicate that the PDO's influence on precipitation is strongest in the eastern U.S. (regional average of 60.1%) and weakest in the central U.S. (regional average of 40.8%) (Table 20). Again, this is contrary to the expected patterns. However, the AMO and PDO spatial trends are consistent with findings from Ning and Bradley

(2014) that in the northeastern U.S., the PDO (as well as the PNA) could explain most of the variance (30.6%) in winter precipitation while the AMO (as well as the NAO) accounted for only 14.6% of the variance.

For the ENSO, a statistically significant difference between averages in the north (6.5%) and south (12.8%) regions was found that confirms earlier studies on the El Niño's strong influence on precipitation across the southern U.S. (Table 20) (e.g. Kiladis and Diaz, 1989; Kurtzman and Scanlon, 2007; Ropelewski and Halpert, 1986). The results also indicate that the ENSO's strongest influence on precipitation is in the central region (Table 20), with the highest average percent variances in the CL and ME aquifers rather than in the western aquifers (CC, PN, and RG) (Table 19). This may coincide with Budikova (2008) who found that an ENSO negative phase (during an AO neutral phase) was associated with dry conditions throughout Texas, along the Gulf Coast, and in Florida.

The aquifer averages for the NAO follow a nearly identical pattern to the ENSO, which is likely due to the overlap in periodicities for these two climate variability modes (Figure 8d). This indicates that the NAO appears to have a relatively high average percent variance in the CC aquifer (10.1%) and a relatively low average in the GLE aquifer (3.6%), when the opposite pattern would have been expected (Table 19). It may be that the ENSO is masking the NAO results. The overlap in the periodicities of the two climate variability modes highlights an important limitation of using the methods herein of statistically analyzing time series to identify influence from specific modes of climate variability.

Anomalous temperature and precipitation changes that are associated with the PNA tend to occur in the areas from the Pacific Northwest, down through the south-central U.S., and across to the southeast. The PNA results for percent variance averages by aquifer agree with these patterns—there is a slight west to east decrease in average percent variance across the aquifers and a statistically significant difference between the average for the SR aquifer (11.7%) which is in the southeast and the GLE aquifer (3.6%) which is in the northeast (Figure 8e and Table 19).

Relative to the other aquifers, there are high averages for AO percent variance in the GLW, SR, and CL aquifers (7.6%, 6.9%, and 4.8%, respectively) (Figure 8f and Table 19). These results may coincide with findings from Budikova (2008) that the AO's major areas of influence on precipitation are the interior upper Midwest, the Florida Peninsula, and the area extending northeast from Texas into the Great Lakes Region, respectively.

In summary, there is a lack of statistically significant evidence of west to east spatial patterns of percent variance averages for precipitation RCs for any climate variability mode. Also, the ENSO (and maybe the NAO) is the only climate variability mode with a robust north to south distinction in percent variance. While some of the results agree with expected spatial patterns based on previous climate variability studies, there are other results that are contrary to expectations.

4.1.2 Possible Explanations for Spatial Patterns in Precipitation Percent Variance Results

Where average percent variance results do not coincide with known spatial patterns, one explanation for this could be that the signals that were identified in the precipitation data are not actually related to the climate variability mode of the same period. Thus, if a RC is not actually an expression of the climate variation of interest, percent variance results likely will not reflect the spatial patterns expected with that mode of climate variability.

Another possible explanation for the percent variance patterns for precipitation is constructive or destructive interference with the modes of climate variability, which are creating quasi-periodic signals that are not consistent with the six modes of interest in this thesis. For example, McCabe et al. (2004) found that hydroclimatic changes associated with the AMO can be altered by the PDO. When the PDO is positive, the increased frequency of drought that occurs across most of the U.S. as a result of a positive AMO becomes more centered in the northwestern U.S, and when the PDO is negative, drought conditions become more centered in the southwestern U.S. This supports the findings in this thesis of higher average AMO percent variance in the western region of the U.S. (Table 20). Budikova (2008) also showed how the precipitation spatial patterns of El Niño in the eastern half of the U.S. are modified by the different phases of the AO.

During an El Niño event, a positive AO is associated with wetter than normal conditions observed in Florida spreading further into the U.S. and along the eastern seaboard to Virginia, while a negative AO is associated with significant drying of the area from eastern Kansas to the Great Lakes region (Budikova, 2008). This might explain why some of the eastern and central aquifers had high ENSO percent variances relative to the western aquifers (Figure 8c and Table 19).

It is also possible that precipitation patterns are influenced by other meteorological and climatic phenomena in addition to the six modes of climate variability evaluated here. For example, one important source of warm season rainfall variations in the southwestern and central U.S. is the North American Monsoon (NAM). Hu and Feng (2008) found that the spatial pattern of NAM rainfall has alternated between these two regions at a multidecadal timescale in the 20th century, and this alternation was found to be linked to the phases of the AMO. This could partially explain the high AMO percent variance of the RG aquifer and other central aquifers relative to the eastern aquifers (Figure 8a and Table 19).

4.1.3 Spatial Patterns of Percent Variance in Groundwater RCs

Percent variance results for groundwater composite RCs were also averaged and compared across aquifers and regions (Figure 9 and Tables 21 and 22). Although AMO-like signals in groundwater were not detected in all aquifers, the groundwater spatial pattern for AMO aquifer averages was similar to the precipitation spatial pattern, with a decreasing trend west to east and a moderate fit for the linear trend line through the data ($R^2 = 0.41$) (Figure 9a). The trend lines for the ENSO and NAO had moderately low fits ($R^2 = 0.30$ and 0.25, respectively) (Figures 9c and 9d), which is an improvement from the fit of the trend lines in the precipitation data. However, the trend lines for the remaining climate variability modes still had weak fits in the groundwater data ($R^2 \leq 0.11$) (Figures 9b, 9e, 9f).

Compared to the precipitation results, there were more statistically significant differences in the groundwater data for both aquifer and regional averages. For example, the groundwater percent variance averages for the PDO were much higher in the RG, CL, and ME aquifers (92.5%, 86.1%, and 81.5%, respectively) relative to the other aquifers, and these averages were all statistically different from the GLW aquifer (43.0%) (Figure 9b and Table 21). This contributes to the statistically significant difference between the north and south regional averages for the PDO (67.8% and 82.9%, respectively) (Table 22). Also, the ENSO and NAO averages for the SR aquifer were much higher than all the other PAs, especially the PN and RG aquifers (Figures 9c and 9d and Table 21), which contributes to the statistically higher regional averages in the east compared to the west and central regions for these two climate variability modes (Table 22).

Because some of the precipitation percent variance results were consistent with expected spatial patterns and other results were inconsistent, it follows that the groundwater percent variance results would have a mix of outcomes as well including a lack of robust west to east spatial patterns. Yet, the spatial patterns for each climate variability mode were not the same between precipitation and groundwater data. This indicates that some other factors are affecting the climate variability signals during their propagation from precipitation to groundwater.

4.1.4 Possible Explanation for Spatial Patterns in Groundwater Percent Variance Results: Damping in the Vadose Zone

Table 18 showed that while the average percent variances for the AMO and PDO increased in groundwater RCs relative to precipitation RCs, the averages in groundwater RCs relative to precipitation RCs decreased for ENSO, NAO, PNA, and AO. This relationship between percent variance and average period was further explored in plots for each aquifer that juxtapose the percent variance results of the precipitation and groundwater composite RCs (Figures 10–17). In each PA, the linear trend lines for the precipitation and groundwater data intersect. The steeper slope of the groundwater trend line compared to the precipitation trend line indicates that climate variability modes with relatively longer periodicities increased their percent variance and that climate variability modes with relatively shorter periodicities decreased their percent variance in groundwater relative to precipitation. This can be explained by the damping depth concept of Dickinson et al. (2014a)—higher frequency sinusoidal signals are damped out sooner than lower frequency signals in the vadose zone and therefore lower frequency signals are more likely to be preserved at the depth of the water table. The filtering of these signals in the vadose zone results in water table variations that are dominated more by signals of longer periods.

Additionally, in plots of percent variance versus average depth to water for each climate variability mode, the AMO and PDO showed a general increase in percent variance with depth while the ENSO, NAO, PNA, and AO showed a decrease in percent variance with depth (Figure 18). Again, these findings are consistent with Dickinson et al. (2014a) that demonstrate a positive relation between the period length of transient infiltration flux and damping depth in the Central Valley PA. They found that nearly 100% of an infiltration flux variation with a 1 year periodicity would be preserved at the depth of the water table (150 meters), while only 40% of an infiltration flux with a 30-day period would be preserved at the water table.

The difference in the slopes of the precipitation and groundwater trend lines from Figures 10–17 was used to represent the relative strength of the damping that occurs in each aquifer and the relative change in the percent variances from precipitation to groundwater. This measure is referred to as the Degree of Damping (DOD). The greater the difference in the slopes, the greater the DOD, and a high DOD indicates that there is more damping of signals with shorter periods, which would cause the distribution of percent variances among climate variability modes in groundwater to be dominated by lower frequency signals in comparison to the distribution in precipitation data. In PAs with a low DOD, higher frequency signals are more able to propagate all the way to the water table and be preserved in groundwater fluctuations, and therefore there would be little difference between groundwater and precipitation in the distribution of percent variances among the climate variability modes. The PA with the smallest DOD was the

GLW aquifer (0.003) and the PA with the greatest DOD was the RG aquifer (0.030) (Table 23).

Conceptually, when each PA is assigned to a nomogram that most closely represents the average infiltration and estimated vadose zone soil type at that PA, the damping factors that occur at the average depth to water for each PA would coincide with the finding that the DOD increases in the following order: GLW, GLE, PN, CC, ME, SR, CL, and RG. In accordance with the DOD order, the nomograms show that virtually no damping of any periodic signal occurred in the GLW and GLE aquifers (Figure 19). The representative soil type of the GL aquifer is sand, which likely explains why the GLW and GLE aquifers, despite having different mean infiltration fluxes, have a damping factor of 1, which indicates 100% of the sinusoidal signals preserved at the depth of the respective water tables. At the depth of the water tables for the PN and CC aquifers, the damping factor is approximately 0.95, which indicates that there is approximately 95% preservation of the lowest frequency signals, and as frequency increases, the damping factor decreases to approximately 0.6, which indicates about 60% preservation of the highest frequency signals in the water table (Figure 19). Evaluation of the damping factor of sinusoidal infiltration fluxes helps explain the tendency for the PN, CC, and GL aquifers to have higher average percent variances for the ENSO, NAO, PNA, and AO signals in groundwater relative to the remaining aquifers (Table 21). Accordingly, the nomogram with the RG aquifer has some of the smallest damping factors and thus the greatest DOD (Figure 19), which explains the relatively high average percent variance for

PDO and relatively low average percent variance for ENSO, NAO, PNA, and AO in groundwater (Table 21). On the nomogram, the damping factor decreases to 0.9 for the lowest frequency signals (90% preservation of signals at the water table), and for the highest frequency signals, the damping factor decreases to 0.2 (20% preservation of the signals at the water table). Although the RG aquifer has a more hydraulically conductive soil type (sandy clay loam) than the CC and PN aquifers (loam or silt and silty clay loam, respectively), the reason for the low damping factor and relatively high DOD can be attributed to the RG aquifer's very low mean infiltration flux.

However, there is a discrepancy between the nomogram and regressions of the percent variance for the ME, SR, and CL aquifers because the nomograms indicate large damping factors and relatively little damping while the difference in the slopes of the precipitation and groundwater trend lines indicates that the signals are strongly damped. Therefore, there could be variables other than soil material, mean infiltration flux, and vadose zone thickness that control damping. Additionally, site specific layering or other heterogeneities in the vadose zone that are not represented in the analytical models could be causing damping of the higher frequency signals. In a study of water percolation through the deep vadose zone of a coastal plain in Israel, Rimon et al. (2007) found that below an intermediate clay layer in a sandy soil column, only a single increase in water content was observed for an entire rainy season with five major precipitation events. Thus, the clay layer acted to filter some but not all of the transient infiltration fluxes that were observed in the upper sand layers. Similarly, heterogeneities in the vadose zone of the ME, CL, and SR aquifers could be damping some of the signals from the climate variability modes, resulting in relatively higher average PDO percent variance in groundwater and low percent variances for the higher frequency climate variability modes (Table 21). Compared to the other PAs in this thesis, the depositional environment and layering of sediment in the ME and CL aquifers is more complex because the aquifers are formed from fluvial, deltaic, and marginal marine deposits, which results in rapid and numerous changes in lithologic facies. Furthermore, interbedding of sand and clay is widespread in these aquifers, which also differentiates them from many other PAs that are generally composed of massive and regionally-extensive sand beds (USGS, 2014b). The SR aquifer is also unique in that it contains limestone and thin clay beds in some areas and has a dual HSG classification. The A/D category indicates that the soil is typically highly conductive, but when not fully drained, it can lead to conditions of restricted water movement (Table 8).

4.1.5 Answers to Research Question #1

The complex interplay of mean infiltration flux, infiltration period, soil type, thickness of the vadose zone, and the possible influence of other variables like layering and heterogeneity makes it difficult to determine which, if any, variable is the dominant control on damping. However, there is still a lot of important information that can be derived from the nomograms regarding the variables that control the damping and filtering of climate variability signals in the vadose zone. Overall, the nomograms show that at very high mean infiltration fluxes, there is little change in the damping factor across various soil types (Figure 19). However, as the mean infiltration flux is decreased, the damping factor also decreases and damping increases across the soil types. In the most conductive soil material (sand), even with large changes in mean flux, the damping factors across different infiltration periods does not change substantially from one mean flux to the next. Yet, in the least conductive soil material (silty clay loam), changes in mean flux produce very large changes in the damping factors and increase the damping of infiltration fluxes. Additionally, when the depth to the water table increases, the damping also increases.

A more detailed sensitivity analysis, including an exploration of the effect of layering and heterogeneity in the vadose zone, is suggested for future research to gain a better understanding of the controls on damping. This additional information will help refine our understanding of the climate variability-groundwater teleconnection.

4.1.6 Spatial Patterns of Percent Variance in Groundwater RCs Reevaluated with the Degree of Damping (DOD)

When average percent variance results for groundwater RCs were replotted with aquifers ordered by the DOD rather than west to east, there was a large improvement in the fit of the linear trend line for the PDO results (an increase in the R^2 from 0.01 to 0.69) (Figure 20b). There were also improvements to the PNA trend line (R^2 increased from 0.11 to 0.25) (Figure 20e) and the AO (R^2 increased from 0.001 to 0.21) (Figure 20f). In contrast, the fit of the AMO trend line decreased from an R^2 of 0.41 to 0.16 (Figure 20a), however, this may be attributed to the absence of AMO signals in the ME, SR, CL, and RG aquifers. The R^2 values for the ENSO and NAO trend lines also had drastic decreases down to 0.035 and 0.0048, respectively (Figures 20c and 20d). However, in these two plots, the average for the SR aquifer stands out as a possible outlier that is skewing the trend. Given the previously mentioned idea that the vadose zone above the SR aquifer may have a unique effect on the propagation of climate variability signals due to its unusual soil conditions, the averages for the SR aquifer were removed from all the percent variance plots to see if the fit of the trend lines could be improved. In these new plots, the R^2 values increased for nearly all the modes of climate variability (Figure 21). In particular, the PDO, PNA, and ENSO trend lines now had moderate to high R^2 values (0.71, 0.59, and 0.49, respectively) (Figure 21b, 21e, 21c). The trend lines also reiterate the earlier finding that for lower frequency climate variability modes (AMO and PDO), percent variance increases as the DOD increases, and for higher frequency climate variability modes (ENSO, NAO, PNA, and AO), percent variance decreases as the DOD increases.

4.2 Lag Correlations

4.2.1 Climate Index-Precipitation Lag Correlations

For climate index-precipitation lag correlations, correlation coefficients were higher (lower) on average with lower frequency (higher frequency) climate variability modes (Table 24). Thus, AMO correlations had the highest coefficients on average (0.59) and AO correlations had the lowest coefficients on average (0.18). This pattern of increasing correlation strength with decreasing frequency of the climate variation supports the pattern of increasing percent variance with decreasing frequency.

Lag times for index-precipitation correlations, however, did not follow the same pattern—the AO and AMO had the longest average lag times (4.5 and 3.5 years, respectively) and the ENSO had the shortest average lag time (1.3 years) (Table 24). A decrease in lag time roughly coincided with a decrease in climate variability periodicity for the AMO, PDO, and ENSO. This conceptually makes sense as the longer (shorter) the period of fluctuation, the more (less) time it takes to reach the point of maximum correlation between the two time series. However, it is possible that when the period of fluctuation shortens, there is a threshold at which the identification of the best point of correlation becomes more inexact due to the high frequency of variations between the two time series. Therefore, the lag time results for the NAO, PNA, and AO should be treated with caution, especially since, as previously shown, correlation strength is low for higher frequency modes of climate variability.

4.2.2 Spatial Patterns of Climate Index-Precipitation Lag Correlations

The spatial patterns of index-precipitation lag correlations are shown in Figure 22 and Tables 25 and 26. On west to east plots of aquifer-averaged maximum correlation coefficients, the trend lines for the PDO and PNA results had moderately low R^2 values (0.26 and 0.28, respectively) while the remaining climate variability modes had trend lines with weak to very weak fits ($R^2 \leq 0.19$) (Figure 22). Contrary to expectations, the

PDO average correlation coefficient was higher in the eastern region (0.45) relative to the western region (0.32) and significantly higher than the central region (0.12) (Table 26). However, ENSO correlations were strongest in the western and southern regions (0.39 and 0.37, respectively) relative to the other regions (Table 26). Like the precipitation percent variance results, there were no consistent west to east spatial patterns for the index-precipitation correlation coefficients.

In the plots of aquifer-averaged lag times for the six modes of climate variability, only the PDO had a moderately high R^2 value for the linear trend line through the data ordered west to east (Figure 23). The PDO plot indicates that the precipitation response to the PDO is faster on average in the western region (0.8 years) than in the eastern region (3.3 years) (Figure 23 and Tables 26 and 27). Although the trend line for the ENSO is a weak fit ($R^2 = 0.15$), the precipitation response to the ENSO is also faster on average in the west and slower going east. The trend line for the NAO results had a moderate R^2 value of 0.28, and the negative slope indicates that precipitation response to the NAO is slower in the western U.S. and increases going east. The AMO trend line, although weak ($R^2 = 0.16$), also mimicked the NAO pattern of decreasing lag times going west to east (Figure 23). Conceptually, the AMO, PDO, ENSO, and NAO trends follow the expected changes in lag time across aquifers based on the spatial location of the PA. Because higher frequency climate variability modes have overall weaker index-precipitation correlations, there is much more uncertainty in the lag times for the PNA and AO.

4.2.3 Precipitation-Groundwater Lag Correlations

Excluding the AO results, the precipitation-groundwater average correlation coefficients seemed to follow the same pattern as the index-precipitation correlations where correlations improved with lower frequency climate variability modes, although the AMO result was limited because only one correlation was possible (Table 28). The AMO had the highest correlation coefficient (0.56) and the PNA had the lowest correlation coefficient (0.42). The AO results were anomalous as the range (0.30 to 0.96) and average (0.78) of the correlation coefficients was much higher relative to all the other modes of climate variability. The precipitation-groundwater lag times also showed some similarities to the pattern in the index-precipitation lag times where the AMO and AO had the longest average lags (4.1 and 2.8 years, respectively) and the ENSO (as well as NAO) had the shortest average lag (1 year) (Table 28). As previously mentioned, there is likely much more uncertainty in the lag correlation results of the higher frequency climate variability modes and especially for the AO.

Overall, average precipitation-groundwater correlations were stronger than average climate index-precipitation correlations—the average correlation coefficients ranged from 0.42 to 0.78 for precipitation-groundwater correlations (Table 28) and 0.18 to 0.59 for index-precipitation correlations (Table 24). This may be explained by the fact that there is a more direct physical connection between precipitation and groundwater fluctuations than between climate variability indices and precipitation.

4.2.4 Spatial Patterns of Precipitation-Groundwater Lag Correlations

For the ENSO, NAO, and PNA, the fits of the trend lines to the average correlation coefficient data where much higher when the results were plotted by the DOD rather than west to east—the R^2 for the ENSO increased from 0.25 to 0.52, the NAO increased from 0.15 to 0.50, and the PNA increased from 0.070 to 0.27 (Figure 24 and Table 29a). The negative slopes of these trend lines indicate decreasing correlation strength with increasing DOD (Figure 24), which supports the idea that as the DOD increases and more of the high frequency signals are damped and filtered out, there is more of a disconnect between the precipitation signals and groundwater signals. The trend line R^2 value for the AO was very low and not significantly different between the two plots (0.03 compared to 0.02), whereas the fit of the line for the PDO got worse when the results were plotted by the DOD (decrease from 0.13 to 0.003 (Table 29a). Finally, the trend across aquifers for the AMO could not be assessed because correlations could only be performed at the PN aquifer.

For lag time averages, the trend lines for all the climate variability modes except the AO were dramatically improved (Figure 25 and Table 29b). The R^2 values when the PDO, ENSO, NAO, and PNA results were plotted west to east were only as high as 0.16, whereas in a DOD order, the R^2 values were 0.26, 0.47, 0.51, and 0.58, respectively. The positive slope of these trend lines indicates that as the DOD increases, average lag times increase (Figure 25).

4.2.5 Index-Groundwater Lag Correlations

Index-groundwater lag correlation results reflect a combination of the index-precipitation and precipitation-groundwater patterns. Excluding the AMO, the average correlation coefficients for each climate variability mode decreased as the frequency of the periodic fluctuation increased, similar to the index-precipitation and precipitation-groundwater results (Table 30). Again, the AO had one of the longest lags (3.3 years) and the ENSO had the shortest lag (2.1 years). However, here, the PDO rather than the AMO had the longest lag (3.6 years).

The R^2 value (0.56) for the AMO trend line did not change whether the correlation coefficient averages were plotted west to east or by the DOD, but the trend was calculated from only a limited number of points, and only the R^2 value for the NAO showed an improvement from 0.007 to 0.41 when plotting the average correlation coefficients by the DOD (Figure 26 and Table 31a). For all the other climate variability modes, the R^2 values were better when averages were plotted west to east (Table 31a). In terms of average lag times, the fit of the trend line to the AMO results again did not change by changing the aquifer order, however, the DOD order was an improvement for the R^2 values for the ENSO, NAO, and PNA (increases from 0.02, 0.001, and 0.004, respectively, to 0.13, 0.54, and 0.23, respectively), while the west to east order had better R^2 values for the PDO (0.26 compared to 0.16) and somewhat for the AO (0.09 compared to 0.009) (Figure 27 and Table 31b).

4.2.6 Answers to Research Question #2

For the ENSO, NAO, and PNA, there is consistent improvement in the spatial characterization of average correlation coefficients and average lag times for precipitation-groundwater and climate index-groundwater correlations when averages are plotted by the DOD rather than west to east. In contrast, the linear trend in the PDO results might be reflected better with a west to east ordering of aquifer averages. This difference between the PDO (low frequency) and ENSO, NAO, and PNA (high frequency) results might be related to the fact that lower frequency signals get damped less and therefore the DOD order may not be as important for spatially characterizing the climate variability modes with longer periods, whereas higher frequency signals are damped more, so the DOD ordering becomes more important for the climate variability modes with shorter periods. Because of the frequent anomalies with the AO results as well as the overall low correlation coefficients, it difficult to assess the AO patterns with high confidence. Finally, more data is needed to better analyze the patterns with the AMO.

4.3 Answers to Research Question #3

One major pattern observed across all the PAs in this thesis as well as the PAs studied in Gurdak (2007) and Kuss (2011) is that average percent variance for each climate variability mode in both precipitation and groundwater data decreased with increasing frequency of the climate variation (Table 32). In other words, lower frequency signals always accounted for more of the variance in precipitation and groundwater fluctuations than higher frequency signals. In addition, average correlation coefficients for each mode of climate variability almost always decreased with increasing frequency for index-precipitation, precipitation-groundwater, and index-groundwater lag correlations (Table 33). These findings highlight the importance of low frequency climate variations on hydrologic fluctuations across the U.S. and indicate that considering these long-term patterns will help with water resource management.

5.0 CONCLUSION

The use of SSA and lag correlations to identify and evaluate quasi-periodic signals in precipitation and groundwater time series that are potentially related to interannual to multidecadal modes of climate variability indicates that the AMO, PDO, ENSO, NAO, PNA, and AO all have significant influence on precipitation and groundwater fluctuations across the U.S. but that lower frequency climate variations have a greater impact on hydrologic patterns than higher frequency climate variations. Low frequency signals also tend to be preserved better in groundwater fluctuations than high frequency signals. This is a result of the soil texture, thickness of the vadose zone, mean infiltration flux, and infiltration period which partially control the DOD that occurs in each PA. The DOD of climate variability signals in the vadose zone is found to be an important element in the identification of spatial patterns in precipitation-groundwater and index-groundwater lag correlations and lag times. For example, average lag times at each PA tend to increase with higher DOD. Therefore, the spatial patterns of the influence of a climate variability mode on groundwater cannot simply be thought of in terms of where the mode of climate variability originates in the ocean or atmosphere because other vadose zone and infiltration properties play a role in how each of the climate variability modes is expressed in groundwater fluctuations in each PA. Therefore, to improve the management of water resources, particularly as the demands for water change with population growth, agricultural activities, and changes in climate, it is essential to consider the impacts of long-term climate variations on groundwater supply as well as how the DOD at each PA will shape the climate variability-groundwater teleconnection.

REFERENCES

Anderson, W.P., Emanuel, R.E., 2008. Effect of interannual and interdecadal climate oscillations on groundwater in North Carolina. Geophysical Research Letters 35, 4. doi:10.1029/2008GL036054

Baede, A.P.M. (Ed.), 2001. Climate Change 2001: The Scientific Basis, Appendix I, in: IPCC Third Assessment Report. Cambridge University Press, Cambridge, U.K., pp. 787–881.

Bakker, M., Nieber, J.L., 2009. Damping of Sinusoidal Surface Flux Fluctuations with Soil Depth. Vadose Zone Journal 8, 119–126. doi:10.2136/vzj2008.0084

Bayari, C.S., Yildiz, F.E., 2012. Effects of the North Atlantic Oscillation and groundwater use on the contraction of Sultansazligi Wetland, Turkey. Hydrogeology Journal 20, 369–383. doi:10.1007/s10040-011-0809-z

Beebee, R.A., Manga, M., 2004. Variation in the relationship between snowmelt runoff in Oregon and ENSO and PDO. Journal of the American Water Resources Association 40, 1011–1024.

Bonsal, B., Shabbar, A., 2011. Large-scale climate oscillations influencing Canada, 1900-2008. Canadian Councils of Resource Ministers, Ottawa.

Brabets, T.P., Walvoord, M.A., 2009. Trends in streamflow in the Yukon River Basin from 1944 to 2005 and the influence of the Pacific Decadal Oscillation. Journal of Hydrology 371, 108–119. doi:10.1016/j.jhydrol.2009.03.018

Bridgman, H.A., Oliver, J.E., 2006. The Global Climate System: Patterns, Processes, and Teleconnections. Cambridge University Press.

Broomhead, D.S., King, G.P., 1986. Extracting qualitative dynamics from experimental data. Physica D: Nonlinear Phenomena 20, 217–236.

Budikova, D., 2008. Effect of the Arctic Oscillation on precipitation in the eastern USA during ENSO winters. Climate Research 37, 3–16. doi:10.3354/cr00749

Cayan, D.R., Redmond, K.T., Riddle, L.G., 1999. ENSO and Hydrologic Extremes in the Western United States*. Journal of Climate 12, 2881–2893.

Chen, Z., Grasby, S.E., Osadetz, K.G., 2004. Relation between climate variability and groundwater levels in the upper carbonate aquifer, southern Manitoba, Canada. Journal of Hydrology 290, 43–62. doi:10.1016/j.jhydrol.2003.11.029

Climate Impacts Group, 2014. About Pacific Northwest Climate [WWW Document]. Climate Impacts Group, University of Washington, Joint Institute for the Study of the Atmosphere and Ocean. URL http://cses.washington.edu/cig/pnwc/pnwc.shtml

Cole, J.E., Overpeck, J.T., Cook, E.R., 2002. Multiyear La Niña events and persistent drought in the contiguous United States. Geophysical Research Letters 29, 4. doi:10.1029/2001GL013561

Dahlman, L., 2009. Climate Variability: Pacific - North American Teleconnection Pattern [WWW Document]. NOAA Climate.gov: science & information for the climatesmart nation. URL https://www.climate.gov/news-features/understanding-climate/climate-variability-pacific-north-american-teleconnection

De Vita, P., Allocca, V., Manna, F., Fabbrocino, S., 2012. Coupled decadal variability of the North Atlantic Oscillation, regional rainfall and karst spring discharges in the Campania region (southern Italy). Hydrology and Earth System Sciences 16, 1389–1399. doi:10.5194/hess-16-1389-2012

Dickinson, J.E., Ferré, T.P.A., Bakker, M., Crompton, B., 2014a. A Screening Tool for Delineating Subregions of Steady Recharge within Groundwater Models. Vadose Zone Journal 13, 15. doi:10.2136/vzj2013.10.0184

Dickinson, J.E., Hanson, R.T., Ferré, T.P.A., Leake, S.A., 2004. Inferring time-varying recharge from inverse analysis of long-term water levels. Water Resources Research 40, 15. doi:10.1029/2003WR002650

Dickinson, J.E., Hanson, R.T., Predmore, S.K., 2014b. HydroClimATe—Hydrologic and Climatic Analysis Toolkit, in: Hydrologic Analysis and Interpretation, Techniques and Methods. U.S. Geological Survey, Reston, Virginia, p. 48.

Earman, S., Dettinger, M., 2011. Potential impacts of climate change on groundwater resources – a global review. Journal of Water and Climate Change 2, 213–229. doi:10.2166/wcc.2011.034

Enfield, D.B., Mestas-Nuñez, A.M., Trimble, P.J., 2001. The Atlantic multidecadal oscillation and its relation to rainfall and river flows in the continental U.S. Geophysical Research Letters 28, 2077–2080.

Feng, S., Hu, Q., Oglesby, R.J., 2011. Influence of Atlantic sea surface temperatures on persistent drought in North America. Climate Dynamics 37, 569–586. doi:10.1007/s00382-010-0835-x

Fleming, S.W., Quilty, E.J., 2006. Aquifer Responses to El Niño-Southern Oscillation, Southwest British Columbia. Ground Water 44, 595–599. doi:10.1111/j.1745-6584.2006.00187.x

Fry, J., Xian, G., Jin, S., Dewitz, J., Homer, C., Yang, L., Barnes, C., Herold, N., Wickham, J., 2011. Completion of the 2006 National Land Cover Database for the Coterminous United States. Photogrammetric Engineering and Remote Sensing 77, 858–864.

Gardner, W.R., 1964. Water movement below the root zone, in: Transactions of the 8th International Congress of Soil Science. International Society of Soil Science, Bucharest, pp. 63–68.

Gershunov, A., Barnett, T.P., 1998. Interdecadal Modulation of ENSO Teleconnections. Bulletin of the American Meteorological Society 79, 2715–2725.

Ghil, M., 2002. Natural Climate Variability, in: Encyclopedia of Global Environmental Change, The Earth System: Physical and Chemical Dimensions of Global Environmental Change. Wiley, Chichester ; New York, p. 6.

Ghil, M., Allen, M.R., Dettinger, M.D., Ide, K., Kondrashov, D., Mann, M.E., Robertson, A.W., Saunders, A., Tian, Y., Varadi, F., Yiou, P., 2002. Advanced Spectra

Methods for Climatic Time Series. Reviews of Geophysics 40, 41. doi:10.1029/2000RG000092

Ghil, M., Mo, K.T., 1991. Intraseasonal Oscillations in the Global Atmosphere. Journal of the Atmospheric Sciences 48, 752–790.

Gurdak, J.J., Hanson, R.T., Green, T.R., 2009. Effects of Climate Variability and Change on Groundwater Resources of the United States (Fact Sheet No. 2009-3074). U.S. Geological Survey.

Gurdak, J.J., Hanson, R.T., McMahon, P.B., Bruce, B.W., McCray, J.E., Thyne, G.D., Reedy, R.C., 2007. Climate Variability Controls on Unsaturated Water and Chemical Movement, High Plains Aquifer, USA. Vadose Zone Journal 6, 533–547. doi:10.2136/vzj2006.0087

Gutzler, D.S., Kann, D.M., Thornbrugh, C., 2002. Modulation of ENSO-Based Long-Lead Outlooks of Southwestern U.S. Winter Precipitation by the Pacific Decadal Oscillation. Weather and Forecasting 17, 1163–1172.

Hamlet, A.F., Lettenmaier, D.P., 2007. Effects of 20th century warming and climate variability on flood risk in the western U.S. Water Resources Research 43, 17. doi:10.1029/2006WR005099

Hanson, R.T., Dettinger, M.D., Newhouse, M.W., 2006. Relations between climatic variability and hydrologic time series from four alluvial basins across the southwestern United States. Hydrogeology Journal 14, 1122–1146. doi:10.1007/s10040-006-0067-7

Hanson, R.T., Newhouse, M.W., Dettinger, M.D., 2004. A methodology to asess relations between climatic variability and variations in hydrologic time series in the southwestern United States. Journal of Hydrology 287, 252–269. doi:10.1016/j.jhydrol.2003.10.006

Helsel, D.R., Hirsch, R.M., 2002. Chapter A3: Statistical Methods in Water Resources, in: Techniques of Water Resources Investigations, Book 4. U.S. Geological Survey, p. 522.

Hidalgo, H.G., 2004. Climate precursors of multidecadal drought variability in the western United States. Water Resources Research 40, 10. doi:10.1029/2004WR003350

Higgins, R.W., Silva, V.B.S., Shi, W., Larson, J., 2007. Relationships between Climate Variability and Fluctuations in Daily Precipitation over the United States. Journal of Climate 20, 3561–3579. doi:10.1175/JCLI4196.1

Holman, I.P., 2006. Climate change impacts on groundwater recharge - uncertainty, shortcomings, and the way forward? Hydrogeology Journal 14, 637–647. doi:10.1007/s10040-005-0467-0

Holman, I.P., Rivas-Casado, M., Bloomfield, J.P., Gurdak, J.J., 2011. Identifying non-stationary groundwater level response to North Atlantic ocean-atmosphere teleconnection patterns using wavelet coherence. Hydrogeology Journal 19, 1269–1278. doi:10.1007/s10040-011-0755-9

Hunter, T., Tootle, G., Piechota, T., 2006. Oceanic-atmospheric variability and western U.S. snowfall. Geophysical Research Letters 33, 5. doi:10.1029/2006GL026600

Hu, Q., Feng, S., 2008. Variation of the North American Summer Monsoon Regimes and the Atlantic Multidecadal Oscillation. Journal of Climate 21, 2371–2383. doi:10.1175/2007JCLI2005.1

Hu, Q., Feng, S., Oglesby, R.J., 2011. Variations in North American Summer Precipitation Driven by the Atlantic Multidecadal Oscillation. Journal of Climate 24, 5555–5570. doi:10.1175/2011JCLI4060.1

Hurrell, J.W., 1995. Decadal Trends in the North Atlantic Oscillation: Regional Temperatures and Precipitation. Science 269, 676–679. doi:10.1126/science.269.5224.676

Hurrell, J.W., Kushnir, Y., Ottersen, G., Visbeck, M., 2003. An overview of the North Atlantic Oscillation, in: Hurrell, J.W., Kushnir, Y., Ottersen, G., Visbeck, M. (Eds.), Geophysical Monograph Series. American Geophysical Union, Washington, D. C., pp. 1–35.

Kiladis, G.N., Diaz, H.F., 1989. Global Climatic Anomalies Associated with Extremes in the Southern Oscillation. Journal of Climate 2, 1069–1090.

Knight, J.R., Folland, C.K., Scaife, A.A., 2006. Climate impacts of the Atlantic Multidecadal Oscillation. Geophysical Research Letters 33, 4. doi:10.1029/2006GL026242

Kondrashov, D., Feliks, Y., Ghil, M., 2005. Oscillatory modes of extended Nile River records (A.D. 622–1922). Geophysical Research Letters 32, 4. doi:10.1029/2004GL022156

Kottek, M., Grieser, J., Beck, C., Rudolf, B., Rubel, F., 2006. World Map of the Köppen-Geiger climate classification updated. Meteorologische Zeitschrift 15, 259–263. doi:10.1127/0941-2948/2006/0130

Kurtzman, D., Scanlon, B.R., 2007. El Niño-Southern Oscillation and the Pacific Decadal Oscillation impacts on precipitation in the southern and central United States: Evaluation of spatial distribution and predictions. Water Resources Research 43, 12. doi:10.1029/2007WR005863

Kuss, A.J.M., 2011. Effects of climate variability on recharge in regional aquifers of the United States. San Francisco State University, San Francisco, CA.

Kutzbach, J.E., 1970. Large-Scale Features of Monthly Mean Northern Hemisphere Anomaly Maps of Sea-Level Pressure. Monthly Weather Review 98, 708–716.

Lapp, S.L., St. Jacques, J.-M., Sauchyn, D.J., Vanstone, J.R., 2013. Forcing of hydroclimatic variability in the northwestern Great Plains since AD 1406. Quaternary International 310, 47–61. doi:10.1016/j.quaint.2012.09.011

Li, F., Song, X., Tang, C., Liu, C., Yu, J., Zhang, W., 2007. Tracing infiltration and recharge using stable isotope in Taihang Mt., North China. Environmental Geology 53, 687–696. doi:10.1007/s00254-007-0683-0

Lorenz, E.N., 1951. Seasonal and Irregular Variations of the Northern Hemisphere Sea-Level Pressure Profile. Journal of Meteorology 8, 1952–1959.

Maheu, C., Cazenave, A., Mechoso, C.R., 2003. Water level fluctuations in the Plata Basin (South America) from Topex/Poseidon Satellite Altimetry. Geophysical Research Letters 30, 4. doi:10.1029/2002GL016033

Mantua, N.J., Hare, S.R., 2002. The Pacific Decadal Oscillation. Journal of Oceanography 58, 35–44.

Mantua, N.J., Hare, S.R., Zhang, Y., Wallace, J.M., Francis, R.C., 1997. A Pacific Interdecadal Climate Oscillation with Impacts on Salmon Production. Bulletin of the American Meteorological Society 78, 1069–1079.

Mattern, S., Vanclooster, M., 2010. Estimating travel time of recharge water through a deep vadose zone using a transfer function model. Environmental Fluid Mechanics 10, 121–135. doi:10.1007/s10652-009-9148-1

Mazouz, R., Assani, A.A., Quessy, J., Légaré, G., 2012. Comparison of the interannual variability of spring heavy flood characteristics of tributaries of the St. Lawrence River in Quebec (Canada). Advances in Water Resources 35, 110–120. doi:10.1016/j.advwatres.2011.10.006

McCabe, G.J., Dettinger, M.D., 1999. Decadal variations in the strength of ENSO teleconnections with precipitation in the western United States. International Journal of Climatology 19, 1399–1410.

McCabe, G.J., Palecki, M.A., 2006. Multidecadal climate variability of global lands and oceans. International Journal of Climatology 26, 849–865. doi:10.1002/joc.1289

McCabe, G.J., Palecki, M.A., Betancourt, J.L., 2004. Pacific and Atlantic Ocean influences on multidecadal drought frequency in the United States. Proceedings of the National Academy of Sciences 101, 4136–4141. doi:10.1073/pnas.0306738101

Nigam, S., Guan, B., Ruiz-Barradas, A., 2011. Key role of the Atlantic Multidecadal Oscillation in 20th century drought and wet periods over the Great Plains. Geophysical Research Letters 38, 6. doi:10.1029/2011GL048650

Nimmo, J.R., 2005. Unsaturated Zone Flow Processes, in: Anderson, M.G., Bear, J. (Eds.), Encyclopedia of Hydrological Sciences: Part 13-Groundwater. John Wiley & Sons, Ltd, Chichester, UK, pp. 2299–2322.

Ning, L., Bradley, R.S., 2014. Winter precipitation variability and corresponding teleconnections over the northeastern United States. Journal of Geophysical Research: Atmospheres 119, 7931–7945. doi:10.1002/2014JD021591

NOAA, 2015. Climate Monitoring: Teleconnections [WWW Document]. National Climatic Data Center. URL http://www.ncdc.noaa.gov/teleconnections/ (accessed 3.15.15).

NOAA, 2005. El Niño and La Niña - Related Winter Features Over North America [WWW Document]. National Weather Service, Climate Prediction Center. URL http://www.cpc.ncep.noaa.gov/products/analysis_monitoring/ensocycle/nawinter.shtml

Peings, Y., Magnusdottir, G., 2014. Forcing of the wintertime atmospheric circulation by the multidecadal fluctuations of the North Atlantic ocean. Environmental Research Letters 9, 8. doi:10.1088/1748-9326/9/3/034018

Perez-Valdivia, C., Sauchyn, D., Vanstone, J., 2012. Groundwater levels and teleconnection patterns in the Canadian Prairies. Water Resources Research 48, 13. doi:10.1029/2011WR010930

Pool, D.R., 2005. Variations in climate and ephemeral channel recharge in southeastern Arizona, United States. Water Resources Research 41, 25. doi:10.1029/2004WR003255

PRISM Climate Group, 2014. 30-Year Normals [WWW Document]. Northwest Alliance for Computational Science and Engineering, PRISM Climate Data. URL http://www.prism.oregonstate.edu/normals/

Renwick, J.A., Wallace, J.M., 1996. Relationships between North Pacific winter-time blocking, El Niño, and the PNA pattern. Monthly Weather Review 124, 2071–2076.

Rijtema, P.E., Wassink, H., 1968. Water in the unsaturated zone. International Association of Scientific Hydrology, Braamstraat 61, Gentbrugge.

Rimon, Y., Dahan, O., Nativ, R., Geyer, S., 2007. Water percolation through the deep vadose zone and groundwater recharge: Preliminary results based on a new vadose zone monitoring system. Water Resources Research 43, 12. doi:10.1029/2006WR004855

Ropelewski, C.F., Halpert, M.S., 1987. Global and regional scale precipitation patterns associated with the El Niño/Southern Oscillation. Monthly Weather Review 115, 1606–1626.

Ropelewski, C.F., Halpert, M.S., 1986. North American Precipitation and Temperature Patterns Associated with the El Niño/Southern Oscillation (ENSO). Monthly Weather Review 114, 2352–2362.

Sabziparvar, A.A., Mirmasoudi, S.H., Tabari, H., Nazemosadat, M.J., Maryanaji, Z., 2011. ENSO teleconnection impacts on reference evapotranspiration variability in some warm climates of Iran. Journal of Climatology 31, 1710–1723. doi:10.1002/joc.2187

Sanford, W.E., Selnick, D.L., 2013. Estimation of Evapotranspiration Across the Conterminous United States Using a Regression With Climate and Land-Cover Data. JAWRA Journal of the American Water Resources Association 49, 217–230.

Schonher, T., Nicholson, S.E., 1989. The Relationship between California Rainfall and ENSO Events. Journal of Climate 2, 1258–1269.

Shang, H., Yan, J., Zhang, X., 2011. El Niño-Southern Oscillation influence on winter maximum daily precipitation in California in a spatial model. Water Resources Research 47, 9. doi:10.1029/2011WR010415

Song, J., Li, C., Zhou, W., Pan, J., 2009. The linkage between the Pacific-North American teleconnection pattern and the North Atlantic Oscillation. Advances in Atmospheric Sciences 26, 229–239. doi:10.1007/s00376-009-0229-3
Sophocleous, M.A., 1991. Stream-floodwave propagation through the Great Bend alluvial aquifer, Kansas: Field measurements and numerical simulations. Journal of Hydrology 124, 207–228.
Stoner, A.M.K., Hayhoe, K., Wuebbles, D.J., 2009. Assessing General Circulation Model Simulations of Atmospheric Teleconnection Patterns. Journal of Climate 22, 4348–4372. doi:10.1175/2009JCLI2577.1
Sukhija, B.S., Reddy, D.V., Nagabhushanam, P., Hussain, S., 2003. Recharge processes: piston flow vs preferential flow in semi-arid aquifers of India. Hydrogeology Journal 11, 387–395. doi:10.1007/s10040-002-0243-3
Sutton, R.T., Hodson, D.L.R., 2005. Atlantic Ocean forcing of North American and European summer climate. Science 309, 115–118.
Thompson, D.W.J., Wallace, J.M., 1998. The Arctic Oscillation signature in the wintertime geopotential height and temperature fields. Geophysical Research Letters 25, 1297–1300.
Townley, L.R., 1995. The response of aquifers to periodic forcing. Advances in Water Resources 18, 125–146.
Tremblay, L., Larocque, M., Anctil, F., Rivard, C., 2011. Teleconnections and interannual variability in Canadian groundwater levels. Journal of Hydrology 410, 178–188. doi:10.1016/j.jhydrol.2011.09.013
USDA NRCS, 2009. Hydrologic Soil Groups, in: National Engineering Handbook Part 630 Hydrology. U.S. Department of Agriculture, Natural Resources Conservation Service, p. 14.
USGS, 2014a. Aquifers: Map of the Principal Aquifers of the United States [WWW Document]. USGS Groundwater Information. URL http://water.usgs.gov/ogw/aquifer/map.html
USGS, 2014b. Ground Water Atlas of the United States [WWW Document]. Ground Water Atlas of the United States. URL http://pubs.usgs.gov/ha/ha730/gwa.html
Van Loon, H., Rogers, J.C., 1978. The Seesaw in Winter Temperatures between Greenland and Northern Europe, Part I: General Description. Monthly Weather Review 106, 296–310.
Vautard, R., Pascal, Y., Ghil, M., 1992. Singular Spectrum Analysis: A toolkit for short, noisy, chaotic time series. Physica D: Nonlinear Phenomena 58, 95–126.
Vega, A.J., Rohli, R.V., Henderson, K.G., 1998. The Gulf of Mexico mid-tropospheric response to El Niño and La Niña forcing. Climate Research 10, 115–125.
Venencio, M. del V., García, N.O., 2011. Interannual variability and predictability of water table levels at Santa Fe Province (Argentina) within the climatic change context. Journal of Hydrology 409, 62–70. doi:10.1016/j.jhydrol.2011.07.039
Vicente-Serrano, S.M., López-Moreno, J.I., Gimeno, L., Nieto, R., Morán-Tejeda, E., Lorenzo-Lacruz, J., Beguería, S., Azorin-Molina, C., 2011. A multiscalar global

evaluation of the impact of ENSO on droughts. Journal of Geophysical Research 116. doi:10.1029/2011JD016039

Wada, Y., van Beek, L.P.H., van Kempen, C.M., Reckman, J.W.T.M., Vasak, S., Bierkens, M.F.P., 2010. Global depletion of groundwater resources. Geophysical Research Letters 37, 5. doi:10.1029/2010GL044571

Walker, G.T., 1924. Correlation in seasonal variations of weather, IX. A further study of world weather. Memoirs of the Indian Meteorological Department 24, 275–332.

Walker, G.T., Bliss, E.W., 1932. World Weather V. Memoirs of the Royal Meteorological Society 4, 53–84.

Wallace, J.M., Gutzler, D.S., 1981. Teleconnections in the Geopotential Height Field during the Northern Hemisphere Winter. Monthly Weather Review 109, 784–812.

Wang, C., Zhang, L., 2013. Multidecadal Ocean Temperature and Salinity Variability in the Tropical North Atlantic: Linking with the AMO, AMOC, and Subtropical Cell. Journal of Climate 26, 6137–6162. doi:10.1175/JCLI-D-12-00721.1

Waswa, G.W., Clulow, A.D., Freese, C., Le Roux, P.A.L., Lorentz, S.A., 2013. Transient Pressure Waves in the Vadose Zone and the Rapid Water Table Response. Vadose Zone Journal 12, 18. doi:10.2136/vzj2012.0054

Wolter, K., Timlin, M.S., 2011. El Niño/Southern Oscillation behaviour since 1871 as diagnosed in an extended multivariate ENSO index. International Journal of Climatology 31, 1074–1087. doi:10.1002/joc.2336

Wolter, K., Timlin, M.S., 1998. Measuring the strength of ENSO events: how does 1997/98 rank? Weather 53, 315–324.

Wolter, K., Timlin, M.S., 1993. Monitoring ENSO in COADS with a seasonally adjusted principal component index, in: Proceedings of the 17th Cliamte Diagnostics Workshop. Norman, Oklahoma, pp. 52–57.

Wyatt, M.G., Kravtsov, S., Tsonis, A.A., 2012. Atlantic Multidecadal Oscillation and Northern Hemisphere's climate variability. Climate Dynamics 38, 929–949. doi:10.1007/s00382-011-1071-8

Yan, T., Pietrafesa, L.J., Dickey, D.A., Gayes, P.T., Bao, S., 2014. Seasonal prediction of landfalling hurricanes along Eastern Seaboard of the United States: Seasonal prediction of landfalling hurricanes along US East Coast. International Journal of Climatology 7. doi:10.1002/joc.4163

Zhang, Y., Wallace, J.M., Battisti, D.S., 1997. ENSO-like interdecadal variability: 1900-93. Journal of climate 10, 1004–1020.

TABLES

California Coastal Basins Groundwater Wells

a) Location Information

Site ID	Site Number	State	Latitude	Longitude
CC_GW_01	394802123115701	CA	39.800	-123.200
CC_GW_02	381700122261401	CA	38.283	-122.438
CC_GW_03	372706122254301	CA	37.452	-122.430
CC_GW_04	371044121414701	CA	37.179	-121.697
CC_GW_05	343840120254701	CA	34.644	-120.431
CC_GW_06	344156119184801	CA	34.699	-119.313
CC_GW_07	340535117573501	CA	34.093	-117.961
CC_GW_08	340413117180501	CA	34.070	-117.302

b) Groundwater Record and Hydrologic Information

Site ID	Starting Year	Ending Year	Length of Record (years)	Number of Monthly Measurements	Measure-ments per year	Hydrologic Soil Group	Average Depth to Water (meters)
CC_GW_01	1951	1988	37	149	4	B	3.0
CC_GW_02	1950	1983	33	134	4	B	5.4
CC_GW_03	1953	1983	30	139	5	B	9.7
CC_GW_04	1937	1983	46	566	12	B	11.9
CC_GW_05	1950	2013	63	514	8	B	7.7
CC_GW_06	1972	2012	40	80	2	B	8.9
CC_GW_07	1932	2013	81	8034	99	N/A	34.6
CC_GW_08	1967	2008	41	161	4	A	13.8
						Aquifer Average:	**11.9**

Table 1. Descriptive attributes for a) the location and b) the groundwater record and hydrology of groundwater wells in the California Coastal Basins aquifer. The Site ID identifies the aquifer name (CC), the site type (GW for groundwater), and the location (01–08 from northwest to southeast). The Hydrologic Soil Group categories are: A for sandy and gravelly textures, B for loamy sand or sandy loam textures, C for loamy and silty textures, and D for clayey textures. N/A = information not available.

Pacific Northwest Regional Group of Groundwater Wells

a) Location Information

Site ID	Site Number	State	Latitude	Longitude
PN_GW_01	441508123053001	OR	44.252	-123.093
PN_GW_02	452033122195901	OR	45.366	-122.334
PN_GW_03	434400121275801	OR	43.733	-121.467
PN_GW_04	454014118410101	OR	45.671	-118.684
PN_GW_05	454104118285901	OR	45.684	-118.484
PN_GW_06	474011117072901	WA	47.670	-117.127
PN_GW_07	475439116503401	ID	47.911	-116.844

b) Groundwater Record and Hydrologic Information

Site ID	Starting Year	Ending Year	Length of Record (years)	Number of Monthly Measurements	Measure-ments per year	Hydrologic Soil Group	Average Depth to Water (meters)
PN_GW_01	1962	2014	52	256	5	C	1.8
PN_GW_02	1962	2014	52	188	4	C	18.9
PN_GW_03	1945	2013	68	245	4	B	7.2
PN_GW_04	1979	2012	33	438	13	B	3.0
PN_GW_05	1979	2012	33	434	13	D	2.8
PN_GW_06	1929	2014	85	1393	16	B	31.5
PN_GW_07	1971	2014	43	484	11	B	124.8
						Aquifer Average:	**27.1**

Table 2. Descriptive attributes for a) the location and b) the groundwater record and hydrology of groundwater wells in the Pacific Northwest regional group of aquifers. The Site ID identifies the aquifer name (PN), the site type (GW for groundwater), and the location (01–07 from southwest to northeast). The Hydrologic Soil Group categories are: A for sandy and gravelly textures, B for loamy sand or sandy loam textures, C for loamy and silty textures, and D for clayey textures.

Rio Grande Groundwater Wells

a) Location Information

Site ID	Site Number	State	Latitude	Longitude
RG_GW_01A	380601105505201	CO	38.100	-105.848
RG_GW_01B	375324105553301	CO	37.890	-105.926
RG_GW_02A	374012105410401	CO	37.670	-105.685
RG_GW_02B	373950105342801	CO	37.664	-105.575
RG_GW_03A	373400105513001	CO	37.575	-105.858
RG_GW_03B	372854105513001	CO	37.488	-105.857
RG_GW_03C	372326107491501	CO	37.391	-105.821
RG_GW_04	370758105564401	CO	37.133	-105.946

b) Groundwater Record and Hydrologic Information

Site ID	Starting Year	Ending Year	Length of Record (years)	Number of Monthly Measurements	Measure-ments per year	Hydrologic Soil Group	Average Depth to Water (meters)
RG_GW_01A	1976	2014	38	419	11	B	6.4
RG_GW_01B	1967	2014	47	448	10	A	3.2
RG_GW_02A	1974	2014	40	452	11	A	1.2
RG_GW_02B	1973	2014	41	417	10	B	24.5
RG_GW_03A	1948	2014	66	176	3	D	1.4
RG_GW_03B	1949	2014	65	171	3	C	1.0
RG_GW_03C	1976	2014	38	433	11	D	2.1
RG_GW_04	1974	2014	40	445	11	D	0.8
						Aquifer Average:	**5.1**

Table 3. Descriptive attributes for a) the location and b) the groundwater record and hydrology of groundwater wells in the Rio Grande aquifer. The Site ID identifies the aquifer name (RG), the site type (GW for groundwater), and the location (01–04 from north to south). Letters at the end of the Site ID indicate that multiple groundwater sites are co-located with a single precipitation site of the same location number. The Hydrologic Soil Group categories are: A for sandy and gravelly textures, B for loamy sand or sandy loam textures, C for loamy and silty textures, and D for clayey textures.

Glacial (Western Section) Groundwater Wells

a) Location Information

Site ID	Site Number	State	Latitude	Longitude
GL_GW_01	475224098443202	ND	47.873	-98.743
GL_GW_02	460444094212501	MN	46.079	-94.357
GL_GW_03	424023091291201	IA	42.673	-91.487
GL_GW_04	434823090461401	WI	43.811	-90.770
GL_GW_05	435759089490001	WI	43.966	-89.817
GL_GW_06	453816087590101	WI	45.638	-87.984

b) Groundwater Record and Hydrologic Information

Site ID	Starting Year	Ending Year	Length of Record (years)	Number of Monthly Measurements	Measure-ments per year	Hydrologic Soil Group	Average Depth to Water (meters)
GL_GW_01	1951	2014	63	543	9	B	6.3
GL_GW_02	1949	2014	65	2421	37	A	4.0
GL_GW_03	1957	2007	50	363	7	B	6.4
GL_GW_04	1934	2014	80	1844	23	B	2.0
GL_GW_05	1969	2013	44	2006	46	A	4.5
GL_GW_06	1939	2013	74	5331	72	B	6.4
						Aquifer Average:	**4.9**

Table 4. Descriptive attributes for a) the location and b) the groundwater record and hydrology of groundwater wells in the western section of the Glacial aquifer. The Site ID identifies the aquifer name (GL), the site type (GW for groundwater), and the location (01–06 from west to east). The Hydrologic Soil Group categories are: A for sandy and gravelly textures, B for loamy sand or sandy loam textures, C for loamy and silty textures, and D for clayey textures.

Glacial (Eastern Section) Groundwater Wells

a) Location Information

Site ID	Site Number	State	Latitude	Longitude
GL_GW_07	433112075091501	NY	43.520	-75.154
GL_GW_08	444904074455201	NY	44.818	-74.764
GL_GW_09	434217073010601	VT	43.705	-73.018
GL_GW_10	425543072175801	NH	42.929	-72.299
GL_GW_11A	415710071402201	RI	41.953	-71.672
GL_GW_11B	415948071325001	RI	41.995	-71.547
GL_GW_11C	415626071254601	RI	41.941	-71.429
GL_GW_12	413148071281601	RI	41.530	-71.471
GL_GW_13	420056070575701	MA	42.016	-70.965
GL_GW_14A	414124070265901	MA	41.690	-70.449
GL_GW_14B	414418070241601	MA	41.738	-70.404

Table 5a. Descriptive attributes for the location of groundwater wells in the eastern section of the Glacial aquifer. The Site ID identifies the aquifer name (GL), the site type (GW for groundwater), and the location (07–14 from northwest to southeast). Letters at the end of the Site ID indicate that multiple groundwater sites are co-located with a single precipitation site of the same location number.

Glacial (Eastern Section) Groundwater Wells

b) Groundwater Record and Hydrologic Information

Site ID	Starting Year	Ending Year	Length of Record (years)	Number of Monthly Measurements	Measure-ments per year	Hydrologic Soil Group	Average Depth to Water (meters)
GL_GW_07	1926	2013	87	4872	56	B	6.9
GL_GW_08	1953	2013	60	3402	57	A	2.0
GL_GW_09	1957	2013	56	634	11	A	11.1
GL_GW_10	1963	2014	51	629	12	C	1.1
GL_GW_11A	1968	2013	45	554	12	A	4.7
GL_GW_11B	1947	2013	66	803	12	B	2.4
GL_GW_11C	1946	2013	67	814	12	B	3.9
GL_GW_12	1954	2013	59	725	12	B	2.6
GL_GW_13	1958	2013	55	655	12	A	2.8
GL_GW_14A	1962	2013	51	618	12	B	15.2
GL_GW_14B	1962	2013	51	623	12	C	14.4
						Aquifer Average:	**6.1**

Table 5b. Descriptive attributes for the groundwater record and hydrology of groundwater wells in the eastern section of the Glacial aquifer. The Site ID identifies the aquifer name (GL), the site type (GW for groundwater), and the location (07–14 from northwest to southeast). Letters at the end of the Site ID indicate that multiple groundwater sites are co-located with a single precipitation site of the same location number. The Hydrologic Soil Group categories are: A for sandy and gravelly textures, B for loamy sand or sandy loam textures, C for loamy and silty textures, and D for clayey textures.

Coastal Lowlands Groundwater Wells

a) Location Information

Site ID	Site Number	State	Latitude	Longitude
CL_GW_01	291949095024801	TX	29.331	-95.047
CL_GW_02	295449095083401	TX	29.914	-95.143
CL_GW_03	294433095044703	TX	29.743	-95.080
CL_GW_04	294527095014902	TX	29.758	-95.030
CL_GW_05	301336093183002	LA	30.227	-93.308
CL_GW_06	312703092224801	LA	31.451	-92.380
CL_GW_07	304116092083601	LA	30.688	-92.142
CL_GW_08	293845092264901	LA	29.646	-92.447
CL_GW_09	295345092100702	LA	29.896	-92.169
CL_GW_10	302703091133703	LA	30.451	-91.227
CL_GW_11	303356091095301	LA	30.566	-91.165

Table 6. Descriptive attributes for a) the location of groundwater wells in the Coastal Lowlands aquifer. The Site ID identifies the aquifer name (CL), the site type (GW for groundwater), and the location (01–11 from southwest to northeast).

Coastal Lowlands Groundwater Wells

b) Groundwater Record and Hydrologic Information

Site ID	Starting Year	Ending Year	Length of Record (years)	Number of Monthly Measurements	Measure-ments per year	Hydrologic Soil Group	Average Depth to Water (meters)
CL_GW_01	1962	2013	51	90	2	C/D	27.7
CL_GW_02	1954	2014	60	616	10	D	28.1
CL_GW_03	1973	2014	41	476	12	D	4.2
CL_GW_04	1972	2014	42	496	12	D	6.6
CL_GW_05	1963	2014	51	156	3	D	20.6
CL_GW_06	1956	2014	58	492	8	C	21.2
CL_GW_07	1957	2014	57	205	4	C	17.1
CL_GW_08	1965	2014	49	139	3	B	2.7
CL_GW_09	1964	2014	50	229	5	D	3.4
CL_GW_10	1966	2014	48	222	5	D	68.5
CL_GW_11	1967	2014	47	219	5	D	15.8
						Aquifer Average:	**19.6**

Table 6. Descriptive attributes for b) the groundwater record and hydrology of groundwater wells in the Coastal Lowlands aquifer. The Site ID identifies the aquifer name (CL), the site type (GW for groundwater), and the location (01–11 from southwest to northeast). The Hydrologic Soil Group categories are: A for sandy and gravelly textures, B for loamy sand or sandy loam textures, C for loamy and silty textures, and D for clayey textures.

Mississippi Embayment Groundwater Wells

a) Location Information

Site ID	Site Number	State	Latitude	Longitude
ME_GW_01A	350910090015102	TN	35.153	-90.031
ME_GW_01B	350432090015101	TN	35.076	-90.031
ME_GW_02	341138091551601	AR	34.195	-91.921
ME_GW_03	332916089432002	MS	33.488	-89.722
ME_GW_04	330609093274302	AR	33.103	-93.462
ME_GW_05	323029091430001	LA	32.508	-91.717
ME_GW_06	324508091252301	LA	32.752	-91.423
ME_GW_07	322627090062401	MS	32.443	-90.107
ME_GW_08	320316093114201	LA	32.055	-93.195
ME_GW_09	320153093583601	LA	32.032	-93.977
ME_GW_10	312206093311001	LA	31.369	-93.520

Table 7a. Descriptive attributes for the location of groundwater wells in the Mississippi Embayment aquifer. The Site ID identifies the aquifer name (ME), the site type (GW for groundwater), and the location (01–10 from northeast to southwest). Letters at the end of the Site ID indicate that multiple groundwater sites are co-located with a single precipitation site of the same location number.

Mississippi Embayment Groundwater Wells

b) Groundwater Record and Hydrologic Information

Site ID	Starting Year	Ending Year	Length of Record (years)	Number of Monthly Measurements	Measure-ments per year	Hydrologic Soil Group	Average Depth to Water (meters)
ME_GW_01A	1945	2013	68	909	13	B	26.2
ME_GW_01B	1949	2013	64	751	12	B	25.1
ME_GW_02	1958	2013	55	502	9	D	70.9
ME_GW_03	1958	1996	38	167	4	C	31.8
ME_GW_04	1967	2013	46	86	2	C	16.2
ME_GW_05	1969	2013	44	144	3	B	6.0
ME_GW_06	1955	2013	58	248	4	C	9.6
ME_GW_07	1957	2013	56	230	4	C	48.9
ME_GW_08	1981	2013	32	159	5	B	5.8
ME_GW_09	1982	2013	31	138	4	B	4.9
ME_GW_10	1965	2013	48	284	6	D	7.5
						Aquifer Average:	**23.0**

Table 7b. Descriptive attributes for the groundwater record and hydrology of groundwater wells in the Mississippi Embayment aquifer. The Site ID identifies the aquifer name (ME), the site type (GW for groundwater), and the location (01–10 from northeast to southwest). Letters at the end of the Site ID indicate that multiple groundwater sites are co-located with a single precipitation site of the same location number. The Hydrologic Soil Group categories are: A for sandy and gravelly textures, B for loamy sand or sandy loam textures, C for loamy and silty textures, and D for clayey textures.

Surficial Groundwater Wells

a) Location Information

Site ID	Site Number	State	Latitude	Longitude
SR_GW_01	335629078115407	NC	33.941	-78.199
SR_GW_02	315950081161201	GA	31.997	-81.270
SR_GW_03	283249081053203	FL	28.548	-81.092
SR_GW_04	281532081345002	FL	28.259	-81.581
SR_GW_05	272504081120101	FL	27.418	-81.200
SR_GW_06	270959082203003	FL	27.167	-82.341
SR_GW_07	263329081394301	FL	26.559	-81.661
SR_GW_08	261200081204901	FL	26.201	-81.346

b) Groundwater Record and Hydrologic Information

Site ID	Starting Year	Ending Year	Length of Record (years)	Number of Monthly Measurements	Measure-ments per year	Hydrologic Soil Group	Average Depth to Water (meters)
SR_GW_01	1986	2014	28	161	6	A	2.2
SR_GW_02	1954	2014	60	630	11	C	1.8
SR_GW_03	1969	2014	45	565	13	A/D	0.7
SR_GW_04	1979	2012	33	300	9	A	3.8
SR_GW_05	1977	2014	37	212	6	A/D	0.8
SR_GW_06	1981	2011	30	177	6	A/D	0.9
SR_GW_07	1975	2014	39	422	11	A/D	1.2
SR_GW_08	1984	2014	30	313	10	A/D	1.0
						Aquifer Average:	**1.6**

Table 8. Descriptive attributes for a) the location and b) the groundwater record and hydrology of groundwater wells in the Surficial aquifer. The Site ID identifies the aquifer name (SR), the site type (GW for groundwater), and the location (01–08 from northeast to southwest). The Hydrologic Soil Group categories are: A for sandy and gravelly textures, B for loamy sand or sandy loam textures, C for loamy and silty textures, and D for clayey textures. A/D indicates a dual soil classification.

California Coastal Basins Precipitation Stations

a) Location Information

Site ID	Site Number	State	Latitude	Longitude
CC_PR_01	USC00042081	CA	39.816	-123.244
CC_PR_02	USC00048351	CA	38.299	-122.462
CC_PR_03	USC00043714	CA	37.472	-122.443
CC_PR_04	USC00043417	CA	37.003	-121.561
CC_PR_05	USC00045064	CA	34.654	-120.451
CC_PR_06	USC00044863	CA	34.833	-118.865
CC_PR_07	USC00047785	CA	34.106	-118.100
CC_PR_08	USC00047306	CA	34.053	-117.189

b) Precipitation Record and Hydrologic Information

Site ID	Starting Year	Ending Year	Length of Record (years)	Average Annual Precipitation (millimeters)	Fraction of Precipitation Lost to ET	Average Annual Infiltration (millimeters)
CC_PR_01	1935	2013	78	1147	0.45	631
CC_PR_02	1952	2013	61	742	0.55	334
CC_PR_03	1939	2014	75	706	0.75	176
CC_PR_04	1957	2014	57	514	0.85	77
CC_PR_05	1950	2013	63	386	0.85	58
CC_PR_06	1948	2014	66	333	0.85	50
CC_PR_07	1939	2014	75	490	0.85	73
CC_PR_08	1898	2014	116	290	0.95	14
					Aquifer Average:	**177**

Table 9. Descriptive attributes for a) the location and b) the precipitation record and hydrology of precipitation stations in the area of the California Coastal Basins aquifer. The Site ID identifies the aquifer name (CC), the site type (PR for precipitation), and the location (01–08 from northwest to southeast).

Pacific Northwest Region Precipitation Stations

a) Location Information

Site ID	Site Number	State	Latitude	Longitude
PN_PR_01	USW00024221	OR	44.127	-123.220
PN_PR_02	USC00352693	OR	45.268	-122.318
PN_PR_03	USC00359316	OR	43.682	-121.687
PN_PR_04	USC00356540	OR	45.720	-118.626
PN_PR_05	USS0018D20S	OR	45.366	-118.450
PN_PR_06	USW00024157	WA	47.621	-117.528
PN_PR_07	USC00100667	ID	47.980	-116.559

b) Precipitation Record and Hydrologic Information

Site ID	Starting Year	Ending Year	Length of Record (years)	Average Annual Precipitation (millimeters)	Fraction of Precipitation Lost to ET	Average Annual Infiltration (millimeters)
PN_PR_01	1939	2014	75	1152	0.35	749
PN_PR_02	1909	2014	105	1520	0.35	988
PN_PR_03	1941	2014	73	558	0.75	140
PN_PR_04	1956	2014	58	436	0.75	109
PN_PR_05	1978	2014	36	705	0.65	247
PN_PR_06	1889	2014	125	419	0.85	63
PN_PR_07	1947	2014	67	864	0.55	389
					Aquifer Average:	**383**

Table 10. Descriptive attributes for a) the location and b) the precipitation record and hydrology of precipitation stations in the area of the Pacific Northwest regional aquifers. The Site ID identifies the aquifer name (PN), the site type (PR for precipitation), and the location (01–07 from southwest to northeast).

Rio Grande Precipitation Stations

a) Location Information

Site ID	Site Number	State	Latitude	Longitude
RG_PR_01	USC00057337	CO	38.086	-106.144
RG_PR_02	USC00053541	CO	37.733	-105.512
RG_PR_03	USW00023061	CO	37.439	-105.861
RG_PR_04	USC00055322	CO	37.174	-105.939

b) Precipitation Record and Hydrologic Information

Site ID	Starting Year	Ending Year	Length of Record (years)	Average Annual Precipitation (millimeters)	Fraction of Precipitation Lost to ET	Average Annual Infiltration (millimeters)
RG_PR_01	1894	2009	115	207	0.85	31
RG_PR_02	1950	2014	64	381	0.95	19
RG_PR_03	1948	2014	66	188	0.95	9
RG_PR_04	1906	2014	108	211	0.75	53
					Aquifer Average:	**28**

Table 11. Descriptive attributes for a) the location and b) the precipitation record and hydrology of precipitation stations in the area of the Rio Grande aquifer. The Site ID identifies the aquifer name (RG), the site type (PR for precipitation), and the location (01–04 from north to south).

Glacial (Western Section) Precipitation Stations

a) Location Information

Site ID	Site Number	State	Latitude	Longitude
GL_PR_01	USW00014912	ND	48.107	-98.868
GL_PR_02	USC00214793	MN	45.966	-94.369
GL_PR_03	USC00132603	IA	42.775	-91.454
GL_PR_04	USC00477997	WI	43.936	-90.816
GL_PR_05	USC00473405	WI	44.119	-89.536
GL_PR_06	USC00204090	MI	45.786	-88.084

b) Precipitation Record and Hydrologic Information

Site ID	Starting Year	Ending Year	Length of Record (years)	Average Annual Precipitation (millimeters)	Fraction of Precipitation Lost to ET	Average Annual Infiltration (millimeters)
GL_PR_01	1921	2013	92	495	0.85	74
GL_PR_02	1913	2013	100	694	0.65	243
GL_PR_03	1934	2014	80	903	0.65	316
GL_PR_04	1936	2014	78	872	0.55	392
GL_PR_05	1903	2014	111	824	0.65	288
GL_PR_06	1899	2013	114	758	0.65	265
					Aquifer Average:	**263**

Table 12. Descriptive attributes for a) the location and b) the precipitation record and hydrology of precipitation stations in the area of the western section of the Glacial aquifer. The Site ID identifies the aquifer name (GL), the site type (PR for precipitation), and the location (01–06 from west to east).

Glacial (Eastern Section) Precipitation Stations

a) Location Information

Site ID	Site Number	State	Latitude	Longitude
GL_PR_07	USC00303851	NY	43.575	-75.521
GL_PR_08	USW00094725	NY	44.936	-74.846
GL_PR_09	USC00431433	VT	43.706	-72.962
GL_PR_10	USC00274399	NH	42.939	-72.325
GL_PR_11	USC00379423	RI	41.984	-71.491
GL_PR_12	USW00014765	RI	41.722	-71.433
GL_PR_13	USC00190860	MA	42.048	-71.005
GL_PR_14	USC00193821	MA	41.665	-70.304

b) Precipitation Record and Hydrologic Information

Site ID	Starting Year	Ending Year	Length of Record (years)	Average Annual Precipitation (millimeters)	Fraction of Precipitation Lost to ET	Average Annual Infiltration (millimeters)
GL_PR_07	1924	2014	90	1425	0.35	926
GL_PR_08	1948	2014	66	933	0.45	513
GL_PR_09	1947	2013	66	1188	0.45	653
GL_PR_10	1893	2014	121	1120	0.45	616
GL_PR_11	1956	2014	58	1278	0.45	703
GL_PR_12	1948	2014	66	1212	0.45	667
GL_PR_13	1930	2014	84	1270	0.45	699
GL_PR_14	1893	2013	120	1109	0.45	610
					Aquifer Average:	**673**

Table 13. Descriptive attributes for a) the location and b) the precipitation record and hydrology of precipitation stations in the area of the eastern section of the Glacial aquifer. The Site ID identifies the aquifer name (GL), the site type (PR for precipitation), and the location (07–14 from northwest to southeast).

Coastal Lowlands Precipitation Stations

a) Location Information

Site ID	Site Number	State	Latitude	Longitude
CL_PR_01	USC00410257	TX	29.157	-95.459
CL_PR_02	USC00416280	TX	30.138	-95.178
CL_PR_03_04	USW00012918	TX	29.638	-95.282
CL_PR_05	USC00416664	TX	30.086	-93.742
CL_PR_06	USC00160098	LA	31.321	-92.461
CL_PR_07	USC00161287	LA	30.959	-92.179
CL_PR_08	USC00167932	LA	29.729	-92.818
CL_PR_09	USW00013976	LA	30.205	-91.988
CL_PR_10	USC00165620	LA	30.364	-91.167
CL_PR_11	USW00013970	LA	30.537	-91.147

b) Precipitation Record and Hydrologic Information

Site ID	Starting Year	Ending Year	Length of Record (years)	Average Annual Precipitation (millimeters)	Fraction of Precipitation Lost to ET	Average Annual Infiltration (millimeters)
CL_PR_01	1913	2014	101	1376	0.65	482
CL_PR_02	1952	2014	62	1336	0.65	468
CL_PR_03_04	1941	2014	73	1356	0.65	475
CL_PR_05	1938	2014	76	1530	0.55	688
CL_PR_06	1892	2014	122	1511	0.55	680
CL_PR_07	1956	2014	58	1549	0.55	697
CL_PR_08	1964	2014	50	1537	0.55	692
CL_PR_09	1893	2014	121	1558	0.55	701
CL_PR_10	1963	2014	51	1569	0.55	706
CL_PR_11	1930	2014	84	1575	0.55	709
					Aquifer Average:	**630**

Table 14. Descriptive attributes for a) the location and b) the precipitation record and hydrology of precipitation stations in the area of the Coastal Lowlands aquifer. The Site ID identifies the aquifer name (CL), the site type (PR for precipitation), and the location (07–14 from southwest to northeast). Note: site CL_PR_03_04 is co-located with CL_GW_03 and CL_GW_04.

Mississippi Embayment Precipitation Stations

a) Location Information

Site ID	Site Number	State	Latitude	Longitude
ME_PR_01	USW00013893	TN	35.056	-89.986
ME_PR_02	USC00035754	AR	34.226	-92.019
ME_PR_03	USC00229743	MS	33.485	-89.624
ME_PR_04	USC00034548	AR	33.295	-93.233
ME_PR_05	USC00160537	LA	32.731	-91.914
ME_PR_06	USC00165090	LA	32.807	-91.173
ME_PR_07	USW00003940	MS	32.321	-90.078
ME_PR_08	USC00160349	LA	32.163	-93.133
ME_PR_09	USC00411578	TX	31.808	-94.164
ME_PR_10	USC00164288	LA	31.375	-93.391

b) Precipitation Record and Hydrologic Information

Site ID	Starting Year	Ending Year	Length of Record (years)	Average Annual Precipitation (millimeters)	Fraction of Precipitation Lost to ET	Average Annual Infiltration (millimeters)
ME_PR_01	1940	2014	74	1356	0.55	610
ME_PR_02	1884	2014	130	1323	0.65	463
ME_PR_03	1953	2014	61	1448	0.55	652
ME_PR_04	1948	2014	66	1332	0.55	599
ME_PR_05	1935	2014	79	1434	0.55	646
ME_PR_06	1926	2014	88	1441	0.65	505
ME_PR_07	1951	2014	63	1402	0.55	631
ME_PR_08	1943	2014	71	1418	0.55	638
ME_PR_09	1939	2014	75	1352	0.65	473
ME_PR_10	1963	2014	51	1431	0.55	644
					Aquifer Average:	**586**

Table 15. Descriptive attributes for a) the location and b) the precipitation record and hydrology of precipitation stations in the area of the Mississippi Embayment aquifer. The Site ID identifies the aquifer name (ME), the site type (PR for precipitation), and the location (01–10 from northeast to southwest).

Surficial Precipitation Stations

a) Location Information

Site ID	Site Number	State	Latitude	Longitude
SR_PR_01	USC00318113	NC	33.994	-78.007
SR_PR_02	USW00003822	GA	32.130	-81.210
SR_PR_03	USC00088942	FL	28.624	-80.815
SR_PR_04	USC00084625	FL	28.276	-81.424
SR_PR_05	USC00082288	FL	27.369	-81.513
SR_PR_06	USC00089176	FL	27.100	-82.436
SR_PR_07	USC00087397	FL	26.916	-81.998
SR_PR_08	USC00086078	FL	26.168	-81.715

b) Precipitation Record and Hydrologic Information

Site ID	Starting Year	Ending Year	Length of Record (years)	Average Annual Precipitation (millimeters)	Fraction of Precipitation Lost to ET	Average Annual Infiltration (millimeters)
SR_PR_01	1891	2014	123	1465	0.55	659
SR_PR_02	1947	2014	67	1240	0.65	434
SR_PR_03	1901	2014	113	1345	0.65	471
SR_PR_04	1959	2014	55	1244	0.65	436
SR_PR_05	1946	2014	68	1229	0.75	307
SR_PR_06	1955	2014	59	1354	0.65	474
SR_PR_07	1965	2014	49	1303	0.65	456
SR_PR_08	1942	2014	72	1419	0.75	355
					Aquifer Average:	**449**

Table 16. Descriptive attributes for a) the location and b) the precipitation record and hydrology of precipitation stations in the area of the Surficial aquifer. The Site ID identifies the aquifer name (SR), the site type (PR for precipitation), and the location (01–08 from northeast to southwest).

DAMP Input Variables

Aquifer	Average Infiltration (meters/day)	Representative Soil Type	Average Depth to Water (meters)
CC	4.9×10^{-4}	Loam or Silt	11.9
PN	1.1×10^{-3}	Silty Clay Loam	27.1
RG	7.6×10^{-5}	Sandy Clay Loam	5.1
GLW	7.2×10^{-4}	Sand	4.9
ME	1.6×10^{-3}	Silty Clay Loam	23.0
CL	1.7×10^{-3}	Silty Clay Loam	19.6
SR	1.2×10^{-3}	Sand or Clay	1.6
GLE	1.8×10^{-3}	Sand	6.1

Table 17. Aquifer-averaged values of daily infiltration, soil type, and depth to water that were input into the DAMP program to create two-dimensional nomograms of the damping factor. Aquifers are listed in west to east order.

Percent Variance of Climate Variability Modes

	Precipitation RCs			Groundwater RCs		
	Minimum	**Maximum**	**Average**	**Minimum**	**Maximum**	**Average**
AMO	41.6%	94.8%	61.3%	59.3%	96.6%	73.5%
PDO	18.5%	94.5%	49.5%	2.3%	99.8%	77.6%
ENSO	0.8%	59.3%	10.7%	0.02%	46.7%	8.8%
NAO	0.3%	40.6%	7.5%	0.02%	37.3%	5.2%
PNA	0.5%	27.7%	7.7%	<0.01%	13.0%	3.4%
AO	0.2%	18.6%	4.7%	<0.01%	7.2%	1.3%

Table 18. Percent variance ranges and averages for precipitation and groundwater reconstructed components (RCs) that fell within the range of each climate variability period.

Percent Variance of Precipitation RCs Averaged by Aquifer

	CC	PN	RG	GLW
AMO	63.0%	73.0%	63.5%	54.6%
PDO	51.8%	52.0%	49.2%	38.7%
ENSO	11.7%	6.5%	6.5%	7.9%
NAO	10.1%	3.8%	3.5%	4.5%
PNA	A,B 9.5%	A,B 8.9%	A,B 5.4%	A,B 10.2%
AO	5.3%	4.3%	2.3%	7.6%

	CL	ME	SR	GLE
AMO	70.4%	56.5%	51.8%	53.6%
PDO	41.5%	41.3%	54.5%	65.0%
ENSO	15.0%	15.5%	11.1%	5.5%
NAO	9.6%	11.0%	9.5%	3.6%
PNA	A,B 6.9%	A,B 5.9%	A 11.7%	B 3.6%
AO	4.8%	0.6%	6.9%	0.7%

Table 19. Aquifer averages of percent variance for precipitation reconstructed components (RCs). Aquifers are ordered from west to east. Letters A and B indicate statistically significant differences between means based on the Tukey-Kramer Honestly Significant Difference test.

Percent Variance of Precipitation RCs Averaged by Region

	West	Central	East
AMO	67.2%	63.0%	52.9%
PDO	51.3%	40.8%	60.1%
ENSO	8.7%	13.5%	8.3%
NAO	6.4%	9.0%	6.5%
PNA	8.4%	7.3%	7.6%
AO	4.3%	4.8%	5.2%

	North	South
AMO	59.5%	62.5%
PDO	54.0%	47.1%
ENSO	A 6.5%	B 12.8%
NAO	A 3.9%	B 9.4%
PNA	7.1%	8.0%
AO	4.9%	4.6%

Table 20. Regional averages of percent variance for precipitation reconstructed components (RCs). The west region includes the CC, PN, and RG aquifers; the central region includes the GLW, CL, and ME aquifers; and the east region includes the SR and GLE aquifers. The north region includes the PN, GLW, and GLE aquifers; and the south region includes the CC, RG, CL, ME, and SR aquifers. Letters A and B indicate statistically significant differences between means based on the Tukey-Kramer Honestly Significant Difference test.

Percent Variance of Groundwater RCs Averaged by Aquifer

	CC		PN		RG		GLW	
AMO		71.0%		96.6%		--		67.1%
PDO	A,B	74.2%	A,B	71.8%	A	92.5%	B	43.0%
ENSO	A,B	9.3%	B	2.9%	B	1.6%	A,B	11.7%
NAO	A,B	5.7%	B	2.3%	B	1.0%	B	2.4%
PNA		3.0%		5.3%		1.2%		3.1%
AO		0.3%		3.3%		0.2%		0.3%

	CL		ME		SR		GLE	
AMO		--		--		--		59.3%
PDO	A	86.1%	A	81.5%	A,B	76.7%	A,B	76.4%
ENSO	A,B	6.5%	A,B	6.9%	A	21.7%	A,B	11.2%
NAO	B	3.8%	B	2.5%	A	15.7%	A,B	6.9%
PNA		1.7%		2.1%		5.8%		5.4%
AO		0.0%		0.4%		0.8%		2.2%

Table 21. Aquifer averages of percent variance for groundwater reconstructed components (RCs). Aquifers are ordered from west to east. Letters A and B indicate statistically significant differences between means based on the Tukey-Kramer Honestly Significant Difference test.

Percent Variance of Groundwater RCs Averaged by Region

	West	Central	East
AMO	83.8%	67.1%	59.3%
PDO	80.1%	76.3%	76.5%
ENSO	A 4.7%	A 7.8%	B 15.8%
NAO	A 3.2%	A 3.0%	B 10.8%
PNA	A,B 3.2%	A 2.1%	B 5.6%
AO	1.4%	0.2%	1.7%

	North	South
AMO	74.3%	71.0%
PDO	A 67.8%	B 82.9%
ENSO	8.8%	8.9%
NAO	4.5%	5.6%
PNA	A 4.8%	B 2.7%
AO	A 2.2%	B 0.4%

Table 22. Regional averages of percent variance for groundwater reconstructed components (RCs). The west region includes the CC, PN, and RG aquifers; the central region includes the GLW, CL, and ME aquifers; and the east region includes the SR and GLE aquifers. The north region includes the PN, GLW, and GLE aquifers; and the south region includes the CC, RG, CL, ME, and SR aquifers. Letters A and B indicate statistically significant differences between means based on the Tukey-Kramer Honestly Significant Difference test.

Degree of Damping (DOD) at Each Aquifer

Aquifer	Slope of Groundwater Trend Line	Slope of Precipitation Trend Line	DOD (difference in slopes)
GLW	0.014	0.011	0.003
GLE	0.028	0.016	0.012
PN	0.031	0.017	0.015
CC	0.031	0.016	0.016
ME	0.037	0.015	0.023
SR	0.037	0.012	0.025
CL	0.040	0.012	0.028
RG	0.043	0.013	0.030

Table 23. The DOD is the difference in the slopes of the trend lines for groundwater and precipitation composite RCs at each aquifer in Figures 10–17. In this table, the aquifers are listed from smallest to greatest DOD.

Climate Index-Precipitation Lag Correlation Results

	Lag Correlation Coefficients			Lag Times (years)		
	Minimum	Maximum	Average	Minimum	Maximum	Average
AMO	0.19	0.81	0.59	0.1	5.0	3.5
PDO	0.16	0.86	0.40	0.1	5.0	2.4
ENSO	0.15	0.58	0.34	0.1	5.0	1.3
NAO	0.15	0.56	0.28	0.1	5.0	2.1
PNA	0.15	0.46	0.24	0.3	4.8	1.9
AO	0.16	0.24	0.18	2.5	5.0	4.5

Table 24. Ranges and averages of maximum correlation coefficients (absolute value) and lag times in each climate variability periodicity for correlations between composite RCs of climate indices and precipitation.

Climate Index-Precipitation Maximum Lag Correlation Coefficients Averaged by Aquifer

	CC		PN		RG		GLW	
AMO		0.59		0.53		0.67		0.44
PDO	A	0.25	A	0.33	A	0.47	A	0.52
ENSO	A	0.47	B,C	0.31	A,B,C	0.33	A,B,C	0.31
NAO		0.28		0.34		0.19		0.17
PNA		0.24		0.20		0.18		0.19
AO		0.17		0.20		0.18		0.17

	CL		ME		SR		GLE	
AMO		0.64		0.45		0.78		0.45
PDO	B	0.26	A	0.59	A	0.46	A	0.45
ENSO	A,B,C	0.34	C	0.24	A,B	0.42	B,C	0.27
NAO		0.28		0.34		0.27		0.22
PNA		0.29		0.26		0.24		0.26
AO		0.17		0.17		0.19		0.17

Table 25. Aquifer averages of maximum lag correlation coefficients (absolute value) for index-precipitation lag correlations. Aquifers are ordered from west to east across the U.S. Letters A, B, and C indicate statistically significant differences between means based on the Tukey-Kramer Honestly Significant Difference test.

Climate Index-Precipitation Maximum Lag Correlation Coefficients Averaged by Region

	West	Central	East
AMO	0.62	0.58	0.58
PDO	A,B 0.32	A 0.12	B 0.45
ENSO	A 0.39	B 0.30	A,B 0.35
NAO	0.29	0.29	0.25
PNA	0.21	0.27	0.25
AO	0.18	0.17	0.18

	North	South
AMO	0.46	0.65
PDO	0.43	0.24
ENSO	A 0.29	B 0.37
NAO	0.26	0.29
PNA	0.22	0.25
AO	0.18	0.18

Table 26. Regional averages of maximum lag correlation coefficients (absolute value) for index-precipitation lag correlations. Letters A and B indicate statistically significant differences between means based on the Tukey-Kramer Honestly Significant Difference test.

Climate Index-Precipitation Correlation Lag Times (Years) Averaged by Aquifer

	CC		PN		RG		GLW	
AMO		5.0		5.0		1.6		5.0
PDO	A	0.3	A,B	0.3	A,B	2.7	A,B	0.5
ENSO	B,C	0.8	A,B,C	1.1	B,C	0.1	A,B	3.1
NAO	A	3.2	A,B	2.4	A	3.8	A,B	2.3
PNA	A	3.9	B	0.8	B	0.5	A,B	1.7
AO		4.5		4.4		4.1		5.0

	CL		ME		SR		GLE	
AMO		4.6		5.0		0.3		3.4
PDO	A,B	2.4	A,B	3.3	A,B	2.2	B	4.4
ENSO	C	0.5	A,B,C	1.6	C	0.3	A	3.5
NAO	A,B	1.8	B	1.0	A	3.3	A,B	1.2
PNA	B	1.9	A,B	2.2	B	1.0	A,B	2.2
AO		3.6		4.0		5.0		4.0

Table 27. Lag times (years) of climate index-precipitation lag correlations averaged by aquifer for each climate variability mode. Aquifers are ordered from west to east. Letters A, B, and C indicate statistically significant differences between means based on the Tukey-Kramer honestly significant difference test.

Precipitation-Groundwater Lag Correlation Results

	Lag Correlation Coefficients			Lag Times (years)		
	Minimum	**Maximum**	**Average**	**Minimum**	**Maximum**	**Average**
AMO	0.56	0.56	0.56	4.1	4.1	4.1
PDO	0.17	0.89	0.54	0.1	5.0	1.7
ENSO	0.16	0.83	0.50	0.1	5.0	1.0
NAO	0.16	0.88	0.51	0.1	4.0	1.0
PNA	0.15	0.81	0.42	0.1	4.9	1.4
AO	0.30	0.96	0.78	0.2	5.0	2.8

Table 28. Ranges and averages of maximum correlation coefficients (absolute value) and lag times in each climate variability periodicity for correlations between composite RCs of precipitation and groundwater.

Changes in R^2 Values with Aquifer Ordering for Precipitation-Groundwater Lag Correlations

a) Maximum Correlation Coefficient Plots

	West to East	DOD
AMO	--	--
PDO	0.13	0.003
ENSO	0.25	0.52
NAO	0.15	0.50
PNA	0.07	0.27
AO	0.03	0.02

b) Correlation Lag Time Plots

	West to East	DOD
AMO	--	--
PDO	0.16	0.26
ENSO	0.01	0.47
NAO	0.007	0.51
PNA	0.3	0.58
AO	0.18	0.003

Table 29. Comparison of R^2 values of trend lines in precipitation-groundwater correlation plots when aquifers were listed on the x-axis in a a) west to east order or by b) smallest to greatest degree of damping (DOD).

Climate Index-Groundwater Lag Correlation Results

	Lag Correlation Coefficients			Lag Times (years)		
	Minimum	Maximum	Average	Minimum	Maximum	Average
AMO	0.22	0.67	0.42	0.1	5.0	2.5
PDO	0.16	0.92	0.52	0.1	5.0	3.6
ENSO	0.15	0.60	0.32	0.2	5.0	2.1
NAO	0.16	0.63	0.34	0.1	5.0	2.5
PNA	0.16	0.52	0.29	0.1	5.0	2.6
AO	0.15	0.41	0.22	0.1	5.0	3.3

Table 30. Ranges and averages of maximum correlation coefficients (absolute value) and lag times (years) in each climate variability periodicity for correlations between composite RCs of climate indices and groundwater.

Changes in R^2 Values with Aquifer Ordering for Climate Index-Groundwater Lag Correlations

a) Maximum Correlation Coefficient Plots

	West to East	DOD
AMO	0.56	0.56
PDO	0.20	0.003
ENSO	0.13	0.13
NAO	0.007	0.41
PNA	0.12	0.10
AO	0.39	0.02

b) Correlation Lag Time Plots

	West to East	DOD
AMO	0.89	0.89
PDO	0.26	0.16
ENSO	0.02	0.13
NAO	0.001	0.54
PNA	0.004	0.23
AO	0.09	0.009

Table 31. Comparison of R^2 values of trend lines in climate index-groundwater correlation plots when aquifers were listed on the x-axis in a a) west to east order or by b) smallest to greatest degree of damping (DOD).

Average Percent Variance Results from Previous Studies

a) Findings from Gurdak (2007)

	Precipitation RCs	Groundwater RCs
AMO	55%	--
PDO	28%	45%
ENSO	1.1%	3.4%
Annual	1.3%	0.9%

b) Findings from Kuss (2011)

	Precipitation RCs	Groundwater RCs
AMO	66%	47%
PDO	53%	39%
ENSO	13%	24%
NAO	27%	--

Table 32. Average percent variance from precipitation and groundwater reconstructed components (RCs) for each climate variability mode from a) Gurdak (2007) and b) Kuss (2011).

Average Lag Correlation Coefficients from Previous Studies

a) Findings from Gurdak (2007)

	I-PR	PR-GW	I-GW
AMO	0.57	--	--
PDO	0.56	0.73	0.73
ENSO	0.29	0.28	0.38
Annual	--	0.14	--

b) Findings from Kuss (2011)

	I-PR	PR-GW	I-GW
AMO	0.33	0.76	0.54
PDO	0.41	0.59	0.33
ENSO	0.36	0.47	0.34
NAO	0.21	0.3	0.14

Table 33. Average maximum lag correlation coefficients from correlations of climate indices-precipitation, precipitation-groundwater, and climate indices-groundwater for each climate variability mode from a) Gurdak (2007) and b) Kuss (2011).

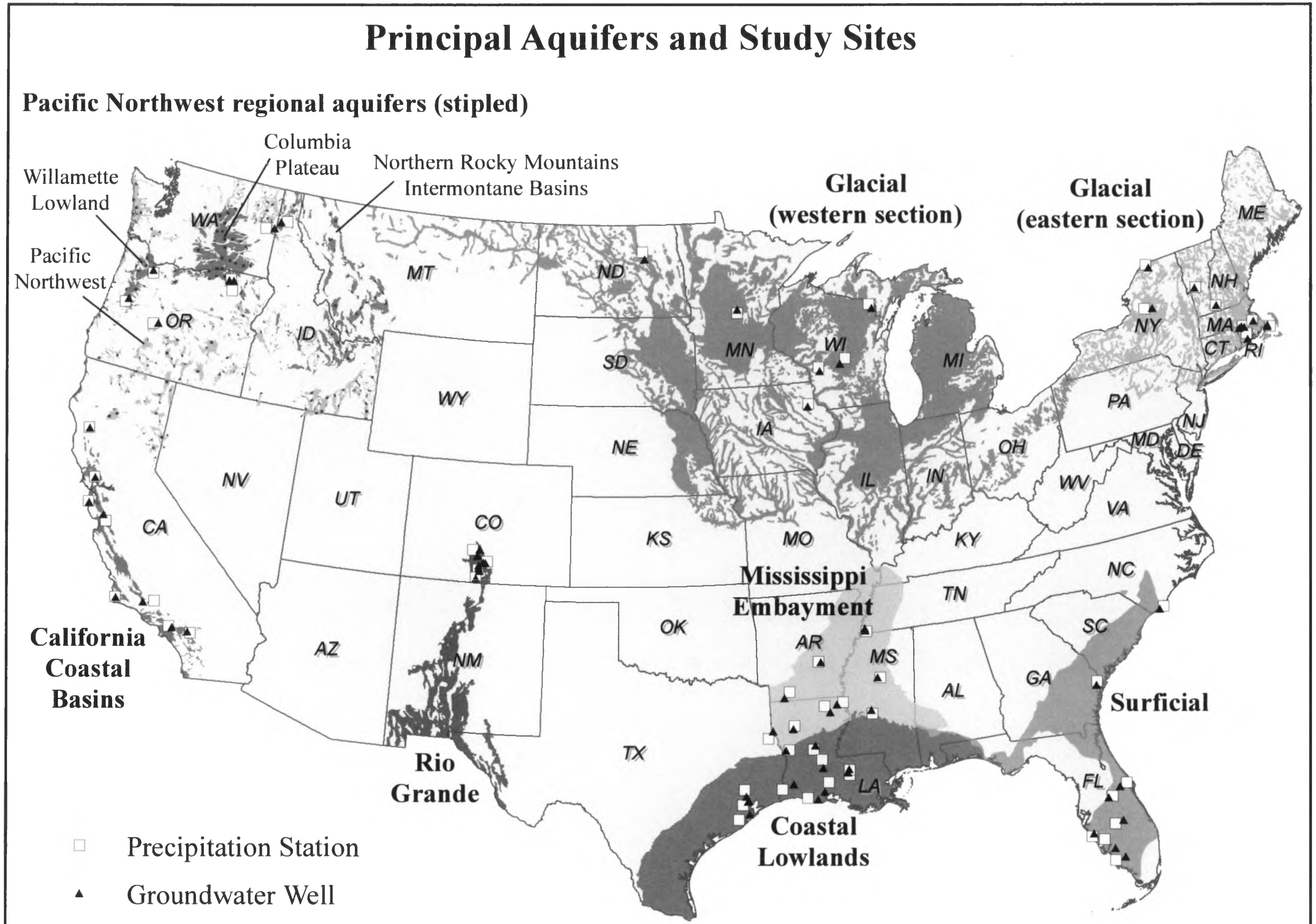

Figure 1. Locations of unconsolidated to semi-consolidated sand and gravel principal aquifers in the United States used in this study. Within the bounds of each aquifer are co-located precipitation and groundwater sites.

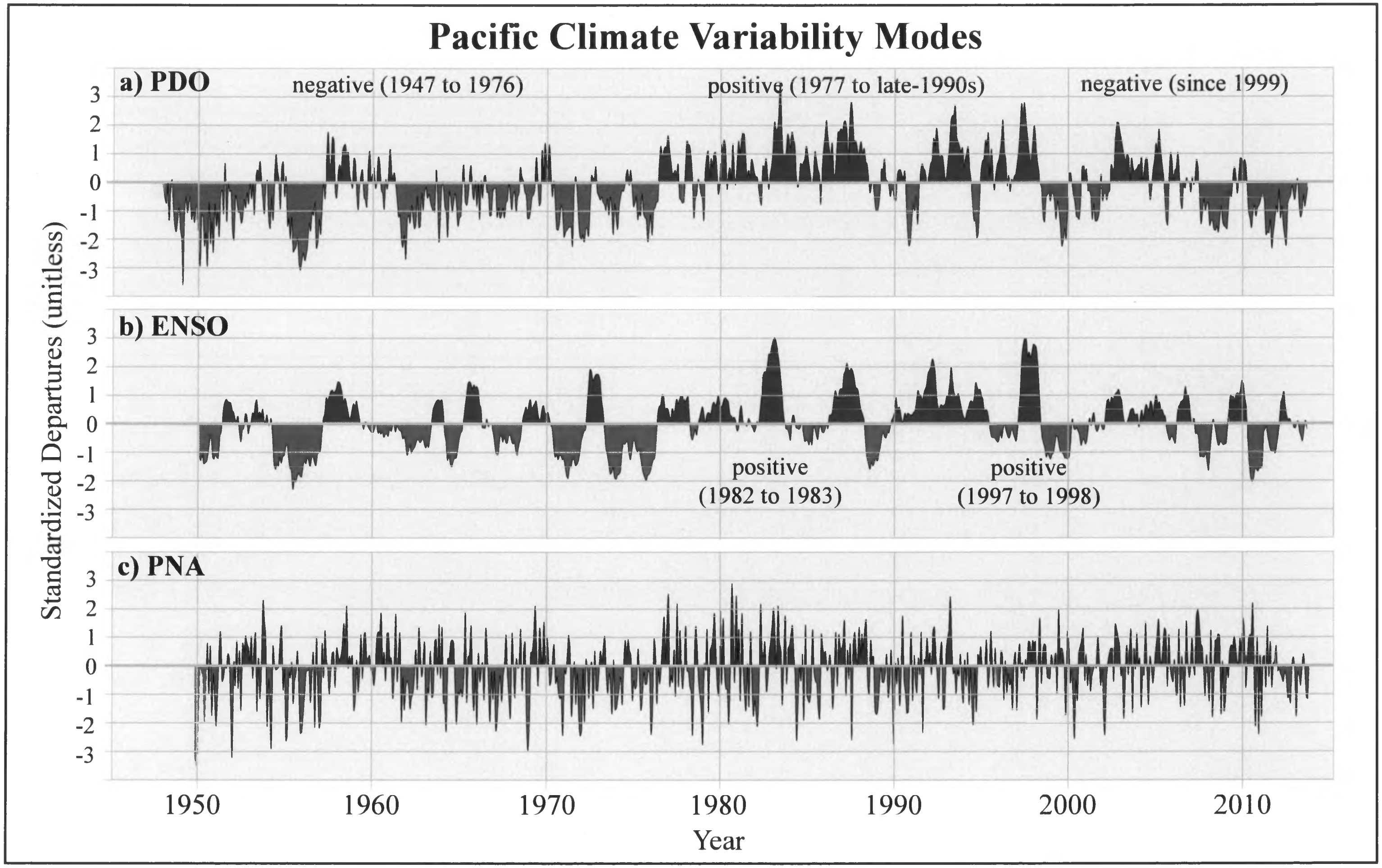

Figure 2. Time series of indices for climate variability modes in the Pacific region. The a) Pacific Decadal Oscillation has a 15 to 30 year cycle, the b) El Niño-Southern Oscillation has a 2 to 7 year cycle, and the c) Pacific/North American Oscillation has a <1 to 4 year cycle. Red signifies a positive phase of the climate variability mode and blue signifies a negative phase. Yellow shaded areas are notable periods of strong and/or persistent phases that were identified in previous literature.

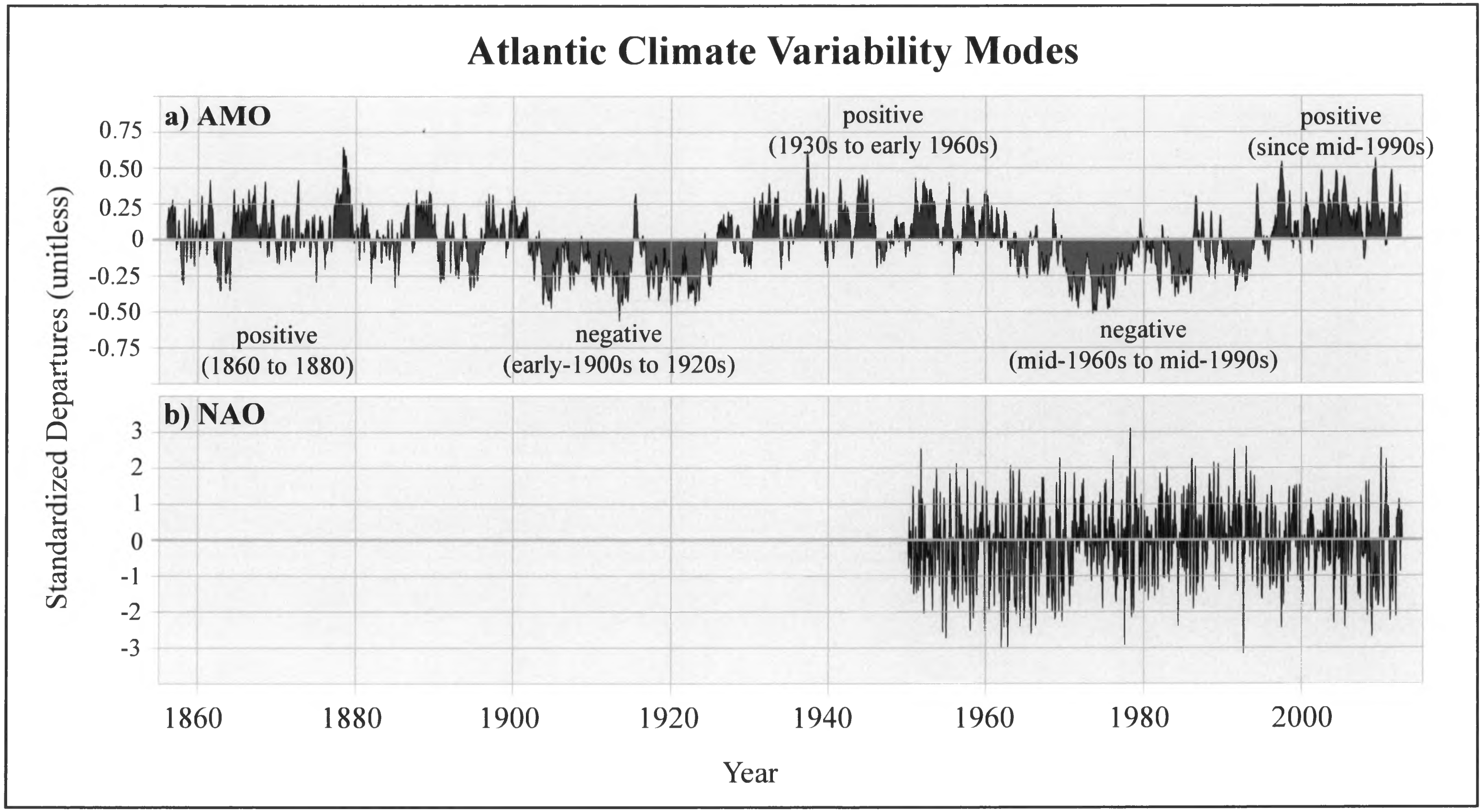

Figure 3. Time series of indices for climate variability modes in the Atlantic region. The a) Atlantic Multidecadal Oscillation has a 50 to 80 year cycle and the b) North Atlantic Oscillation has a 3 to 6 year cycle. Red signifies a positive phase of the climate variability mode and blue signifies a negative phase. Yellow shaded areas are notable periods of strong and/or persistent phases that were identified in previous literature.

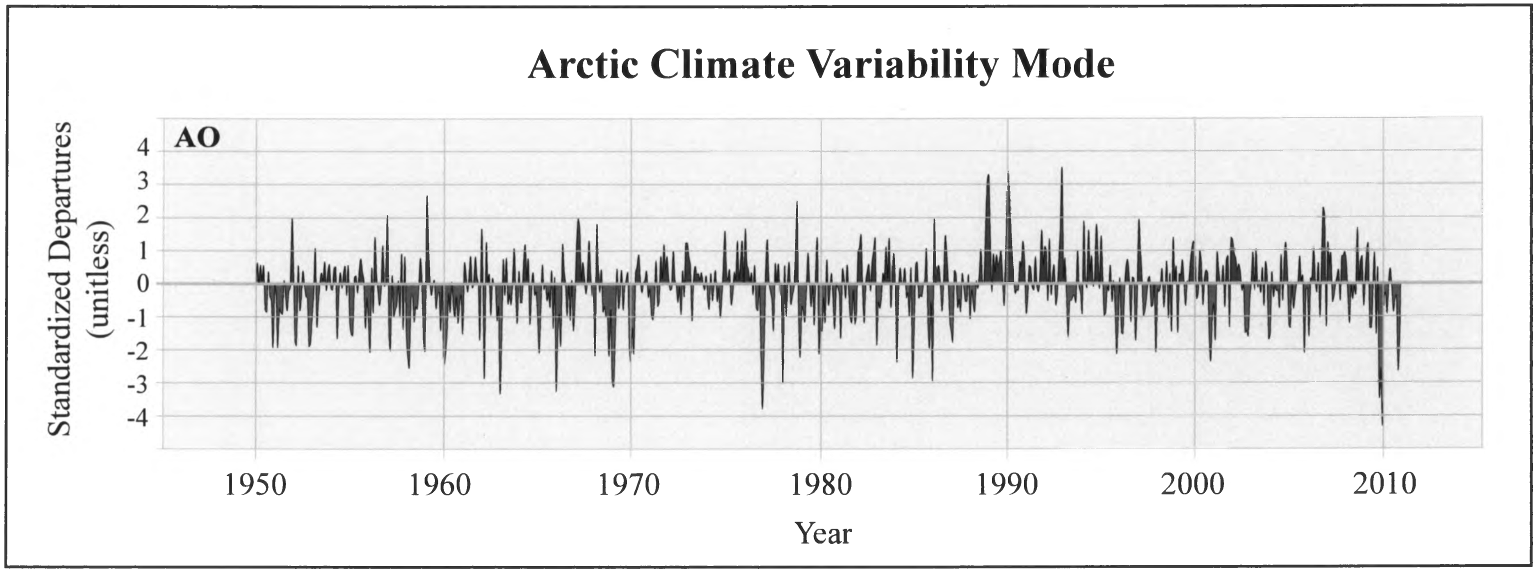

Figure 4. Time series of the Arctic Oscillation index. The AO has a 6 to 12 month cycle. Red signifies a positive phase of the climate variability mode and blue signifies a negative phase.

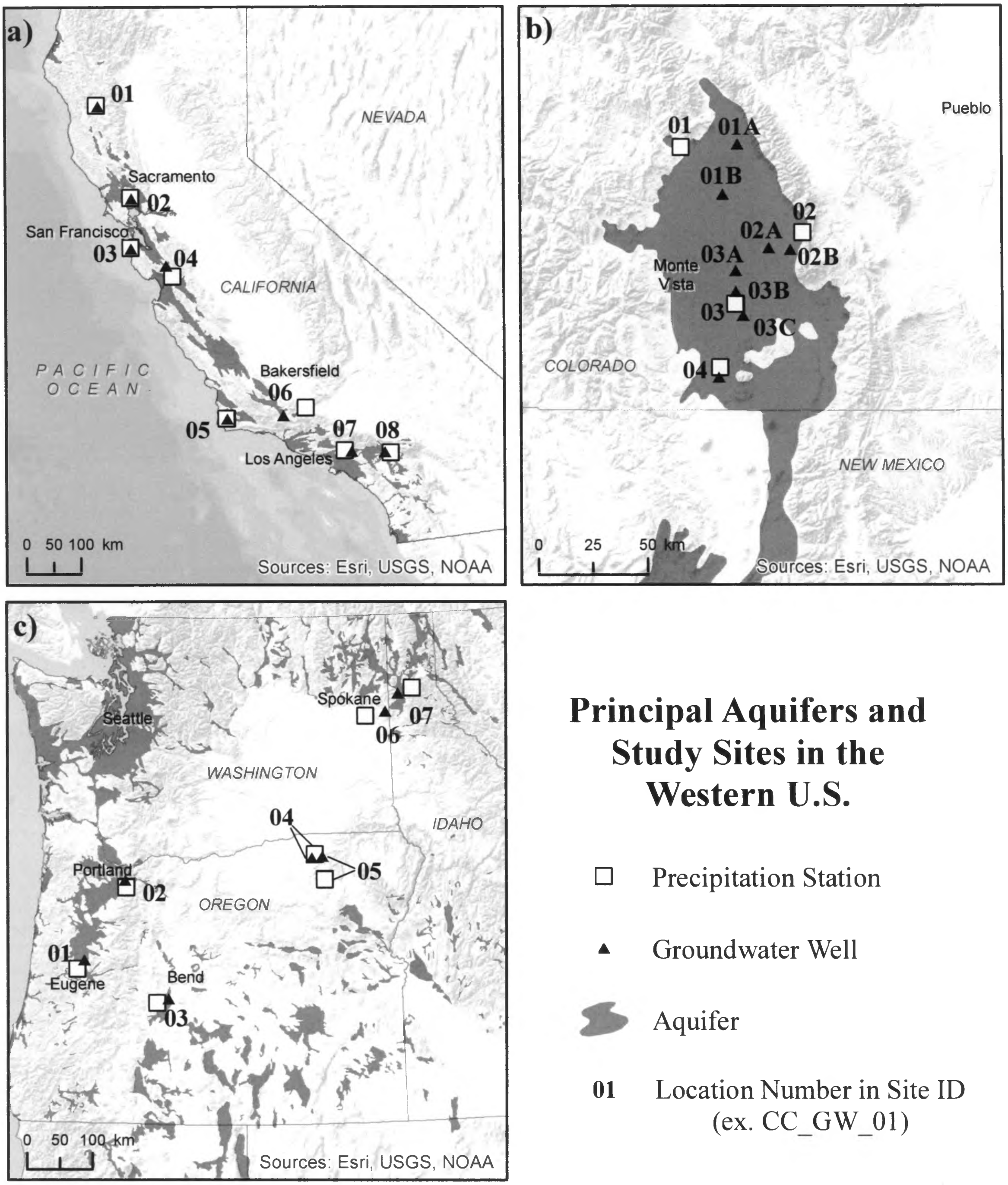

Figure 5. Locations of co-located precipitation and groundwater sites in the a) California Coastal Basins, b) Rio Grande, and c) Pacific Northwest regional aquifers. For this thesis, these aquifers are considered as part of the western region of the U.S.

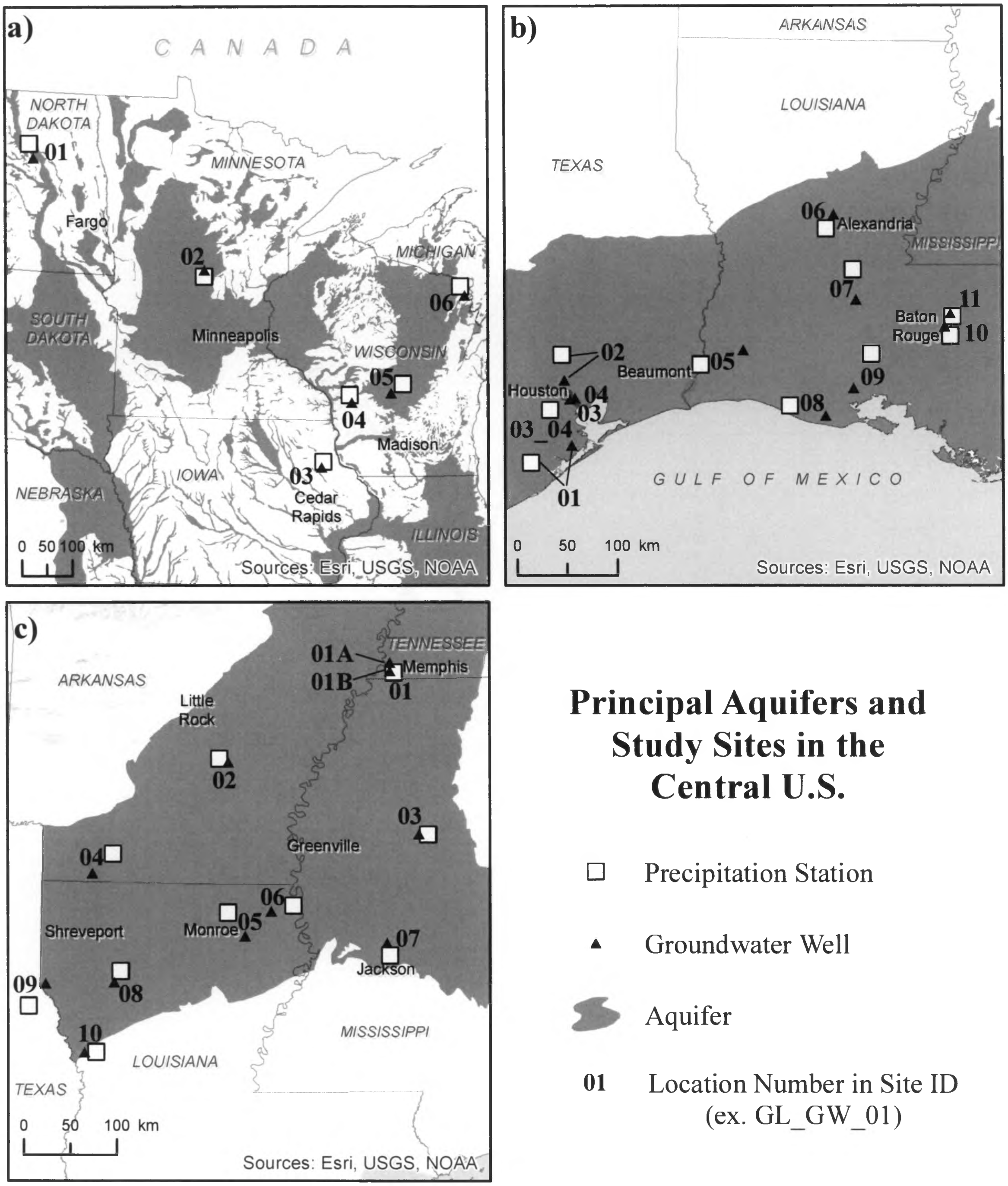

Figure 6. Locations of co-located precipitation and groundwater sites in the a) Glacial (western section), b) Coastal Lowlands, and c) Mississippi Embayment aquifers. For this thesis, these aquifers are considered as part of the central region of the U.S.

Principal Aquifers and Study Sites in the Eastern U.S.

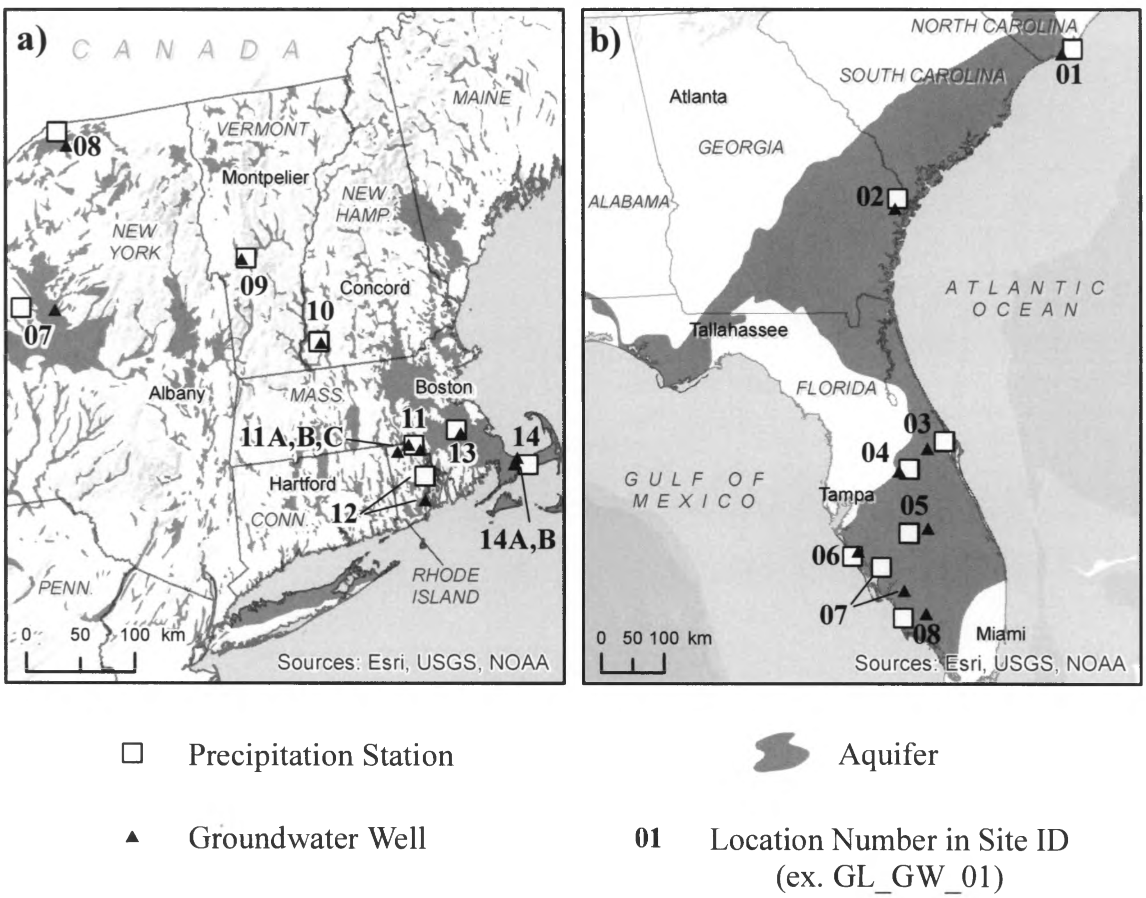

Figure 7. Locations of co-located precipitation and groundwater sites in the a) Glacial (eastern section) and b) Surficial aquifers. For this thesis, these aquifers are considered as part of the eastern region of the U.S.

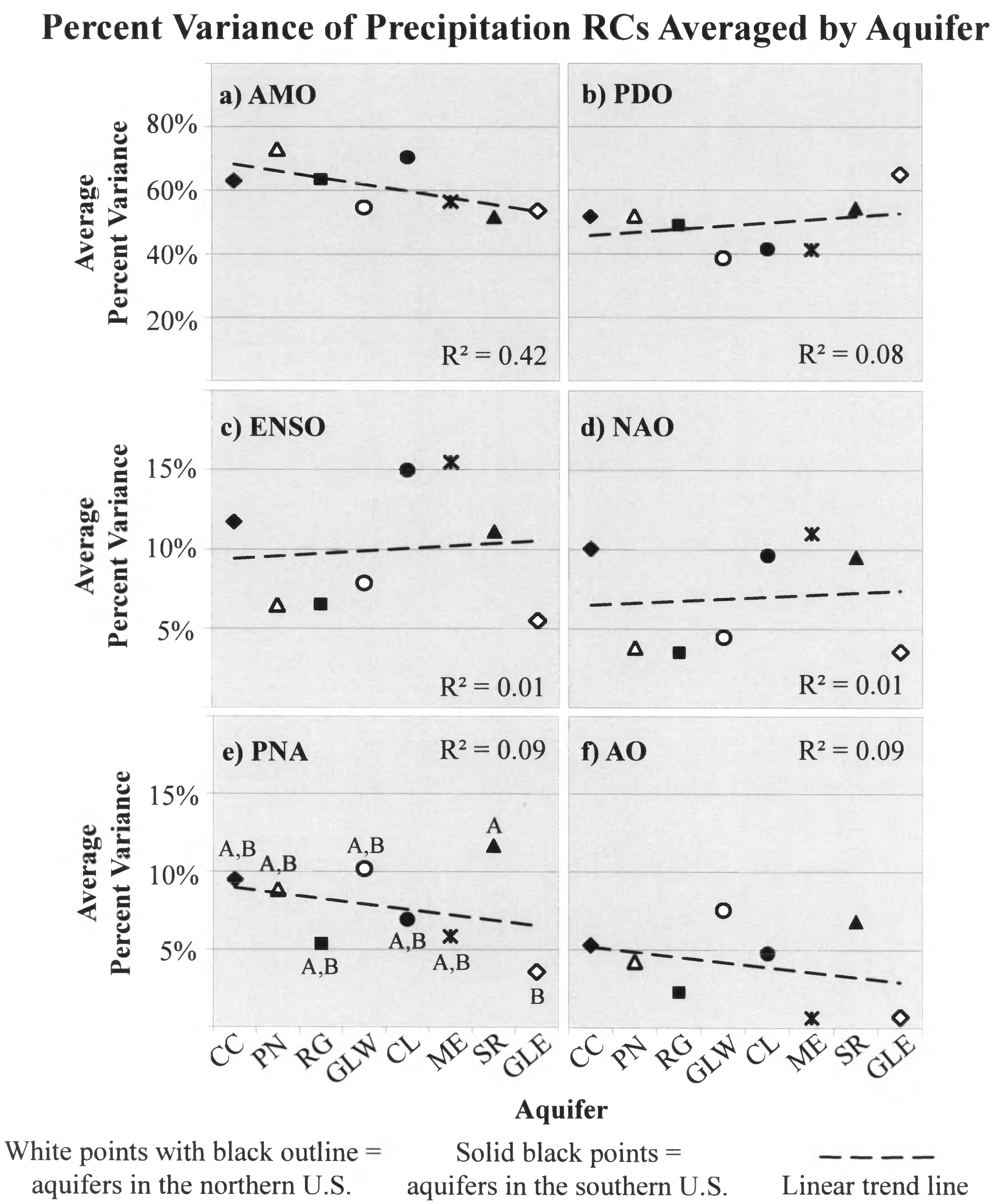

Figure 8. Percent variance of precipitation reconstructed components (RCs) averaged by aquifer for each climate variability mode. Aquifers are ordered from west to east. Letters A and B indicate statistically significant differences between means based on the Tukey-Kramer Honestly Significant Difference test.

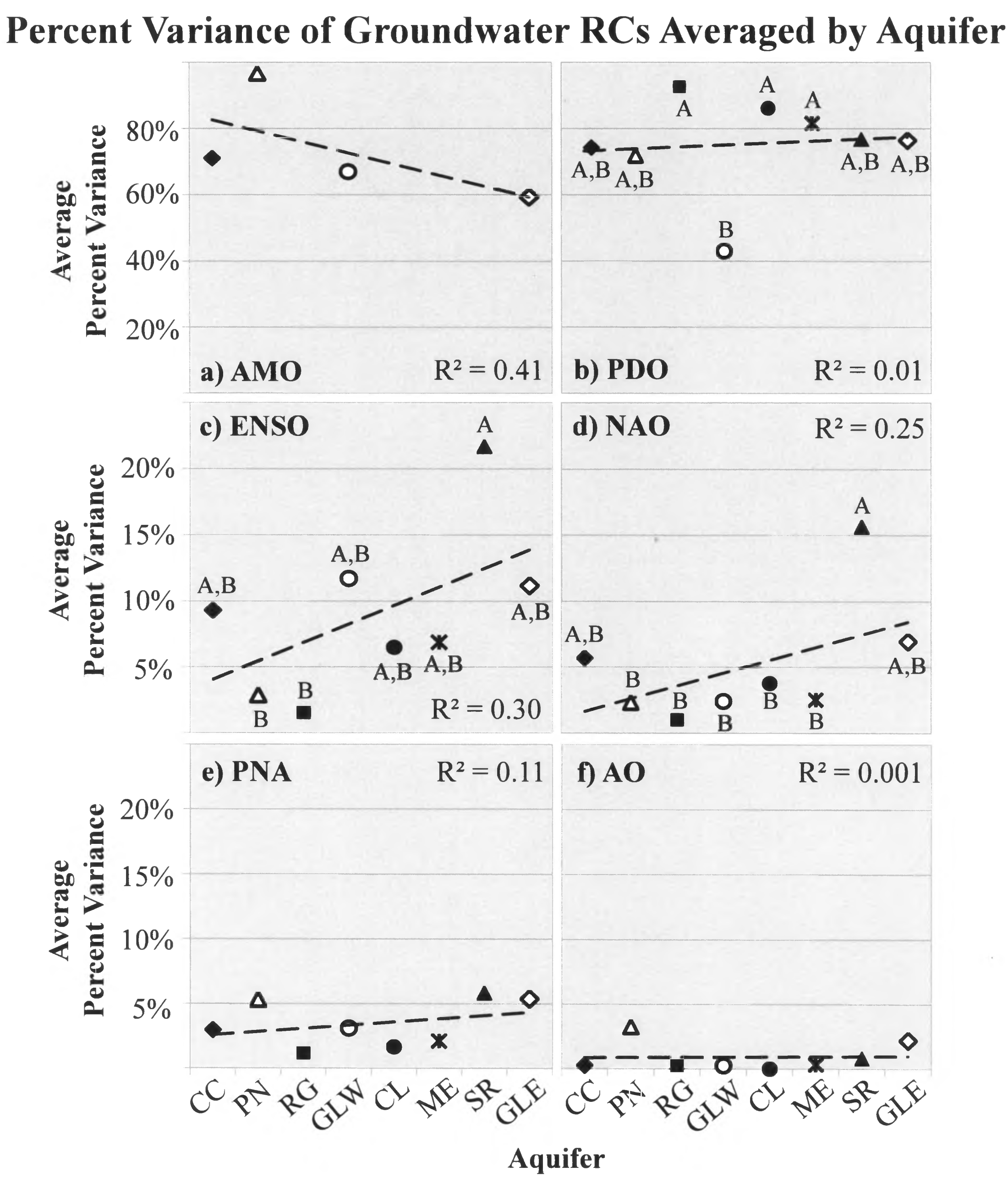

White points with black outline = aquifers in the northern U.S. Solid black points = aquifers in the southern U.S. – – – – Linear trend line

Figure 9. Percent variance of groundwater reconstructed components (RCs) averaged by aquifer for each climate variability mode. Aquifers are ordered from west to east. Letters A and B indicate statistically significant differences between means based on the Tukey-Kramer Honestly Significant Difference test.

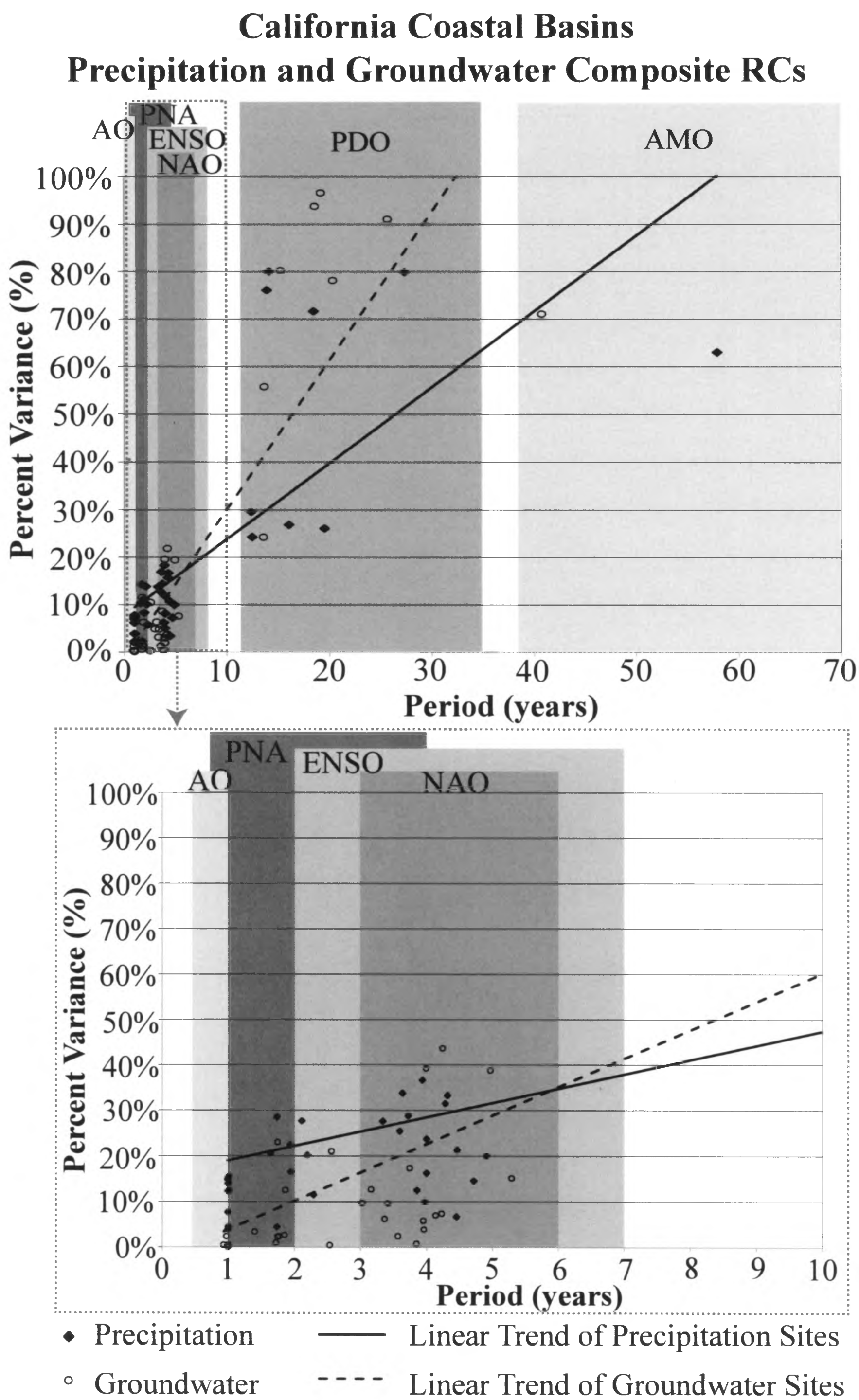

Figure 10. Percent variance and period of all the precipitation and groundwater composite RCs in the California Coastal Basins aquifer.

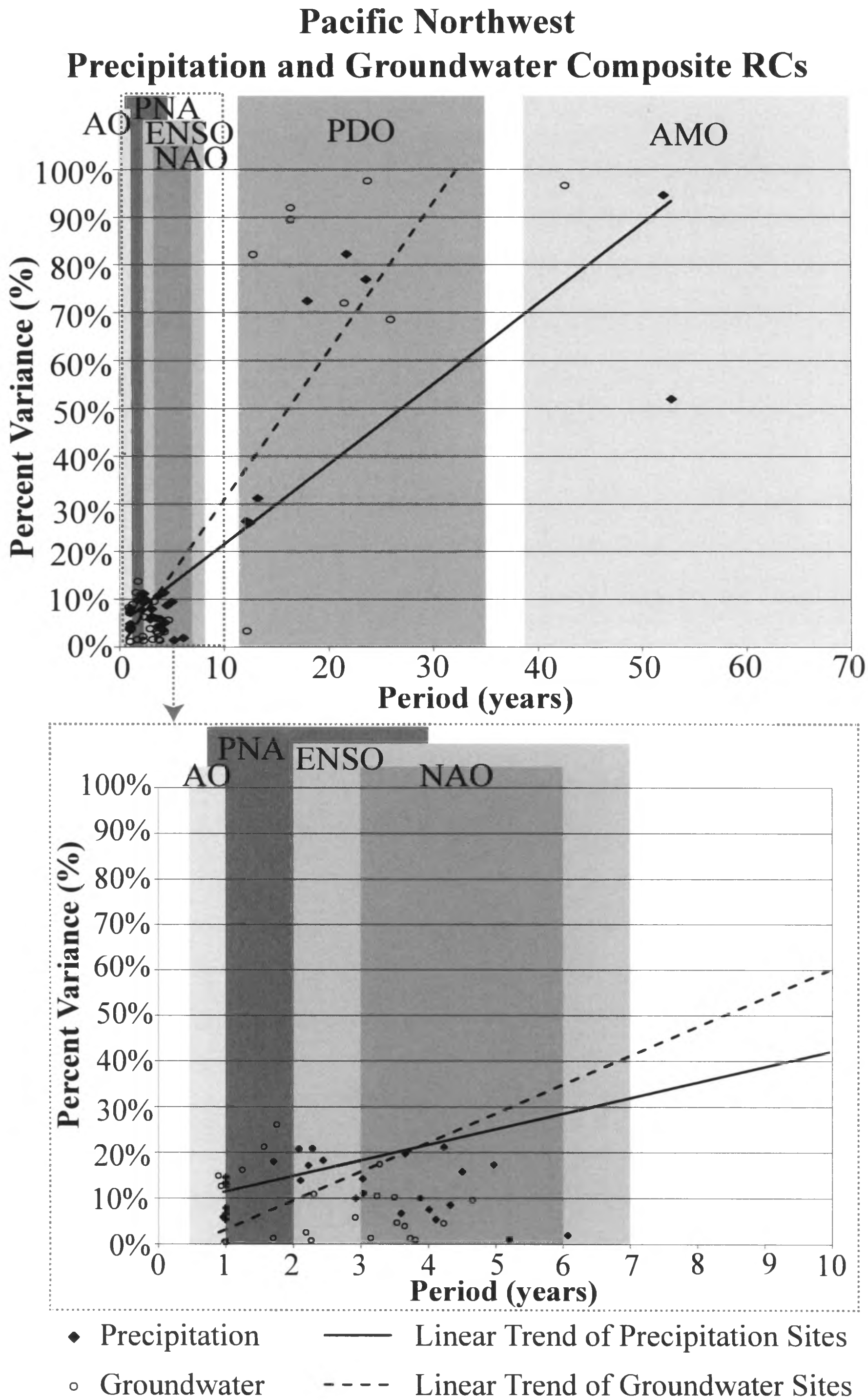

Figure 11. Percent variance and period of all the precipitation and groundwater composite RCs in the Pacific Northwest regional group of aquifers.

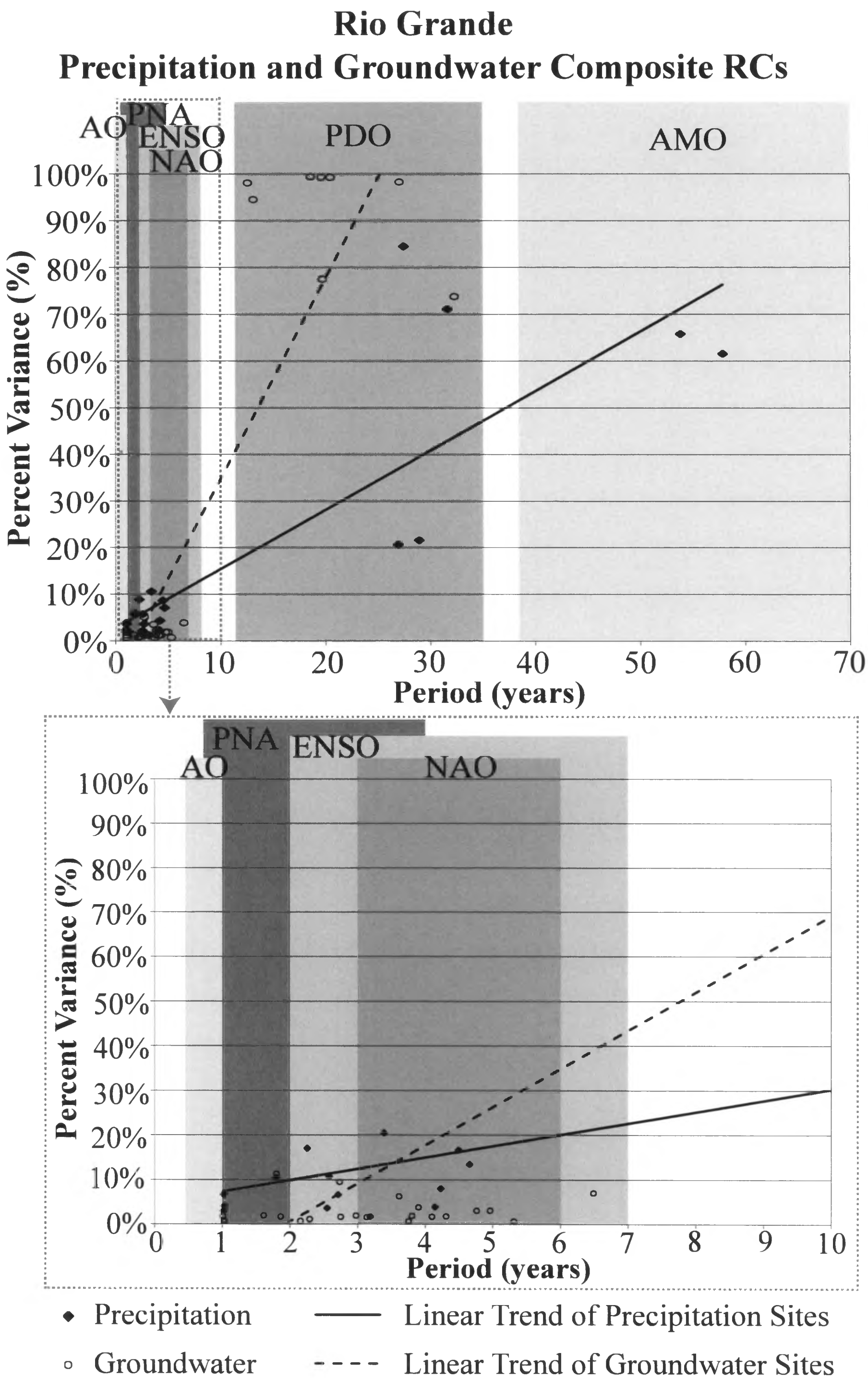

Figure 12. Percent variance and period of all the precipitation and groundwater composite RCs in the Rio Grande aquifer.

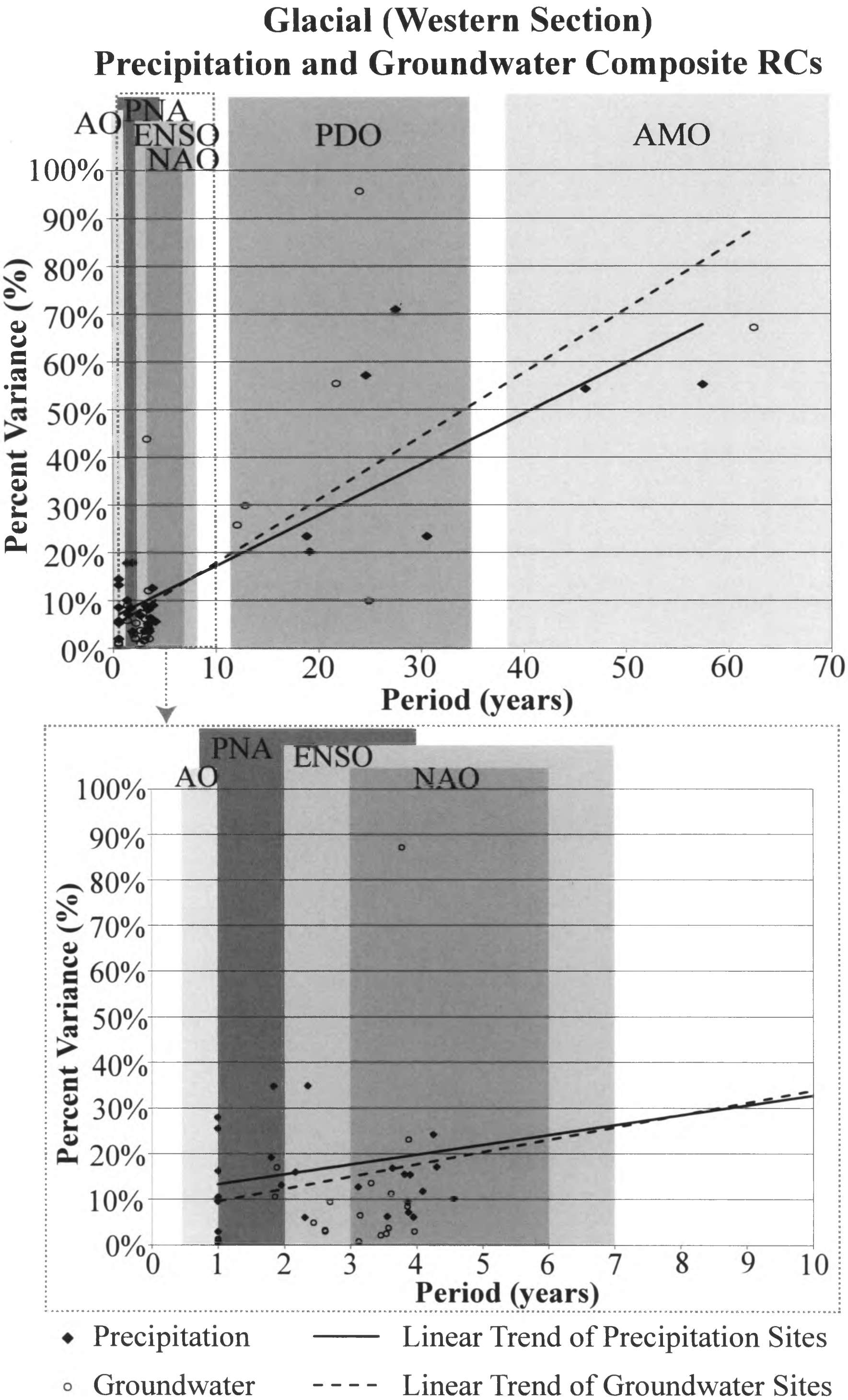

Figure 13. Percent variance and period of all the precipitation and groundwater composite RCs in the western section of the Glacial aquifer.

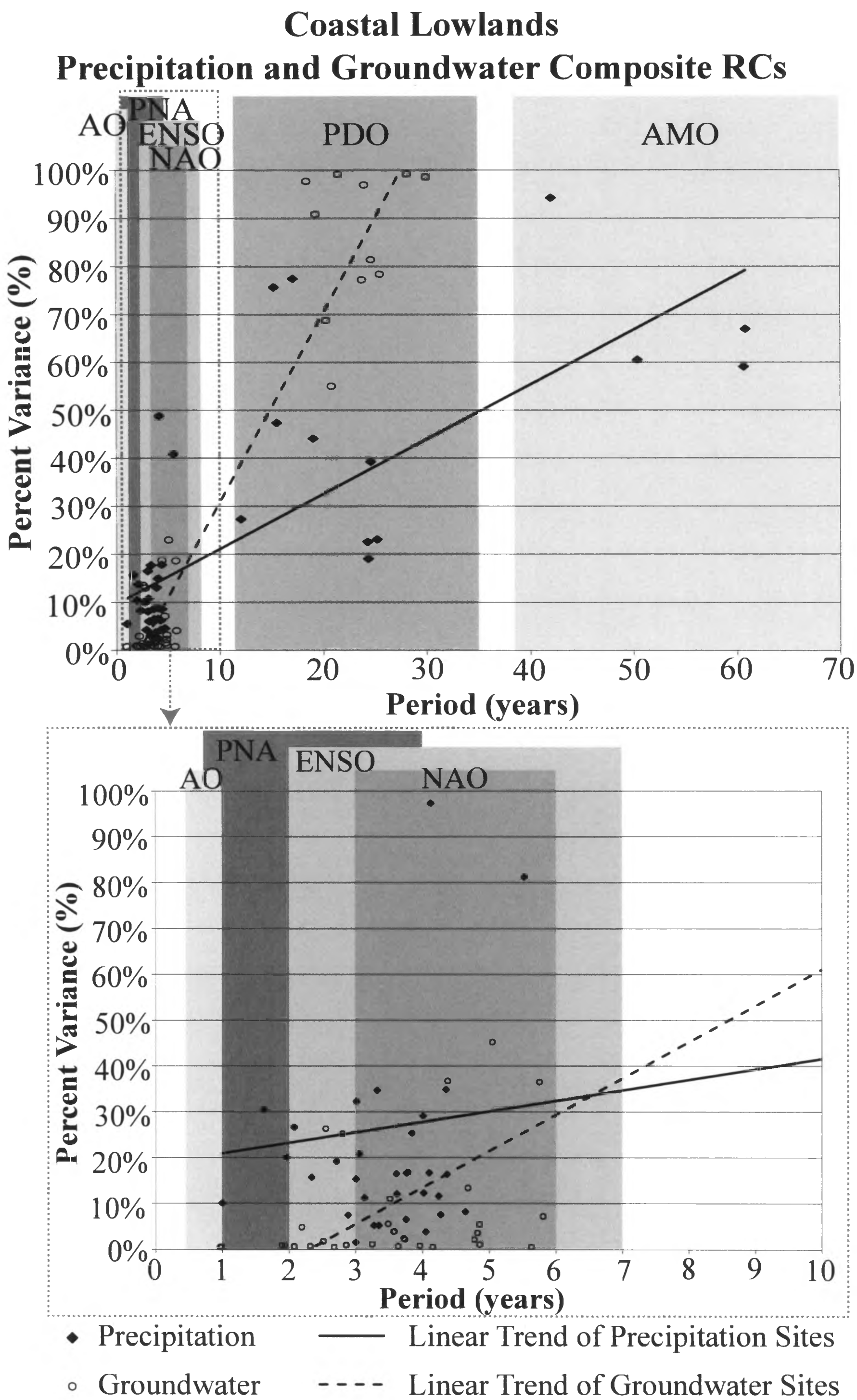

Figure 14. Percent variance and period of all the precipitation and groundwater composite RCs in the Coastal Lowlands aquifer.

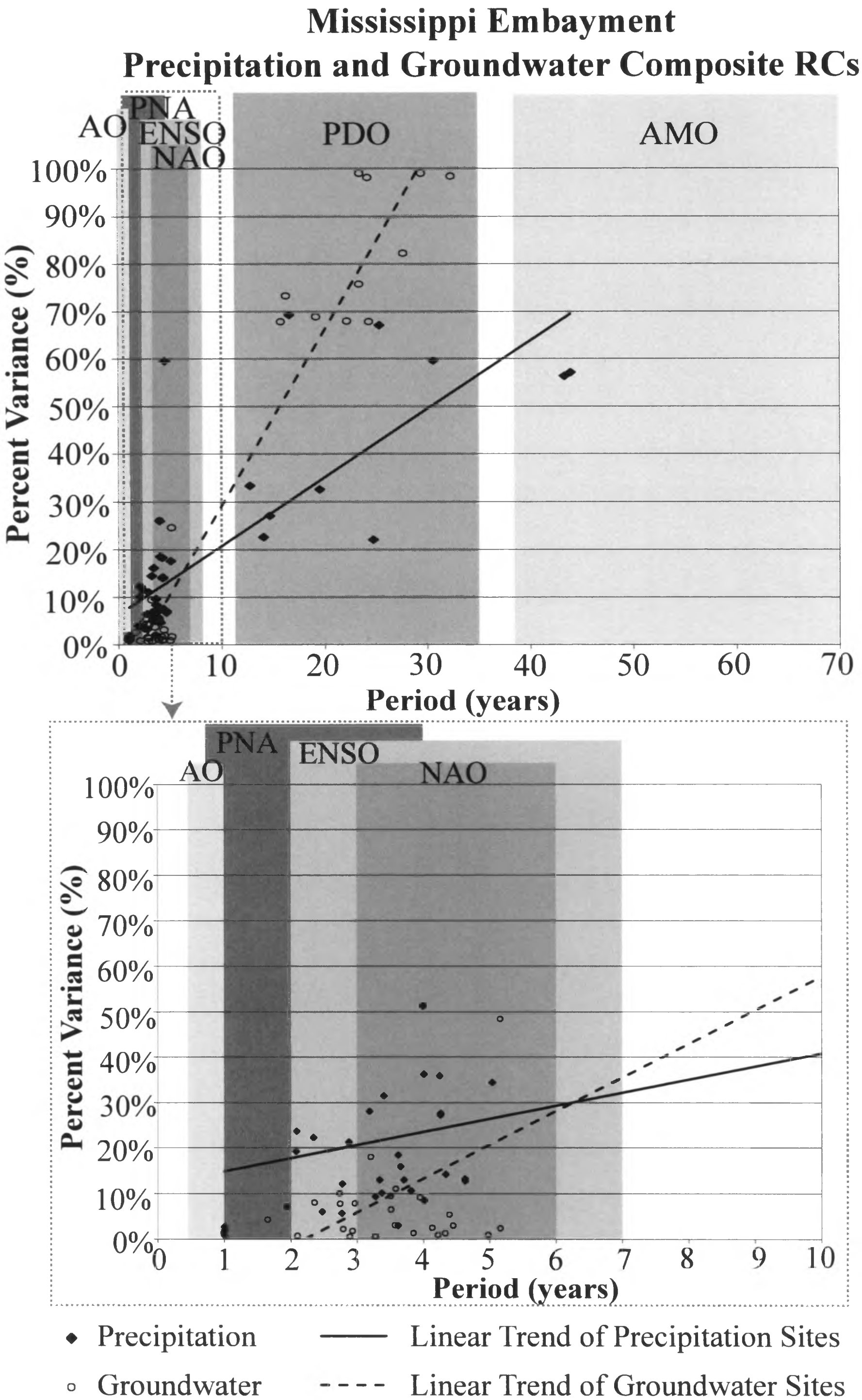

Figure 15. Percent variance and period of all the precipitation and groundwater composite RCs in the Mississippi Embayment aquifer.

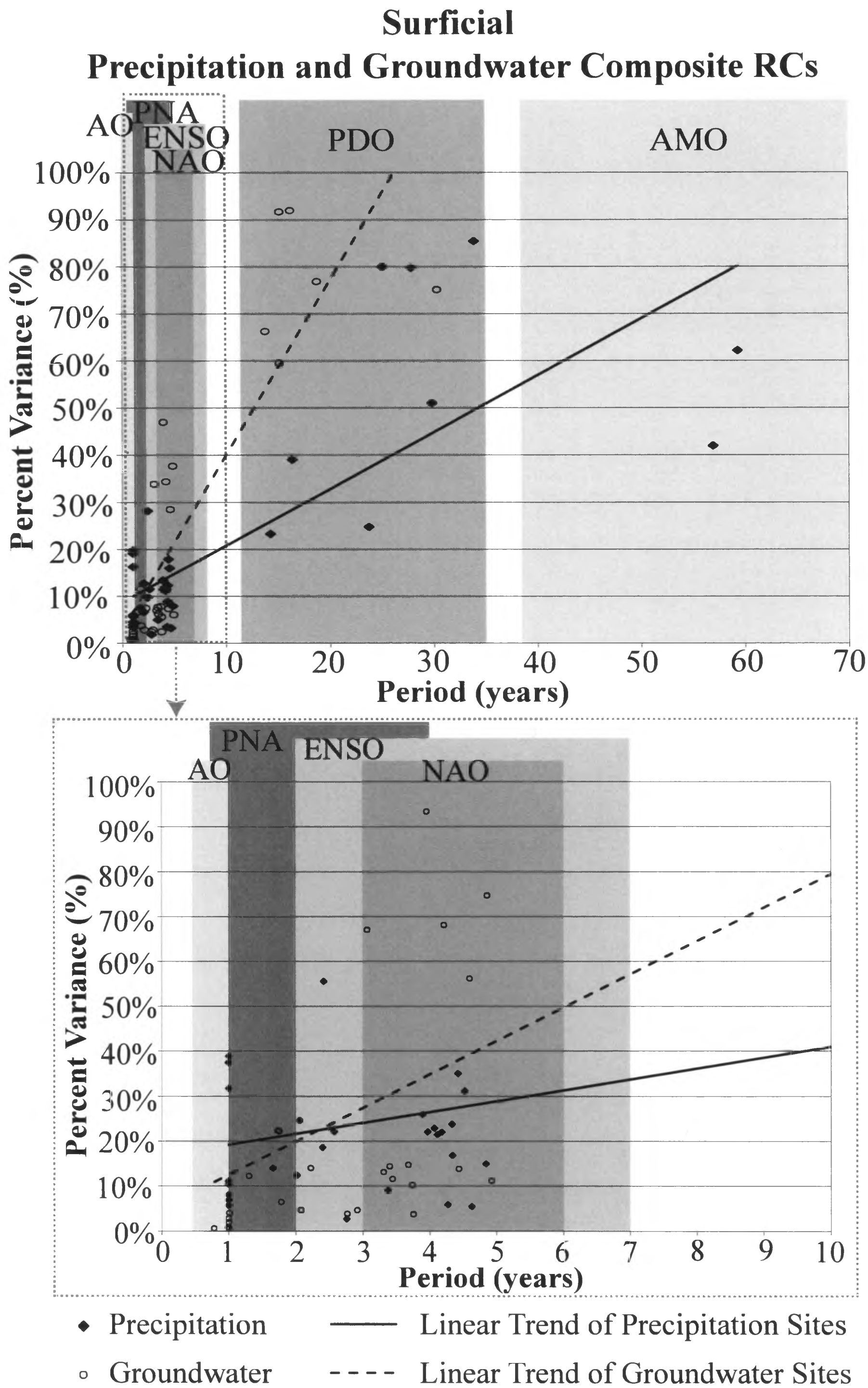

Figure 16. Percent variance and period of all the precipitation and groundwater composite RCs in the Surficial aquifer.

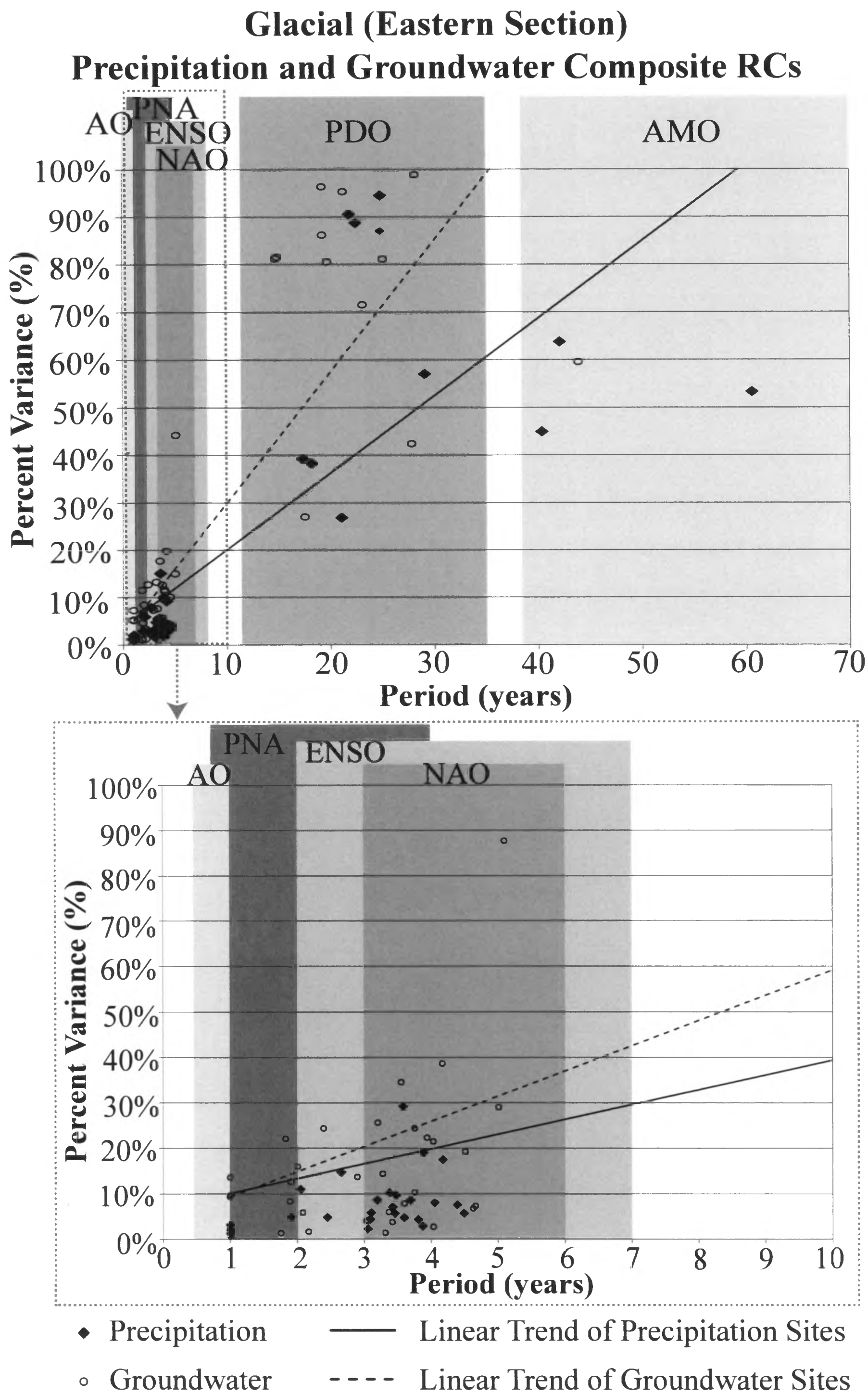

Figure 17. Percent variance and period of all the precipitation and groundater composite RCs in the eastern section of the Glacial aquifer.

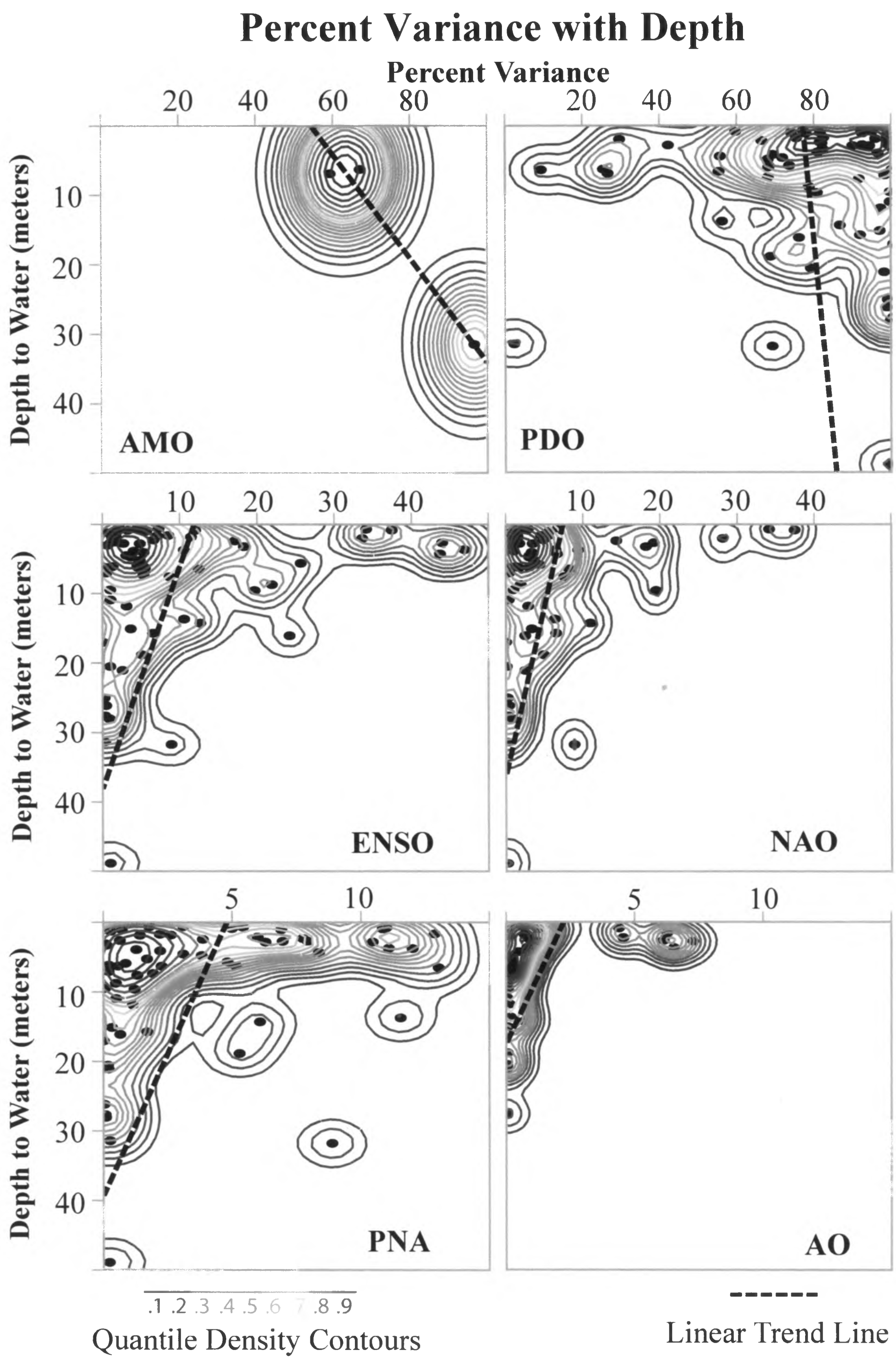

Figure 18. Plots showing how percent variance changes with depth in the vadose zone for each climate variability mode. Quantile density contours indicate what percentage of the points are concentrated in certain areas of the plot.

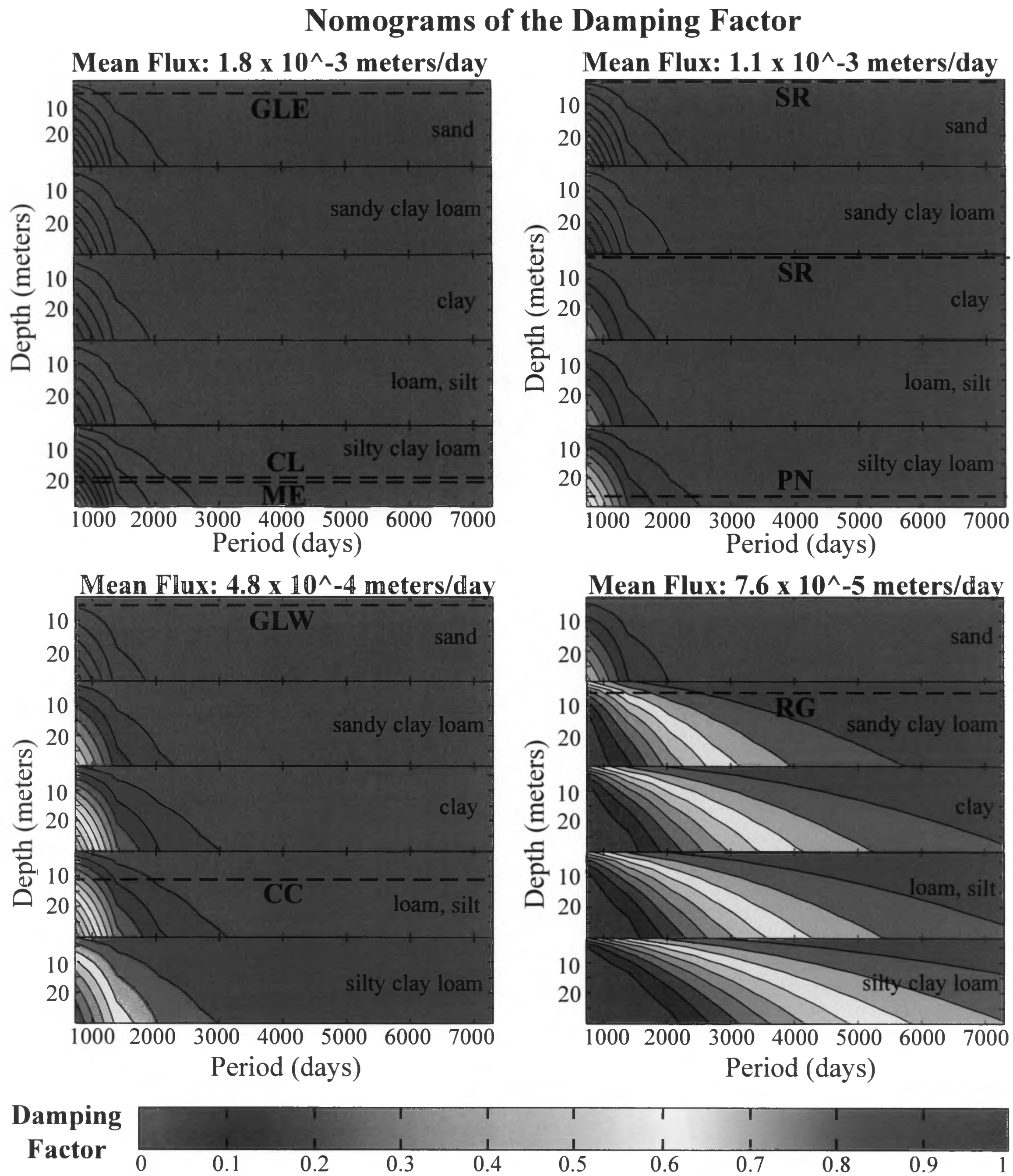

Figure 19. Nomograms showing the damping factors for six selected soil types and four different mean infiltration fluxes. Each aquifer is labeled on the plot that it most closely coincides with and a dashed line is placed at the average depth to water value of the aquifer. Following the dashed line across shows how the damping factor changes with periodicity for that particular aquifer.

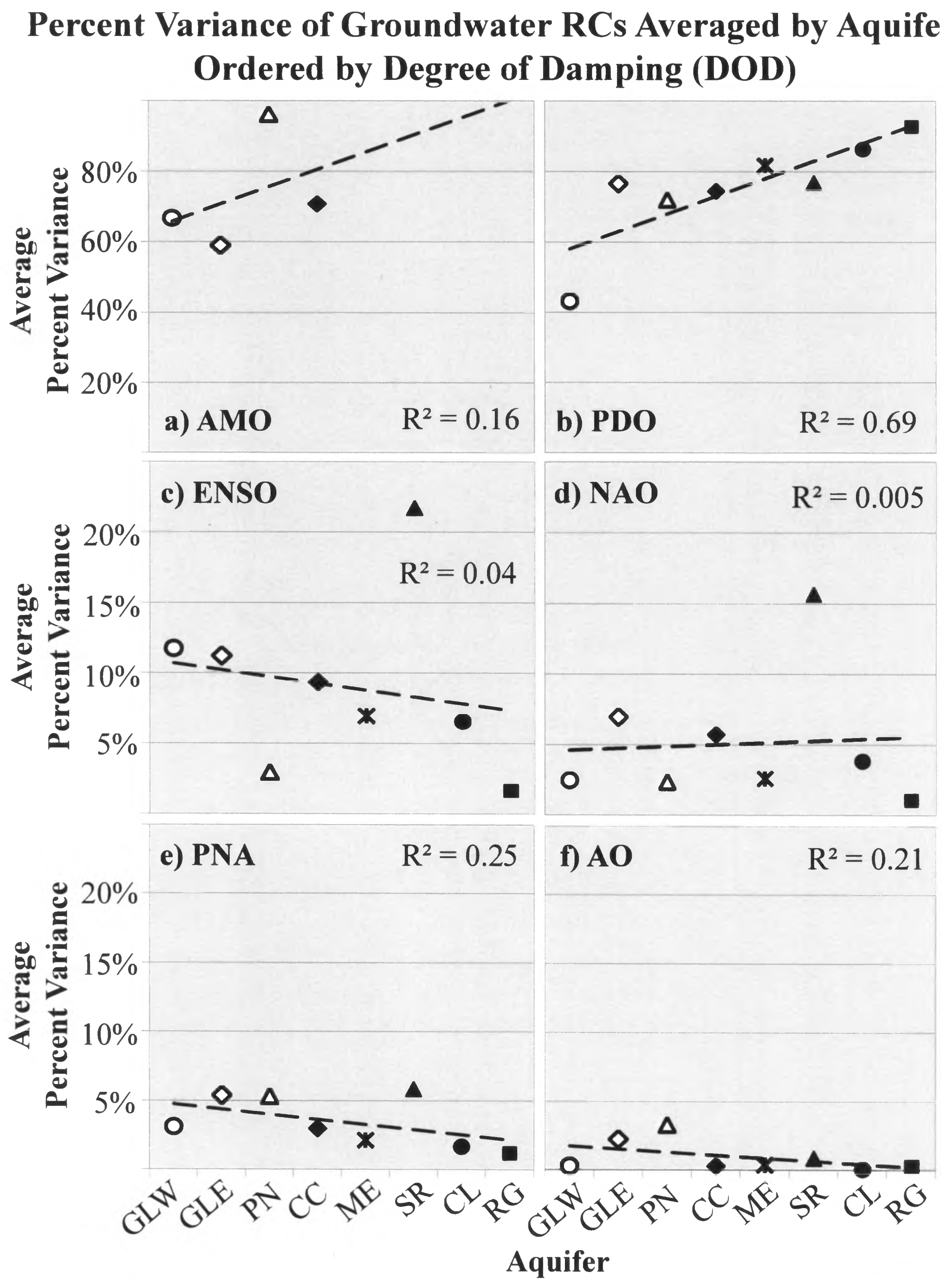

Solid black points = aquifers in southern U.S.

White points with black outline = aquifers in northern U.S.

– – – – Linear trend line

Figure 20. Percent variances of groundwater reconstructed components (RCs) averaged by aquifer for each climate variabilty mode. Aquifers are ordered from smallest to greatest DOD.

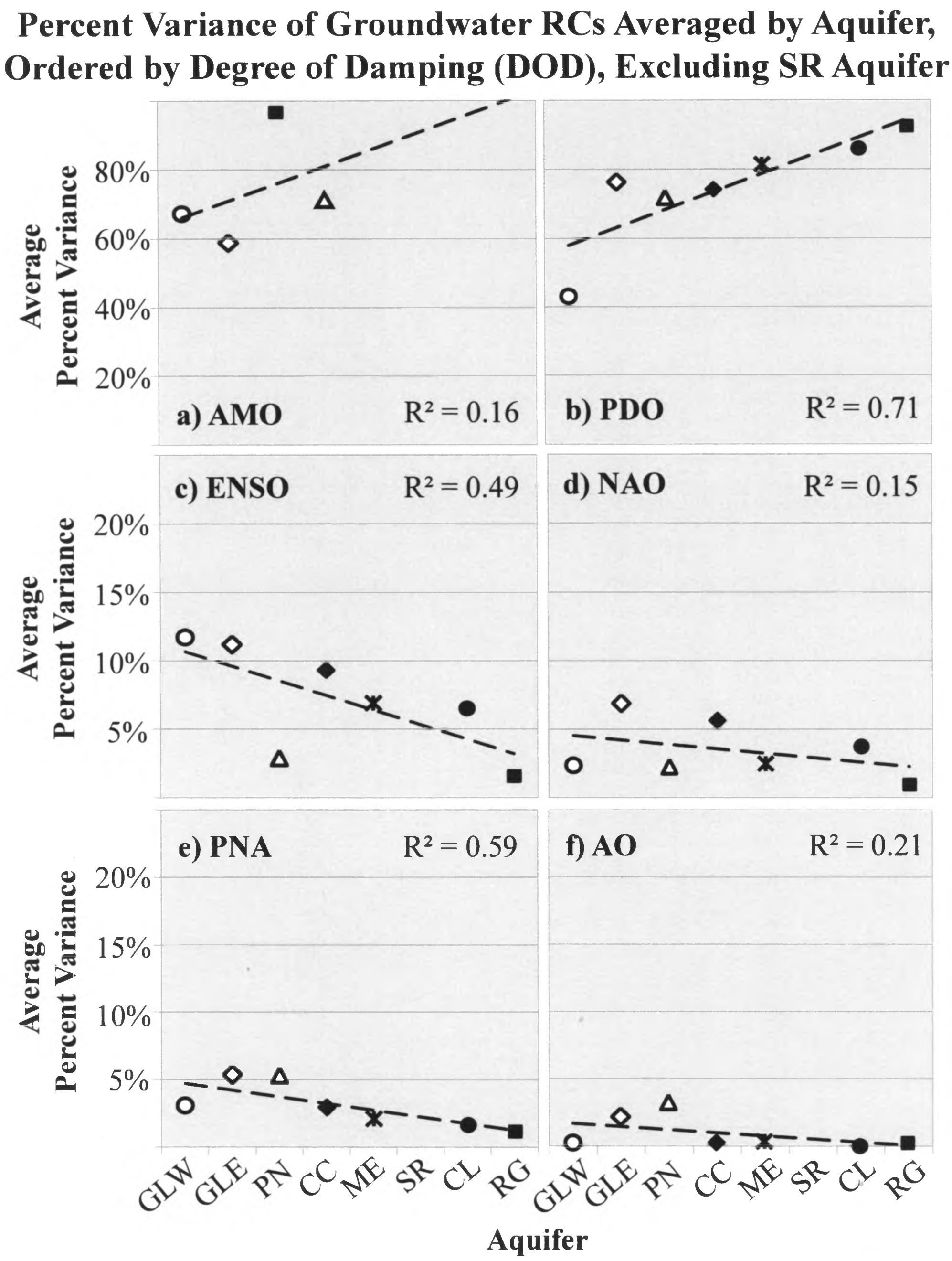

Solid black points = aquifers in southern U.S.

White points with black outline = aquifers in northern U.S.

Linear trend line

Figure 21. Percent variances of groundwater reconstructed components (RCs) averaged by aquifer for each climate variabilty mode, with the anomalous results from the SR aquifer removed. Aquifers are ordered from smallest to greatest DOD.

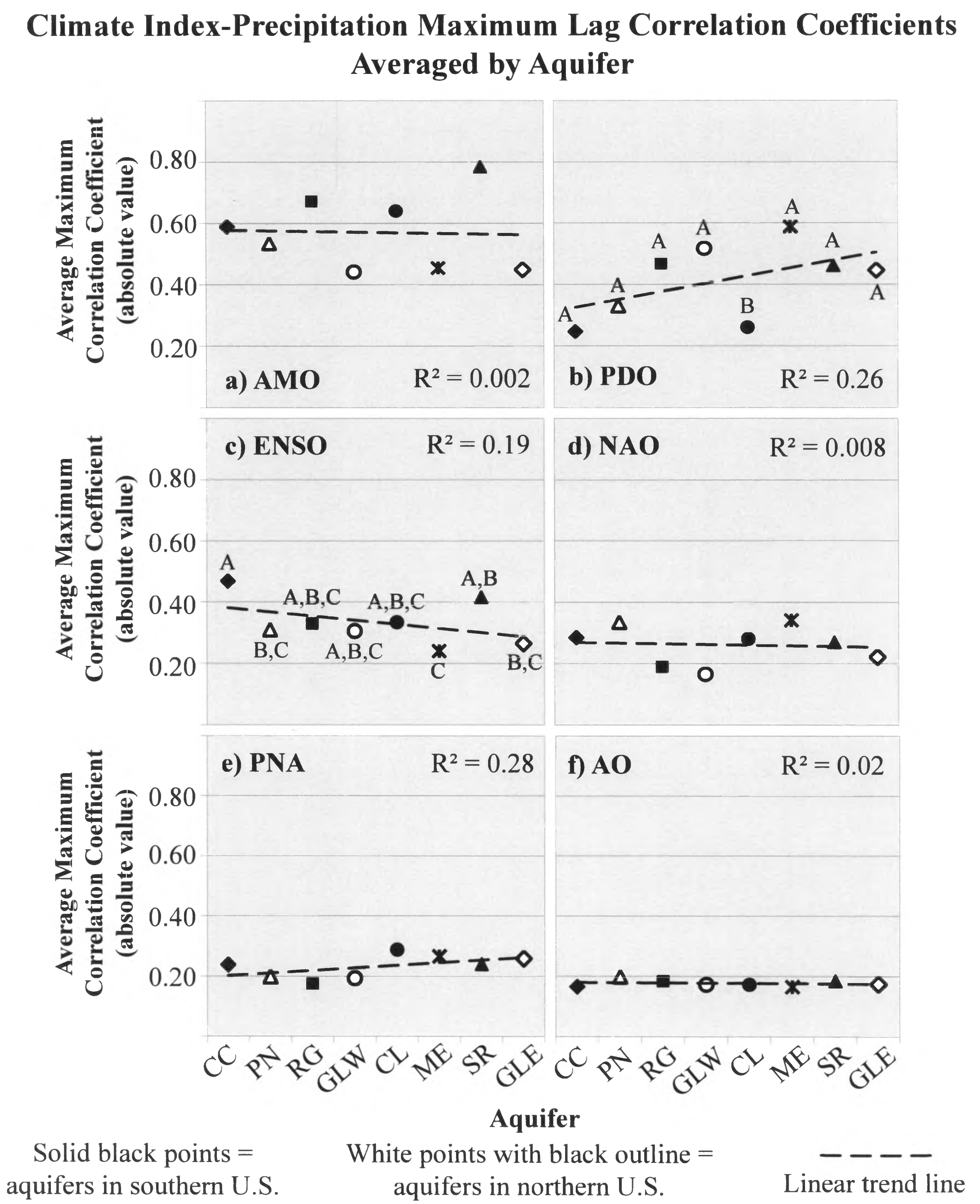

Figure 22. Correlation coefficients of climate index-precipitation lag correlations averaged by aquifer for each climate variabilty mode. Aquifers are ordered from west to east. Letters A, B, & C indicate statistically significant differences between averages.

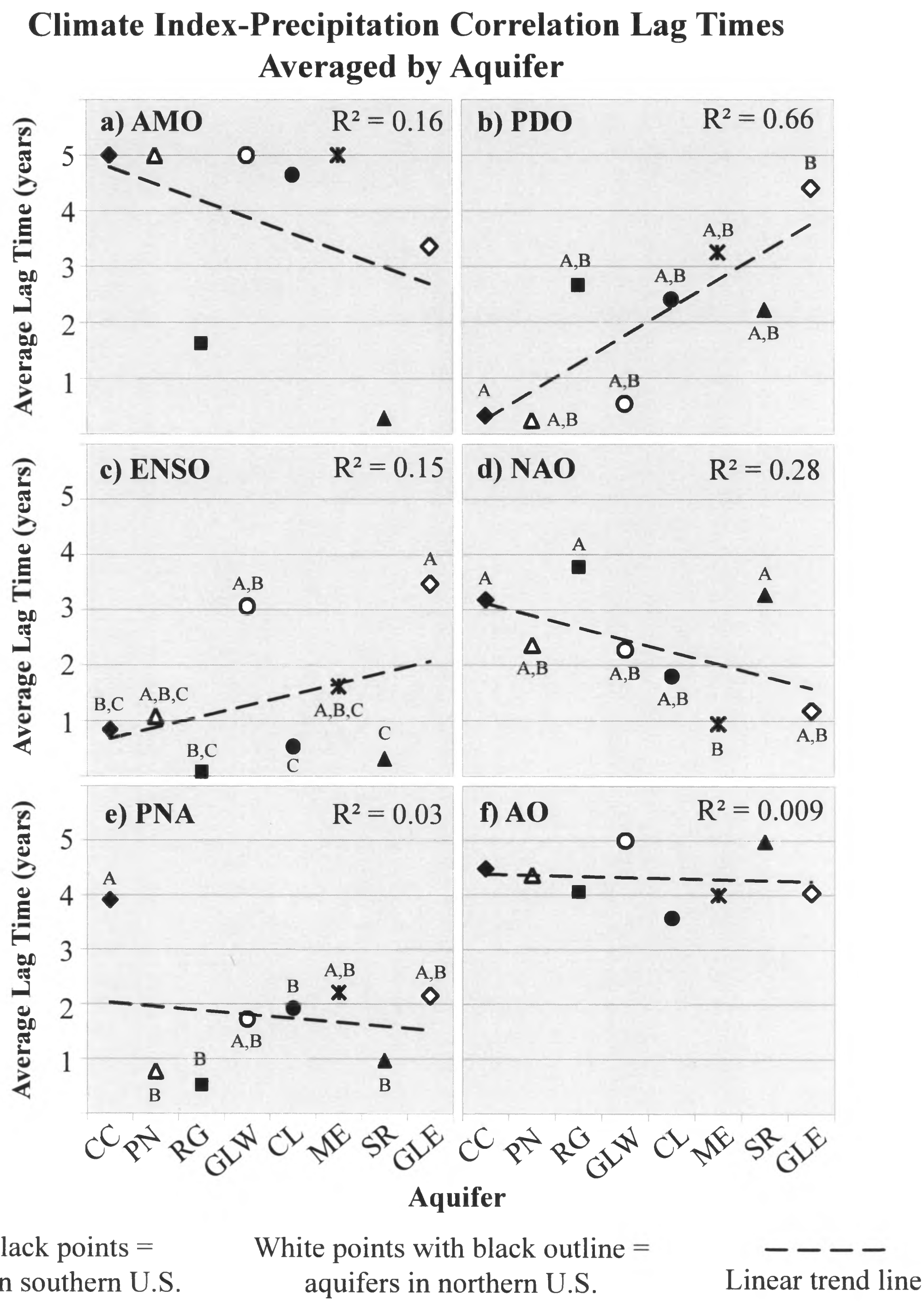

Figure 23. Lag times of climate index-precipitation lag correlations averaged by aquifer for each climate variabilty mode. Aquifers are ordered from west to east. Letters A, B, and C indicate statistically significant differences between averages.

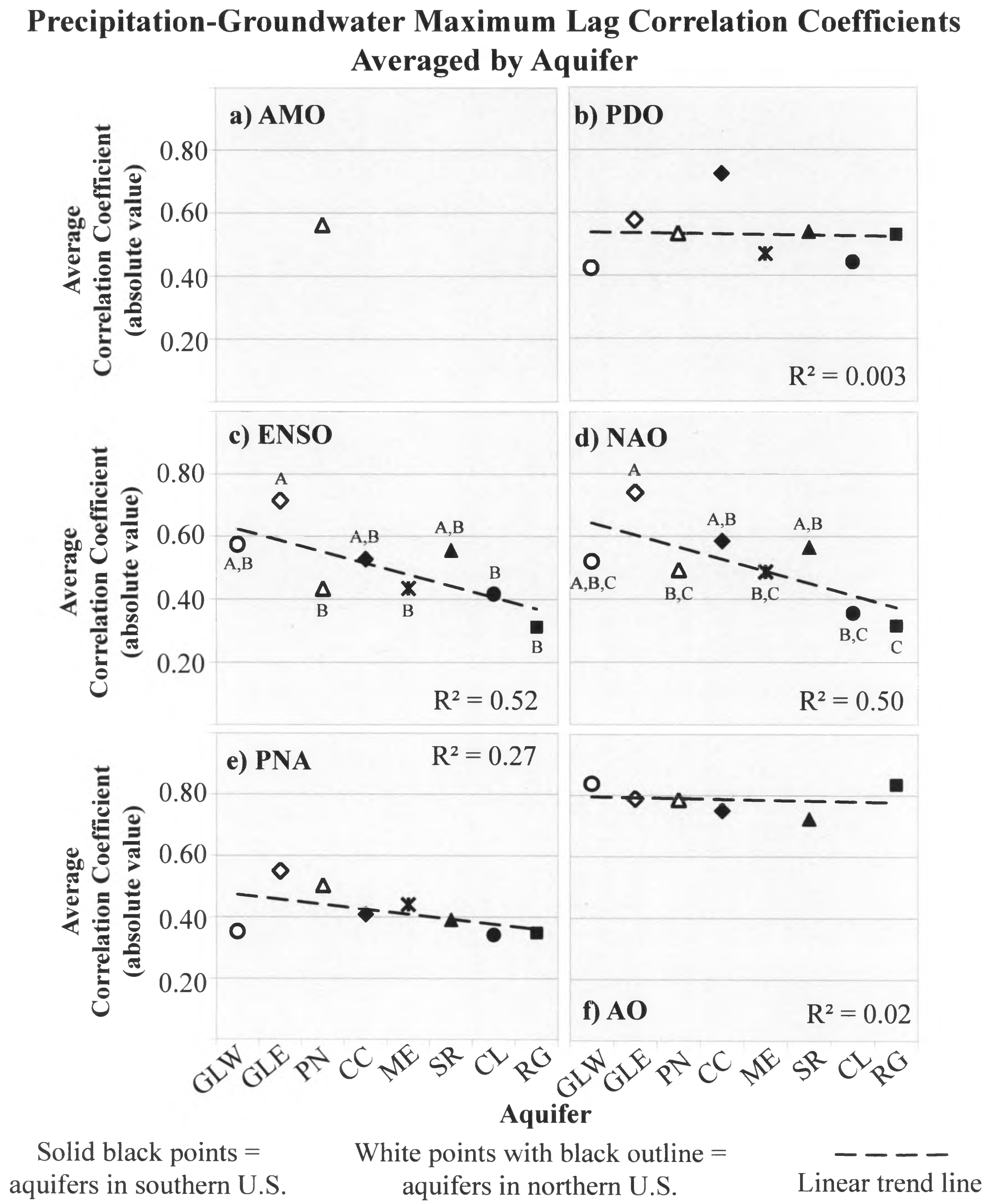

Figure 24. Correlation coefficients of precipitation-groundwater lag correlations averaged by aquifer for each climate variabilty mode. Aquifers are ordered from smallest to greatest degree of damping. Letters A, B, and C indicate statistically significant differences between averages.

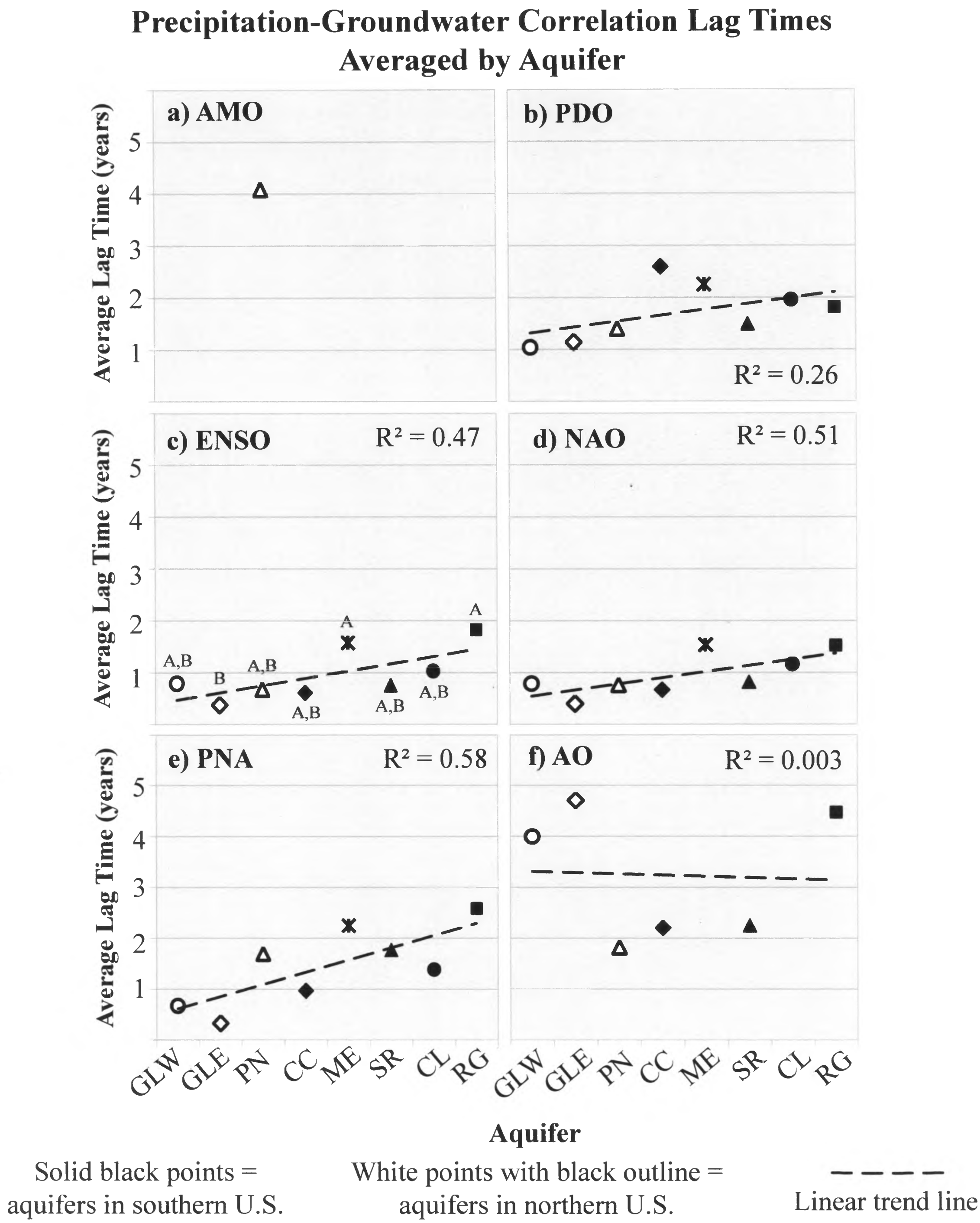

Figure 25. Lag times (years) of precipitation-groundwater lag correlations averaged by aquifer for each climate variabilty mode. Aquifers are ordered from smallest to greatest DOD.

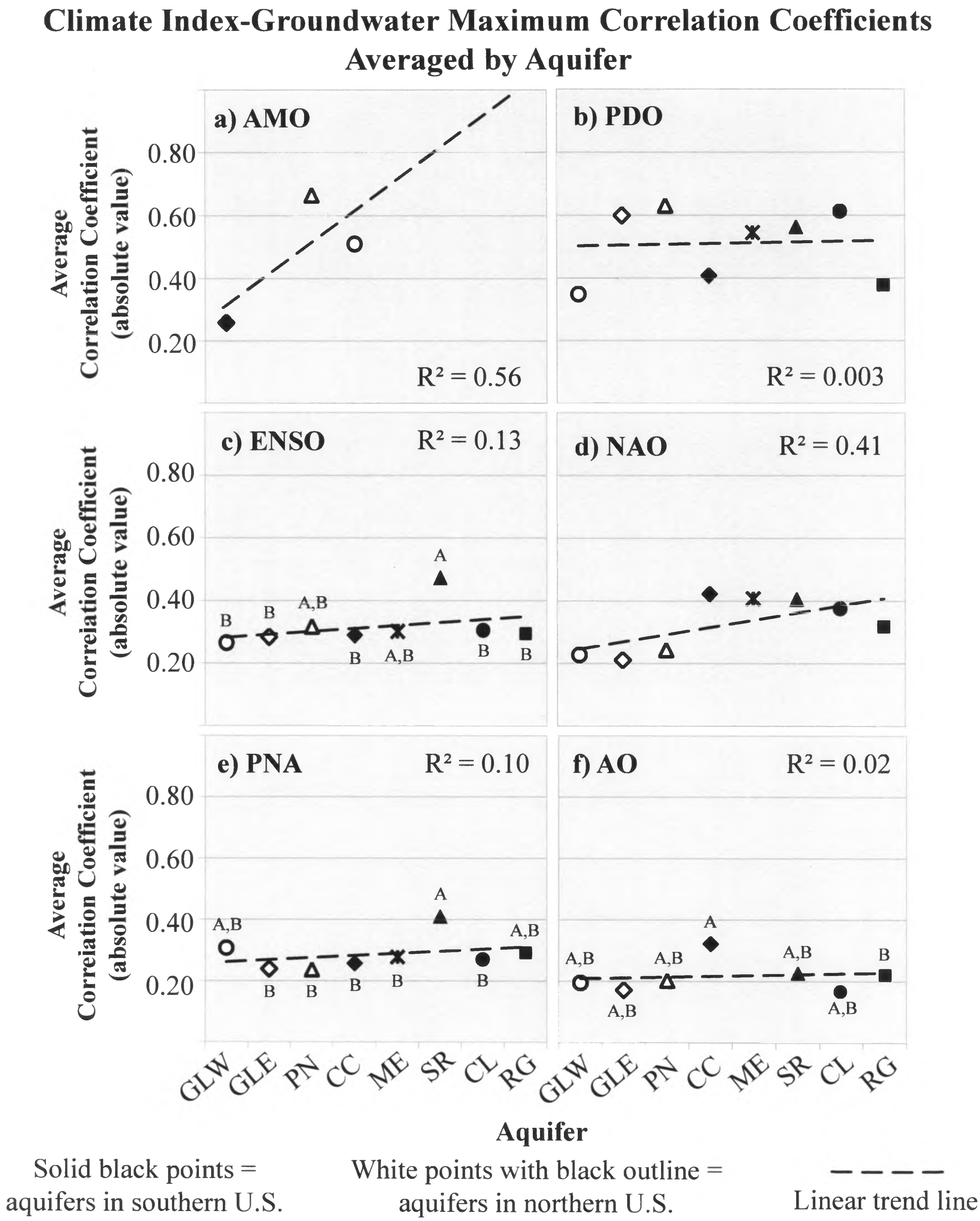

Figure 26. Correlation coefficients of climate index-groundwater lag correlations averaged by aquifer for each climate variabilty mode. Aquifers are ordered from smallest to greatest DOD.

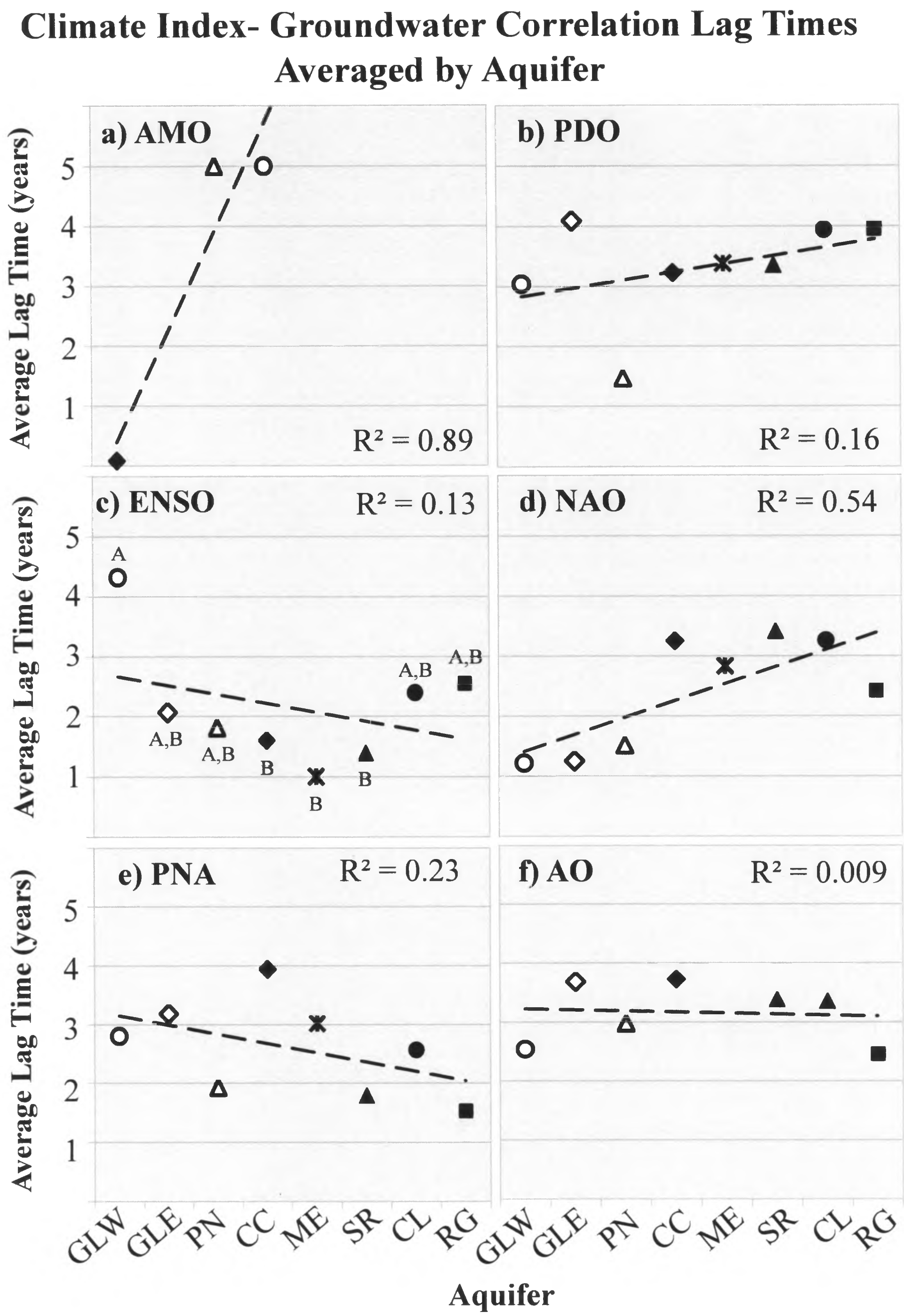

Solid black points = aquifers in southern U.S.

White points with black outline = aquifers in northern U.S.

Linear trend line

Figure 27. Lag times (years) of climate index-groundwater lag correlations averaged by aquifer for each climate variabilty mode. Aquifers are ordered from smallest to greatest DOD.

APPENDIX A

This appendix lists the distances between co-located precipitation and groundwater sites at each principal aquifer.

California Coastal Basins Study Sites

Precipitation Station	Co-located Groundwater Well	Distance Between Sites (kilometers)
CC_PR_01	CC_GW_01	4.1
CC_PR_02	CC_GW_02	2.8
CC_PR_03	CC_GW_03	2.6
CC_PR_04	CC_GW_04	23.3
CC_PR_05	CC_GW_05	2.2
CC_PR_06	CC_GW_06	43.2
CC_PR_07	CC_GW_07	12.9
CC_PR_08	CC_GW_08	10.6

Pacific Northwest Region Study Sites

Precipitation Station	Co-located Groundwater Well	Distance Between Sites (kilometers)
PN_PR_01	PN_GW_01	17.2
PN_PR_02	PN_GW_02	11.0
PN_PR_03	PN_GW_03	18.4
PN_PR_04	PN_GW_04	7.1
PN_PR_05	PN_GW_05	35.7
PN_PR_06	PN_GW_06	30.4
PN_PR_07	PN_GW_07	22.5

Rio Grande Study Sites

Precipitation Station	Co-located Groundwater Well	Distance Between Sites (kilometers)
RG_PR_01	RG_GW_01A	26.1
RG_PR_01	RG_GW_01B	29.0
RG_PR_02	RG_GW_02A	16.7
RG_PR_02	RG_GW_02B	9.5
RG_PR_03	RG_GW_03A	15.1
RG_PR_03	RG_GW_03B	5.5
RG_PR_03	RG_GW_03C	6.4
RG_PR_04	RG_GW_04	4.7

Glacial Study Sites

Precipitation Station	Co-located Groundwater Well	Distance Between Sites (kilometers)
GL_PR_01	GL_GW_01	27.6
GL_PR_02	GL_GW_02	12.7
GL_PR_03	GL_GW_03	11.7
GL_PR_04	GL_GW_04	14.4
GL_PR_05	GL_GW_05	28.1
GL_PR_06	GL_GW_06	18.3
GL_PR_07	GL_GW_07	29.8
GL_PR_08	GL_GW_08	14.7
GL_PR_09	GL_GW_09	4.5
GL_PR_10	GL_GW_10	2.3
GL_PR_11	GL_GW_11A	15.3
GL_PR_11	GL_GW_11B	4.7
GL_PR_11	GL_GW_11C	6.9
GL_PR_12	GL_GW_12	21.9
GL_PR_13	GL_GW_13	4.8
GL_PR_14	GL_GW_14A	12.2
GL_PR_14	GL_GW_14B	11.4

Coastal Lowlands Study Sites

Precipitation Station	Co-located Groundwater Well	Distance Between Sites (kilometers)
CL_PR_01	CL_GW_01	44.8
CL_PR_02	CL_GW_02	24.9
CL_PR_03_04	CL_GW_03	22.9
CL_PR_03_04	CL_GW_04	27.8
CL_PR_05	CL_GW_05	44.9
CL_PR_06	CL_GW_06	16.4
CL_PR_07	CL_GW_07	30.1
CL_PR_08	CL_GW_08	37.2
CL_PR_09	CL_GW_09	38.6
CL_PR_10	CL_GW_10	11.1
CL_PR_11	CL_GW_11	3.6

Mississippi Embayment Study Sites

Precipitation Station	Co-located Groundwater Well	Distance Between Sites (kilometers)
ME_PR_01	ME_GW_01A	11.4
ME_PR_01	ME_GW_01B	4.7
ME_PR_02	ME_GW_02	9.6
ME_PR_03	ME_GW_03	9.1
ME_PR_04	ME_GW_04	30.4
ME_PR_05	ME_GW_05	30.7
ME_PR_06	ME_GW_06	24.3
ME_PR_07	ME_GW_07	13.8
ME_PR_08	ME_GW_08	13.4
ME_PR_09	ME_GW_09	30.6
ME_PR_10	ME_GW_10	12.3

Surficial Study Sites

Precipitation Station	Co-located Groundwater Well	Distance Between Sites (kilometers)
SR_PR_01	SR_GW_01	18.7
SR_PR_02	SR_GW_02	15.9
SR_PR_03	SR_GW_03	28.8
SR_PR_04	SR_GW_04	15.6
SR_PR_05	SR_GW_05	31.8
SR_PR_06	SR_GW_06	12.2
SR_PR_07	SR_GW_07	50.9
SR_PR_08	SR_GW_08	37.4

APPENDIX B

This appendix lists the significant reconstructed components (RCs) for each aquifer that fall within the periods of the six climate variability modes of interest. A dashed line indicates no significant RC for the specified climate variability mode.

California Coastal Basins RCs for the AMO & PDO

	AMO			PDO		
Site ID	**RCs**	**Average Period (years)**	**Percent Variance (%)**	**RCs**	**Average Period (years)**	**Percent Variance (%)**
Precipitation Sites						
CC_PR_01	--	--	--	2	19.5	26.0
CC_PR_02	--	--	--	1,2	14.0	76.1
CC_PR_03	--	--	--	2	12.4	29.5
CC_PR_04	--	--	--	1,2	14.1	80.1
CC_PR_05	--	--	--	1,2	18.5	71.6
CC_PR_06	--	--	--	1,2	27.4	79.9
CC_PR_07	--	--	--	2	12.5	24.3
CC_PR_08	1	57.9	63.0	2,3	16.1	26.9
Groundwater Sites						
CC_GW_01	--	--	--	1,2	18.6	93.7
CC_GW_02	--	--	--	--	--	--
CC_GW_02	--	--	--	1	15.3	80.2
CC_GW_04	--	--	--	1,2	19.2	96.5
CC_GW_05	--	--	--	1,2	25.7	91.0
CC_GW_06	--	--	--	1	20.4	78.1
CC_GW_07	1	40.8	71.0	2	13.6	24.2
CC_GW_08	--	--	--	1	13.7	55.8

California Coastal Basins RCs for the ENSO & NAO

	ENSO			NAO		
Site ID	**RCs**	**Average Period (years)**	**Percent Variance (%)**	**RCs**	**Average Period (years)**	**Percent Variance (%)**
Precipitation Sites						
CC_PR_01	3,4,5,8,9,10	3.9	6.2	4,5,8	4.0	5.0
CC_PR_02	3,4,7,8,9	3.3	13.8	3,4,7	4.0	11.8
CC_PR_03	3,4,7,8,9,10	3.6	16.9	3,4,7,8	4.3	15.7
CC_PR_04	3,6,7	4.0	8.1	3,6	4.7	7.3
CC_PR_05	3,4,7,8	3.7	14.4	3,4	4.9	10.0
CC_PR_06	3,4,7,8,9	3.6	12.7	3,4,7	4.5	10.6
CC_PR_07	3,4,7,8,9	3.9	18.3	3,4,7,8	4.3	16.6
CC_PR_08	5,6,9,10	4.5	3.3	5,6,9,10	4.5	3.3
Groundwater Sites						
CC_GW_01	3,4,7	3.0	4.8	3	4.1	3.5
CC_GW_02	3,4	3.4	4.8	3	4.2	3.7
CC_GW_02	2,3,4	4.0	19.6	2,3	5.0	19.4
CC_GW_04	3,4,5	3.4	3.1	3,4	4.0	2.9
CC_GW_05	3,4,5,6,7	3.7	8.6	3,4	5.3	7.6
CC_GW_06	2,3,4,5	4.2	21.8	3,4	4.0	1.9
CC_GW_07	4,5,6,7,8,9	3.6	1.2	3,5,6	3.8	0.3
CC_GW_08	3,4,5	2.6	10.5	3	3.2	6.3

California Coastal Basins RCs for the PNA & AO

	PNA			AO		
Site ID	RCs	Average Period (years)	Percent Variance (%)	RCs	Average Period (years)	Percent Variance (%)
Precipitation Sites						
CC_PR_01	5,6,7,8,9,10	2.3	5.7	6,7	1.0	2.2
CC_PR_02	5,6,7,8,9,10	1.9	11.2	5,6	1.0	7.0
CC_PR_03	5,6,7,8,9,10	2.2	10.1	5,6	1.0	6.2
CC_PR_04	4,5,7,8,9,10	1.6	10.3	4,5	1.0	7.4
CC_PR_05	5,6,7,8,9,10	1.7	14.2	5,6	1.0	7.7
CC_PR_06	5,6,7,8,9,10	1.9	8.3	5,6	1.0	3.8
CC_PR_07	5,6,7,8,9,10	2.1	13.8	5,6	1.0	6.2
CC_PR_08	7,8,10	1.7	2.2	7,8	1.0	1.9
Groundwater Sites						
CC_GW_01	3,4,5,6,7,8,9,10	1.9	6.3	5,6,10	1.0	1.2
CC_GW_02	4,5,6,7,8,9,10	1.4	1.7	6,7,10	0.9	0.2
CC_GW_02	3,4,5,6,7,8	1.8	1.2	7,8	1.0	0.0
CC_GW_04	4,5,6,7,8,9,10	1.7	1.1	8,9	1.0	0.1
CC_GW_05	5,6,7,8,9,10	1.9	1.3	8,9,10	1.0	0.2
CC_GW_06	4,5,6,7,8,9,10	1.7	0.5	9,10	1.0	0.0
CC_GW_07	6,7,8,9,10	2.5	0.2	--	--	--
CC_GW_08	3,4,5,6,7,8,9,10	1.7	11.5	9,10	1.0	0.1

Pacific Northwest RCs for the AMO & PDO

	AMO			PDO		
Site ID	RCs	Average Period (years)	Percent Variance (%)	RCs	Average Period (years)	Percent Variance (%)
Precipitation Sites						
PN_PR_01	--	--	--	2	12.5	25.3
PN_PR_02	1	52.9	51.5	2,3	13.2	30.4
PN_PR_03	--	--	--	2	12.2	25.6
PN_PR_04	--	--	--	1,2	21.8	82.1
PN_PR_05	--	--	--	1	18.0	72.1
PN_PR_06	1,2	52.2	94.5	--	--	--
PN_PR_07	--	--	--	1,2	23.7	76.7
Groundwater Sites						
PN_GW_01	--	--	--	1,2	12.9	81.9
PN_GW_02	--	--	--	1	26.0	68.2
PN_GW_03	--	--	--	1,2	23.8	97.6
PN_GW_04	--	--	--	1,2	16.5	89.4
PN_GW_05	--	--	--	1,2	16.5	91.9
PN_GW_06	1,2	42.8	96.6	3	12.2	2.3
PN_GW_07	--	--	--	1	21.6	71.7

Pacific Northwest RCs for the ENSO & NAO

	ENSO			NAO		
Site ID	RCs	Average Period (years)	Percent Variance (%)	RCs	Average Period (years)	Percent Variance (%)
Precipitation Sites						
PN_PR_01	3,6,7,8,9,10	3.7	9.7	6,7	4.1	2.5
PN_PR_02	6,7,8,9,10	4.5	7.7	7,8,9	4.3	4.0
PN_PR_03	3,4,7,8,9,10	3.0	5.3	4,7	4.0	3.6
PN_PR_04	3,4,5	4.2	10.4	3,4	5.0	8.5
PN_PR_05	3,4	2.9	4.8	3	3.6	3.2
PN_PR_06	5,6	6.1	0.8	6	5.2	0.3
PN_PR_07	4,5,8,9	3.0	6.9	4,5	3.9	4.8
Groundwater Sites						
PN_GW_01	3,6,7	3.3	8.5	3	4.7	4.6
PN_GW_02	3,4,5,6	3.3	5.0	3,4,5	3.5	4.9
PN_GW_03	4,5,6,7,8	3.2	0.5	4,5,6	3.7	0.4
PN_GW_04	5,6	2.9	2.7	5	3.7	1.7
PN_GW_05	6	2.2	1.1	--	--	--
PN_GW_06	5,6	3.8	0.2	5,6	3.8	0.2
PN_GW_07	3,4,5	3.5	2.1	3,4	4.2	2.1

Pacific Northwest RCs for the PNA & AO

	PNA			AO		
Site ID	**RCs**	**Average Period (years)**	**Percent Variance (%)**	**RCs**	**Average Period (years)**	**Percent Variance (%)**
Precipitation Sites						
PN_PR_01	4,5,7,8,9,10	2.1	10.2	4,5	1.0	7.1
PN_PR_02	4,5,8,9,10	2.4	8.9	4,5	1.0	6.5
PN_PR_03	5,6,7,8,9,10	2.1	6.7	5,6	1.0	3.7
PN_PR_04	4,5,6,7	2.2	8.4	6,7	1.0	3.1
PN_PR_05	3,4,5,6,7,8,9	1.7	8.8	5,6,9	1.0	2.7
PN_PR_06	--	--	--	--	--	--
PN_PR_07	4,5,6,7,8,9,10	2.3	10.2	6,7	1.0	2.5
Groundwater Sites						
PN_GW_01	4,5,6,7,8,9,10	1.8	12.8	4,5	1.0	6.2
PN_GW_02	3,4,5,6,7,8,9,10	2.3	5.2	10	1.0	0.0
PN_GW_03	5,6,7,8,9,10	2.3	0.2	10	1.0	0.0
PN_GW_04	3,4,5,6,7,8,9,10	1.6	10.4	3,4,9,10	0.9	7.2
PN_GW_05	3,4,5,6,7,8,9,10	1.2	7.9	3,4,5,9,10	0.9	6.1
PN_GW_06	5,6	3.8	0.2	--	--	--
PN_GW_07	4,5,6,7,8,9,10	1.7	0.4	8,9	1.0	0.0

Rio Grande RCs for the AMO & PDO

	AMO			PDO		
Site ID	RCs	Average Period (years)	Percent Variance (%)	RCs	Average Period (years)	Percent Variance (%)
Precipitation Sites						
RG_PR_01	1	58.0	61.3	2	29.0	21.1
RG_PR_02	--	--	--	1	31.7	70.9
RG_PR_03	--	--	--	1,2	27.5	84.4
RG_PR_04	1	54.0	65.6	2	27.0	20.2
Groundwater Sites						
RG_GW_01A	--	--	--	1,2	18.7	99.4
RG_GW_01B	--	--	--	1,2	19.7	99.3
RG_GW_02A	--	--	--	1	19.8	77.4
RG_GW_02B	--	--	--	1,2	20.6	99.3
RG_GW_03A	--	--	--	1,2	27.2	98.3
RG_GW_03B	--	--	--	1	32.4	73.6
RG_GW_03C	--	--	--	1,2	12.7	98.1
RG_GW_04	--	--	--	1,2	13.2	94.5

Rio Grande RCs for the ENSO & NAO

	ENSO			NAO		
Site ID	**RCs**	**Average Period (years)**	**Percent Variance (%)**	**RCs**	**Average Period (years)**	**Percent Variance (%)**
Precipitation Sites						
RG_PR_01	4,5,6,7,10	4.5	8.1	4,5,6,7,10	4.5	8.1
RG_PR_02	7,8,9	2.5	1.5	7	3.2	0.6
RG_PR_03	3,4,7,8,9,10	3.4	10.0	4	4.1	1.7
RG_PR_04	4,5,6,9,10	4.6	6.5	5,6,9,10	4.2	3.7
Groundwater Sites						
RG_GW_01A	3,4,5	2.7	0.5	3,4	3.1	0.5
RG_GW_01B	3,4,5	3.8	0.6	3,4	4.3	0.6
RG_GW_02A	3,4	3.9	1.6	3	4.9	1.3
RG_GW_02B	3,4	5.3	0.1	4	3.7	0.1
RG_GW_03A	4,5,6,7,8	3.0	0.7	4,5	4.1	0.6
RG_GW_03B	3	6.5	3.2	--	--	--
RG_GW_03C	3	4.8	1.2	3	4.8	1.2
RG_GW_04	3,4,5	2.7	4.5	3	3.6	2.9

Rio Grande RCs for the PNA & AO

	PNA			AO		
Site ID	**RCs**	**Average Period (years)**	**Percent Variance (%)**	**RCs**	**Average Period (years)**	**Percent Variance (%)**
Precipitation Sites						
RG_PR_01	6,7,8,9,10	2.6	5.1	8,9	1.0	1.8
RG_PR_02	4,5,6,7,8,9,10	1.8	5.0	4,5,6	1.0	3.2
RG_PR_03	4,5,6,7,8,9,10	2.2	8.3	5,6	1.0	3.0
RG_PR_04	6,7,8,9,10	2.7	3.0	7,8	1.0	1.2
Groundwater Sites						
RG_GW_01A	3,4,5,6,7,8,9	1.8	0.6	7,8	1.0	0.0
RG_GW_01B	5,6,7	2.1	0.1	--	--	--
RG_GW_02A	4,5,6,7,8,9,10	1.6	0.7	7,8	1.0	0.1
RG_GW_02B	4	3.7	0.1	--	--	--
RG_GW_03A	5,6,7,8,9,10	2.3	0.3	--	--	--
RG_GW_03B	--	--	--	--	--	--
RG_GW_03C	--	--	--	--	--	--
RG_GW_04	3,4,5,6,7,8,9,10	1.8	5.4	6,7	1.0	0.6

Glacial RCs for the AMO & PDO

	AMO			PDO		
Site ID	**RCs**	**Average Period (years)**	**Percent Variance (%)**	**RCs**	**Average Period (years)**	**Percent Variance (%)**
Precipitation Sites						
GL_PR_01	1	46.2	54.2	2	30.8	22.9
GL_PR_02	--	--	--	1,2	24.9	57.0
GL_PR_03	--	--	--	--	--	--
GL_PR_04	--	--	--	2	19.4	19.7
GL_PR_05	--	--	--	1,2	27.8	70.9
GL_PR_06	1	57.5	55.1	2	19.2	22.9
GL_PR_07	--	--	--	1,2	22.5	88.7
GL_PR_08	--	--	--	1,2	21.9	90.5
GL_PR_09	--	--	--	1,2	24.8	94.5
GL_PR_10	1	60.6	52.9	2,3	17.3	38.8
GL_PR_11	--	--	--	1	29.1	56.7
GL_PR_12	--	--	--	1,2	24.8	87.0
GL_PR_13	1	42.1	63.5	2	21.0	26.3
GL_PR_14	1	40.3	44.5	2,3	18.2	37.8

Glacial RCs for the AMO & PDO

	AMO			PDO		
Site ID	RCs	Average Period (years)	Percent Variance (%)	RCs	Average Period (years)	Percent Variance (%)
Groundwater Sites						
GL_GW_01	1	62.5	67.1	2	12.5	25.3
GL_GW_02	--	--	--	1,2	24.4	95.9
GL_GW_03	--	--	--	3	25.2	9.2
GL_GW_04	--	--	--	2	13.3	29.4
GL_GW_05	--	--	--	1	22.1	55.3
GL_GW_06	--	--	--	--	--	--
GL_GW_07	1	43.9	59.3	2	17.6	26.4
GL_GW_08	--	--	--	1,2	21.3	95.3
GL_GW_09	--	--	--	1,2	28.2	98.9
GL_GW_10	--	--	--	1,2	14.7	81.1
GL_GW_11A	--	--	--	1	23.1	71.3
GL_GW_11B	--	--	--	1,2	25.1	81.0
GL_GW_11C	--	--	--	1,2	19.7	80.4
GL_GW_12	--	--	--	1,2	14.9	81.4
GL_GW_13	--	--	--	1	27.8	42.0
GL_GW_14A	--	--	--	1,2	19.2	96.3
GL_GW_14B	--	--	--	1,2	19.3	86.1

Glacial RCs for the ENSO & NAO

	ENSO			NAO		
Site ID	**RCs**	**Average Period (years)**	**Percent Variance (%)**	**RCs**	**Average Period (years)**	**Percent Variance (%)**
Precipitation Sites						
GL_PR_01	4,7,8,9,10	3.6	8.3	7,8,9	3.9	7.5
GL_PR_02	6,7,8,9,10	4.3	12.0	7,8,9	4.1	5.7
GL_PR_03	7,8,9,10	3.1	6.2	7,8	3.9	4.5
GL_PR_04	3,6,7,8,9,10	3.8	7.6	6,7,8	3.9	3.4
GL_PR_05	4,8,9,10	4.3	8.4	8,9,10	3.6	2.9
GL_PR_06	5,6,7,10	4.6	4.9	6,7,10	4.0	2.9
GL_PR_07	4,5,6,7,8,9	3.5	4.6	4,5,6	4.4	3.5
GL_PR_08	3,4,5	4.5	2.5	4,5	3.5	2.5
GL_PR_09	4,5,6,7	3.1	1.9	4,5	3.9	1.1
GL_PR_10	6,7,8,9,10	3.6	2.1	6,7,8,9	3.8	1.9
GL_PR_11	3,4,5,6,7	3.6	14.4	4	3.4	3.3
GL_PR_12	4,5,6	3.4	4.8	4,5	3.7	4.0
GL_PR_13	4,5,6,7,8	3.5	4.5	4,5,6	4.0	3.7
GL_PR_14	5,6,7,8,9,10	3.9	9.3	5,6,7,8,9	4.2	8.5

Glacial RCs for the ENSO & NAO

	ENSO			NAO		
Site ID	**RCs**	**Average Period (years)**	**Percent Variance (%)**	**RCs**	**Average Period (years)**	**Percent Variance (%)**
Groundwater Sites						
GL_GW_01	4,5	4.0	1.3	4,5	4.0	1.3
GL_GW_02	3,4,5,6,7	3.9	4.0	4,5	3.5	1.0
GL_GW_03	4,5,6	2.7	4.5	4	3.1	3.0
GL_GW_04	3,4,5,6,7,8,9	3.9	11.4	5,6	3.5	0.9
GL_GW_05	2,3,4,5	3.8	43.5	3,4	3.3	6.6
GL_GW_06	4,5,6,7,8	3.6	5.5	5,6	3.6	1.7
GL_GW_07	--	--	--	--	--	--
GL_GW_08	4,5,8	3.0	1.7	4,5	3.4	1.5
GL_GW_09	3,4,5,6	4.0	1.0	4,5	3.3	0.4
GL_GW_10	3,4,7,8	3.8	11.9	4	3.4	2.7
GL_GW_11A	3	4.6	3.1	3	4.6	3.1
GL_GW_11B	4,7,8,9,10	2.9	6.6	4,7	3.8	4.9
GL_GW_11C	3,6,7,8	4.0	10.5	3,6,7	4.5	9.3
GL_GW_12	3,4,5,6,9	3.6	17.0	3,4	5.0	14.3
GL_GW_13	2,3,4	5.1	43.8	3,4	4.2	19.1
GL_GW_14A	3,4,5,6	3.6	3.6	3,4	4.7	3.3
GL_GW_14B	3,4,5,6	3.2	12.6	3,4	3.9	10.9

Glacial RCs for the PNA & AO

	PNA			AO		
Site ID	**RCs**	**Average Period (years)**	**Percent Variance (%)**	**RCs**	**Average Period (years)**	**Percent Variance (%)**
Precipitation Sites						
GL_PR_01	5,6,8,9,10	2.2	7.8	5,6	1.0	5.1
GL_PR_02	4,5,8,9,10	2.4	17.3	4,5	1.0	12.6
GL_PR_03	4,5,6,8,9,10	1.8	17.3	4,5,6	1.0	13.8
GL_PR_04	4,5,8,9,10	2.0	6.4	4,5	1.0	4.6
GL_PR_05	5,6,7,9,10	1.8	9.4	5,6,7	1.0	8.0
GL_PR_06	7,8,9,10	2.3	2.8	8,9	1.0	1.3
GL_PR_07	6,7,8,9,10	2.4	2.1	10	1.0	0.3
GL_PR_08	4,5,6,7,8,9,10	2.0	5.2	6,7	1.0	1.2
GL_PR_09	5,6,7,8,9,10	1.9	2.1	8,9	1.0	0.6
GL_PR_10	8,9,10	3.0	0.8	--	--	--
GL_PR_11	4,5,6,7	2.7	7.1	--	--	--
GL_PR_12	4,5,6	3.4	4.8	--	--	--
GL_PR_13	5,6,7,8	3.1	2.6	--	--	--
GL_PR_14	7,8,9,10	3.2	4.0	--	--	--

Glacial RCs for the PNA & AO

	PNA			AO		
Site ID	**RCs**	**Average Period (years)**	**Percent Variance (%)**	**RCs**	**Average Period (years)**	**Percent Variance (%)**
Groundwater Sites						
GL_GW_01	5	3.1	0.2	--	--	--
GL_GW_02	4,5,6,7,8,9	2.6	1.3	--	--	--
GL_GW_03	4,5,6,7,8,9,10	1.9	5.1	8,9	1.0	0.3
GL_GW_04	5,6,7,8,9,10	2.6	1.4	--	--	--
GL_GW_05	3,4,5,6,7,8,9,10	1.9	8.3	7,8	1.0	0.4
GL_GW_06	5,6,7,8,9,10	2.4	2.2	10	1.0	0.1
GL_GW_07	--	--	--	--	--	--
GL_GW_08	4,5,6,7,8,9,10	2.1	2.6	6,7	1.0	0.7
GL_GW_09	4,5,6,7,8,9,10	2.2	0.5	10	1.0	0.0
GL_GW_10	4,5,6,7,8,9	1.8	10.8	5,6	1.0	4.4
GL_GW_11A	3	4.6	3.1	--		0.0
GL_GW_11B	5,6,7,8,9,10	2.0	7.7	5,6	1.0	4.5
GL_GW_11C	4,5,6,7,8	2.4	12.0	4,5	1.0	6.5
GL_GW_12	5,6,7,8,9,10	1.9	3.8	7,8	1.0	0.8
GL_GW_13	4	3.3	6.9	--		0.0
GL_GW_14A	5,6,7,8,9,10	1.8	0.3	8,9	1.0	0.0
GL_GW_14B	4,5,6,7,8,9,10	1.9	6.0	7,8	1.0	0.7

Coastal Lowlands RCs for the AMO & PDO

	AMO			PDO		
Site ID	RCs	Average Period (years)	Percent Variance (%)	RCs	Average Period (years)	Percent Variance (%)
Precipitation Sites						
CL_PR_01	1	50.4	60.6	2	25.2	22.6
CL_PR_02	--	--	--	1	15.5	47.2
CL_PR_03_04	--	--	--	2	12.1	26.9
CL_PR_05	--	--	--	1,2	15.3	75.9
CL_PR_06	1	60.8	67.1	2	24.3	18.5
CL_PR_07	--	--	--	1	19.1	43.9
CL_PR_08	--	--	--	1	24.6	39.0
CL_PR_09	1	60.7	59.2	2	24.3	22.1
CL_PR_10	--	--	--	1,2	17.1	77.7
CL_PR_11	1,2	42.0	94.8	--	--	--
Groundwater Sites						
CL_GW_01	--	--	--	1,2	21.5	99.7
CL_GW_02	--	--	--	1,2	30.0	99.1
CL_GW_03	--	--	--	1	20.3	68.9
CL_GW_04	--	--	--	1	20.8	55.0
CL_GW_05	--	--	--	1	25.5	78.6
CL_GW_06	--	--	--	1,2	24.0	97.4
CL_GW_07	--	--	--	1,2	28.2	99.8
CL_GW_08	--	--	--	1,2	18.4	98.2
CL_GW_09	--	--	--	1	24.7	81.7
CL_GW_10	--	--	--	1	23.8	77.4
CL_GW_11	--	--	--	1,2	19.3	91.3

Coastal Lowlands RCs for the ENSO & NAO

	ENSO			NAO		
Site ID	**RCs**	**Average Period (years)**	**Percent Variance (%)**	**RCs**	**Average Period (years)**	**Percent Variance (%)**
Precipitation Sites						
CL_PR_01	4,5,6,7,8,9,10	3.8	8.1	5,6,7	4.3	3.5
CL_PR_02	3,4,5,6	4.0	14.4	4,5	3.6	5.8
CL_PR_03_04	4,5,6,7,8	3.1	10.2	4,5,6	3.6	8.0
CL_PR_05	3,4,5,6,7	4.4	17.3	4,5,6	4.1	8.1
CL_PR_06	4,5,6,7,8,9,10	4.4	8.0	6,7,8,9	3.8	3.0
CL_PR_07	3,4,5,6,7	3.3	17.2	4,5	3.0	7.5
CL_PR_08	2,3,4,5	4.1	48.7	2,3	5.5	40.6
CL_PR_09	5,6,7,8,9,10	4.0	5.9	5,6,7,8,9	4.2	5.6
CL_PR_10	3,4,5,6	3.0	16.0	3,4	3.8	12.5
CL_PR_11	3,4,5,6,7	4.6	3.9	4,5,6,7	4.1	1.7
Groundwater Sites						
CL_GW_01	3,4,5,6,7	3.3	0.3	3,4	4.9	0.3
CL_GW_02	3,4,5,6,7	3.7	0.9	3,4,5	4.8	0.8
CL_GW_03	3,4,5	3.5	5.3	3	5.8	3.4
CL_GW_04	3,4,5	2.8	12.4	3	3.8	8.2
CL_GW_05	3,4,5,6	3.7	1.0	4	3.6	0.1
CL_GW_06	3,4,5,6,7,8	3.5	2.5	3,4,5	4.9	2.5
CL_GW_07	4,5	4.2	0.0	4	5.6	0.0
CL_GW_08	3,4,5,6	3.6	1.7	3,4	4.8	1.6
CL_GW_09	2,3,4,5,6	4.4	18.2	2,3,4	5.8	18.1
CL_GW_10	2,3,4,5	5.1	22.5	4	4.0	0.2
CL_GW_11	3,4	4.7	6.5	3,4	4.7	6.5

Coastal Lowlands RCs for the PNA & AO

	PNA			AO		
Site ID	RCs	Average Period (years)	Percent Variance (%)	RCs	Average Period (years)	Percent Variance (%)
Precipitation Sites						
CL_PR_01	6,7,8,9,10	2.9	3.5	--	--	--
CL_PR_02	4,5,6,7,8	2.7	9.4	--	--	--
CL_PR_03_04	5,6,7,8,9,10	2.3	7.7	--	--	--
CL_PR_05	5,6,7	3.1	5.4	--	--	--
CL_PR_06	7,8,9,10	3.3	2.4	--	--	--
CL_PR_07	4,5,6,7,8,9,10	2.1	13.1	--	--	--
CL_PR_08	4,5,6,7,8,9,10	1.6	15.1	6,7,8	1.0	4.8
CL_PR_09	7,8,9,10	3.3	2.4	--	--	--
CL_PR_10	4,5,6,7,8,9	2.0	9.8	--	--	--
CL_PR_11	6,7	3.0	0.5	--	--	--
Groundwater Sites						
CL_GW_01	4,5,6,7,8,9,10	2.1	0.1	10	1.0	0.0
CL_GW_02	5,6,7,8,9,10	2.1	0.1	--	--	--
CL_GW_03	4,5,6	2.2	2.2	--	--	--
CL_GW_04	3,4,5,6	2.6	13.0	--	--	--
CL_GW_05	4,5,6,7,8,9,10	1.9	0.2	7,8	1.0	0.0
CL_GW_06	5,6,7,8,9,10	1.9	0.2	9,10	1.0	0.0
CL_GW_07	5	2.7	0.0	--	--	--
CL_GW_08	4,5,6,7	2.5	0.6	--	--	--
CL_GW_09	5,6	2.3	0.1	--	--	--
CL_GW_10	4,5,6	2.9	0.2	--	--	--
CL_GW_11	4	3.6	1.7	--	--	--

Mississippi Embayment RCs for the AMO & PDO

	AMO			PDO		
Site ID	RCs	Average Period (years)	Percent Variance (%)	RCs	Average Period (years)	Percent Variance (%)
Precipitation Sites						
ME_PR_01	--	--	--	2	24.7	21.5
ME_PR_02	1	43.3	56.1	2,3	19.5	32.1
ME_PR_03	--	--	--	1	30.6	59.4
ME_PR_04	--	--	--	1,2	16.6	69.1
ME_PR_05	--	--	--	--	--	--
ME_PR_06	1	43.9	56.8	2	14.6	26.6
ME_PR_07	--	--	--	1	25.3	66.9
ME_PR_08	--	--	--	2	14.1	22.1
ME_PR_09	--	--	--	--	--	--
ME_PR_10	--	--	--	2	12.7	32.9
Groundwater Sites						
ME_GW_01A	--	--	--	1,2	24.2	98.1
ME_GW_01B	--	--	--	1,2	32.3	98.4
ME_GW_02	--	--	--	1	27.7	82.1
ME_GW_03	--	--	--	1	19.2	68.7
ME_GW_04	--	--	--	1	23.4	75.6
ME_GW_05	--	--	--	1	22.2	67.8
ME_GW_06	--	--	--	1,2	29.5	99.0
ME_GW_07	--	--	--	1,2	23.5	99.0
ME_GW_08	--	--	--	1	16.3	73.1
ME_GW_09	--	--	--	1	15.8	67.6
ME_GW_10	--	--	--	1	24.3	67.6

Mississippi Embayment RCs for the ENSO & NAO

	ENSO			NAO		
Site ID	RCs	Average Period (years)	Percent Variance (%)	RCs	Average Period (years)	Percent Variance (%)
Precipitation Sites						
ME_PR_01	3,4,5,6,10	4.0	18.0	3,4,5	5.0	17.0
ME_PR_02	5,6,7,8,9	4.6	6.4	5,6,7,8,9	4.6	6.2
ME_PR_03	3,4,5,6,7	3.4	15.6	3,4,5	4.3	13.4
ME_PR_04	4,5,6,7	3.2	13.9	3,4,5,6	4.0	25.5
ME_PR_05	4,5,6,7,8,9	3.8	5.1	4,5,6	4.0	4.0
ME_PR_06	4,5,6,7,8	3.7	7.8	4,5,6	4.3	6.9
ME_PR_07	3,4,5,6	2.9	10.4	3,4	3.6	9.0
ME_PR_08	3,4,5,6	4.3	13.6	4,5	3.7	6.3
ME_PR_09	4,5,6,7,8	3.4	4.8	4,5,6	4.0	4.0
ME_PR_10	1,3,4,5	4.5	59.3	3,4	4.2	17.8
Groundwater Sites						
ME_GW_01A	4,5,6	3.8	0.4	4,5	4.3	0.4
ME_GW_01B	4	5.0	0.2	4	5.0	0.2
ME_GW_02	3,4,5,6,7	3.6	1.3	3,4,5	4.4	1.2
ME_GW_03	3,4	3.2	8.8	3,4	3.2	8.8
ME_GW_04	2,3,4	5.2	24.1	3,4	4.4	2.5
ME_GW_05	3,4,5	3.5	4.5	3,4	3.9	4.4
ME_GW_06	3,4,5	4.1	1.0	3,4,5	4.1	1.0
ME_GW_07	3,4,5	5.2	1.0	4,5	4.2	0.2
ME_GW_08	2,3,4	4.0	25.5	3	3.0	3.7
ME_GW_09	3,4	2.7	3.6	3	3.5	3.0
ME_GW_10	3,4,5,9	3.6	5.3	--	--	--

Mississippi Embayment RCs for the PNA & AO

	PNA			AO		
Site ID	RCs	Average Period (years)	Percent Variance (%)	RCs	Average Period (years)	Percent Variance (%)
Precipitation Sites						
ME_PR_01	5,6,7,8,9,10	1.9	3.3	7,8,9	1.0	1.1
ME_PR_02	8,9	3.6	1.3	--	--	--
ME_PR_03	4,5,6,7,8,9,10	2.1	9.4	9,10	1.0	0.8
ME_PR_04	5,6,7	2.8	5.8	--	--	--
ME_PR_05	5,6,7,8,9	2.8	2.6	--	--	--
ME_PR_06	5,6,7,8	3.3	4.4	--	--	--
ME_PR_07	3,4,5,6,7,8,9,10	2.1	11.6	9,10	1.0	0.5
ME_PR_08	4,5,6	3.3	6.3	--	--	--
ME_PR_09	5,6,7,8,9,10	2.5	2.8	10	1.0	0.2
ME_PR_10	4,5,6,7	2.3	10.9	--	--	--
Groundwater Sites						
ME_GW_01A	6	2.9	0.0	--	--	--
ME_GW_01B	--	--	--	--	--	--
ME_GW_02	5,6,7,8,9	2.1	0.1	--	--	--
ME_GW_03	3,4	3.2	8.8	--	--	--
ME_GW_04	4	2.9	0.6	--	--	--
ME_GW_05	4,5	2.8	0.8	--	--	--
ME_GW_06	5	3.3	0.0	--	--	--
ME_GW_07	4,5	4.2	0.2	--	--	--
ME_GW_08	3,4	2.7	4.8	--	--	--
ME_GW_09	3,4,5	2.4	3.8	--	--	--
ME_GW_10	4,5,6,7,8,9,10	1.6	1.9	6,7,8	1.0	0.4

Surficial RCs for the AMO & PDO

	AMO			PDO		
Site ID	RCs	Average Period (years)	Percent Variance (%)	RCs	Average Period (years)	Percent Variance (%)
Precipitation Sites						
SR_PR_01	1	59.3	61.9	2	23.7	24.3
SR_PR_02	--	--	--	1,2	25.1	79.9
SR_PR_03	1	56.9	41.6	2	14.2	22.8
SR_PR_04	--	--	--	1,2	27.8	79.6
SR_PR_05	--	--	--	1,2	33.9	85.3
SR_PR_06	--	--	--	1	29.8	50.7
SR_PR_07	--	--	--	1	16.3	38.7
SR_PR_08	--	--	--	--	--	--
Groundwater Sites						
SR_GW_01	--	--	--	1	13.8	66.0
SR_GW_02	--	--	--	1	30.3	74.9
SR_GW_03	--	--	--	1,2	15.2	91.6
SR_GW_04	--	--	--	--	--	--
SR_GW_05	--	--	--	1	18.8	76.7
SR_GW_06	--	--	--	1	15.2	59.3
SR_GW_07	--	--	--	1,2	16.2	91.9
SR_GW_08	--	--	--	--	--	--

Surficial RCs for the ENSO & NAO

	ENSO			NAO		
Site ID	**RCs**	**Average Period (years)**	**Percent Variance (%)**	**RCs**	**Average Period (years)**	**Percent Variance (%)**
Precipitation Sites						
SR_PR_01	5,6,7,8,9	4.3	2.8	5,6,7,8	4.6	2.6
SR_PR_02	3,4,5,8	3.9	12.8	3,4,5	4.3	11.8
SR_PR_03	4,5,6,7,8	4.5	15.4	5,6,7,8	4.1	11.3
SR_PR_04	3,4,7,8	4.0	10.9	4,7	3.4	4.4
SR_PR_05	3,4,7,8	4.3	8.3	3,4,7	4.8	7.3
SR_PR_06	3,4,7	4.2	10.9	3,4,7	4.2	10.9
SR_PR_07	5,6	4.1	10.6	5,6	4.1	10.6
SR_PR_08	5,6,7	4.4	17.4	5,6,7	4.4	17.4
Groundwater Sites						
SR_GW_01	2,3,4	3.1	33.5	2	4.6	28.0
SR_GW_02	3,4,5,6,7	3.4	7.0	3,4	4.9	5.4
SR_GW_03	3,4,5	3.7	7.2	3,4	4.4	6.8
SR_GW_04	2,3,4	4.0	46.7	3	3.3	6.4
SR_GW_05	3,4,5	2.9	2.2	3	3.8	1.7
SR_GW_06	2,3	4.2	34.0	2,3	4.2	34.0
SR_GW_07	3,4	3.4	5.6	3,4	3.4	5.6
SR_GW_08	2,3	4.9	37.3	2,3	4.9	37.3

Surficial RCs for the PNA & AO

	PNA			AO		
Site ID	**RCs**	**Average Period (years)**	**Percent Variance (%)**	**RCs**	**Average Period (years)**	**Percent Variance (%)**
Precipitation Sites						
SR_PR_01	7,8,9,10	2.8	1.2	10	1.0	0.2
SR_PR_02	4,5,6,7,8	2.4	9.2	6,7	1.0	2.7
SR_PR_03	6,7,8,9,10	2.6	10.9	9,10	1.0	3.3
SR_PR_04	4,5,6,7,8,9,10	2.1	12.2	5,6	1.0	5.4
SR_PR_05	5,6,7,8	2.0	6.1	5,6	1.0	3.9
SR_PR_06	5,6,7	1.7	6.9	5,6	1.0	5.1
SR_PR_07	3,4,6	1.0	19.3	3,4	1.0	15.7
SR_PR_08	3,4,6,7	2.4	27.7	3,4	1.0	18.6
Groundwater Sites						
SR_GW_01	3,4,5,6,7,8,9,10	1.3	6.0	7,8,9,10	0.8	0.1
SR_GW_02	5,6,7,8,9	2.1	2.2	--	--	--
SR_GW_03	4,5,6,7,8,9,10	1.8	3.1	9,10	1.0	0.2
SR_GW_04	3,4,5,6,7,8	1.7	11.0	7,8	1.0	0.8
SR_GW_05	3,6	2.8	1.8	--	--	--
SR_GW_06	3,4,5,6,7	1.8	10.9	6,7	1.0	1.8
SR_GW_07	3,4,5,6	2.2	6.9	5,6	1.0	1.2
SR_GW_08	3	3.7	5.0	--	--	--